THE UNIVERSITY *of* EDINBURGH

Using induced pluripotent stem cells to model glial-neuronal interactions in TDP-43 proteinopathies

Andrea Serio

Thesis submitted to the University of Edinburgh for the Degree of Doctor of Philosophy

March 2013

DECLARATION

The experiments presented in this thesis represent the unaided work of the author, except when clearly stated in the text. The work described in this thesis has not been previously accepted for nor is currently being submitted for another degree or qualification

Andrea Serio

March 2013

ACKNOWLEDGMENTS

A lot of people need to be thanked for their support and the help provided during my PhD. I would like to thank Professor Siddharthan Chandran, my PhD supervisor, for giving me the possibility of working on this project and for his guidance and support throughout these years. I also want to thank Professor Ian Wilmut, my second supervisor, for his advices and guidance. Needles to say, none of this project could have been completed with the help, supervision, guidance and support of all the members of the Chandran Lab. In particular I need to thank Bilada Bilican, David Hampton, David Story, Matthew Livesey, Karen Burr, Ghazal Haghi, Nina Rzechorzek, Shyamanga Booroah, Kunal Gupta and Dario Magnani for their help and support. All these people played a incredibly important role in this project over the years, and some are also responsible for having maintained the author's sanity over the legendary "second year blues" and other rough moments. For their scientific and personal support, I am deeply grateful.

Over the last four years I have been lucky enough to work with fantastic people in Edinburgh, but also –thanks to our collaborations- I had the opportunity to know and work with outstanding scientist. For this reason I want to thank Tom Maniatis and his lab from Columbia University and Christopher Shaw and his lab from King's College London. Thanks to constant communication, support and constructive criticisms from all people involved, these collaborations helped shaping this project.

Amongst the collaborations that have influenced my PhD, I am especially grateful to Steven Finkbeiner at the Gladstone Institute, San Francisco, for welcoming me in his lab, allowing me to learn new techniques and develop this project, but most of all for allowing me to meet and work with all the fantastic people in his lab. And this brings me directly to Sami Barmada, who I need to thank for his helpful advice, patience, hospitality and above all for his friendship, with helped me more than he will ever realize.

(Oh, thanks for Climbing and Burritos as well)

I need also to thank the Euan MacDonald Centre for Motor Neurone Research, and all the people that created it and worked with us in these

years (a special mention to Chloe Kippen): they helped us to put what we do into a great deal of prospective.
Another person that I have be grateful to (even if she does not realize that) is Chen Zhao, for being a great student as well as a great friend, and for allowing me to learn something important about myself as I was teaching her.
Thanks to my friend Yu, that has being alongside me for an interesting and never boring (although at time difficult) ride.
I want to thank my parents and my whole family, for always been there and for teaching me so much about the man ones wants to be and the man ones should become.

This thesis is dedicated to the person that most of all has had an impact on my life, my work and my future: Silvia. There are many things I need to thank you for and certainly not enough words do so properly. Without all your endless patience, your love and you zealous dedication to the cause of making me the happiest man alive, none of this would have happened.
Thank you for making the impossible happen on a daily basis, for cancelling the distance between Africa and Australia, for allowing eucalyptus and ponds to stay in the same place.

ABSTRACT

Amyotrophic Lateral Sclerosis (ALS) is an incurable late onset neurodegenerative disorder characterised by the specific loss of motor neurones (MNs). It has been recently demonstrated that Transactive response DNA-binding protein (TDP-43) is the dominant disease protein in both ALS and a sub-group of frontotemporal lobar degeneration (FTLD-TDP). Moreover, the identification of *TARDBP* mutations in familial ALS confirms a mechanistic link between the observed mis-accumulation of TDP-43 and neurodegeneration but also provides an opportunity to establish an *in vitro* platform to model these diseases, based on patient-derived induced pluripotent stem cells (iPSCs). This study presents the optimization of an iPSC-based platform to study the consequences of TDP-43 M337V mutation in human functional populations of MNs and astrocytes in isolation as well as in co-culture.

To develop this platform, two protocols to differentiate patient-derived iPSCs into functional MNs and astrocytes were first optimized, and the obtained cellular populations were then used to characterize the behaviour of mutant TDP-43 and its effect on the different cell types.

This study show that it is possible to use iPSC-based platforms to recapitulate *in vitro* key aspects of TDP-43 proteinopathies such as MN cell autonomous toxicity and TDP-43 accumulation, but they can also be used to highlight previously unrecognised disease specific mechanisms and to test novel therapeutic approaches. Moreover, by performing co-culture experiments it was possible to evaluate the effects of M337V astrocytes on the survival of wild-type and M337V TDP-43 motor neurons, showing that mutant TDP-43 astrocytes do not adversely affect survival of co-cultured neurons. This iPSC-based platform represents an *in vitro* model to study both the effect of somatic mutations on isolated patient-specific cultures, but also to investigate cellular autonomy and neurodegeneration in the context of TDP-43 proteinopathies.

Publications related to this thesis:

Bilican B., **Serio A.** *et al*. Mutant induced pluripotent stem cell lines recapitulate aspects of TDP-43 proteinopathies and reveal cell-specific vulnerability. *Proc Natl Acad Sci USA* (2012)

Serio, A. *et al.* Astrocyte pathology and the absence of non-cell autonomy in an induced pluripotent stem cell model of TDP-43 proteinopathy. *Proc Natl Acad Sci USA* (2013)

Barmada S.J., **Serio A,** *et al.* Small-molecule autophagy inducers enhance TDP43 clearance and prevent TDP43-mediated toxicity in primary rodent and human stem cell-derived neurons. (in preparation)

TABLE OF CONTENTS

Chapter 1: Introduction

1.1) Genetics and pathology of Amyotrophic Lateral Sclerosis

1.1.1) Introduction to the Pathology

Motor neurone diseases (MND) are a class of untreatable neurodegenerative disorders, characterized by a premature loss of motor neurons in the spinal cord and brain stem [1,2]. Within the spectrum of MNDs, amyotrophic lateral sclerosis (ALS) is an adult onset disease that starts as focal muscular weakness caused by specific loss of motor neurons (MNs), and progressively spreads to affect all muscle groups eventually causing death by respiratory failure[3] or complications of the treatment involved (i.e. mechanical ventilation). The mechanism(s) that lead to specific loss of motor neurons is at present unclear.

This form of motor neuron disease has a typical age of onset between 50 and 60 years and leads to spasticity, hyper-reflexia (upper motor neurons), generalized weakness, muscle atrophy (lower motor neurons), and paralysis[4]; ultimately death occurs in consequence to fatal respiratory paralysis typically within 1 to 5 years from clinical diagnosis. The lifetime risk for this neurodegenerative disorder is approximately 1 in 2000, with a UK prevalence of 4.0 to 4.7 per 100.000 population [5].

Pathologically, loss of motor neurons is accompanied by reactive gliosis[6] , intracytoplasmic neurofilament abnormalities, and axonal spheroids[7]. In end-stage disease, there is significant loss of large myelinated fibers in the corticospinal tracts and ventral roots as well as evidence of Wallerian degeneration and atrophy of the myelinated fibers [8]. Selectivity of death occurs even among motor neurons: the neurons that control the bladder (i.e., Onuf's nucleus in the sacral cord) and eye movements are relatively spared [9]. From a neuropathological point of view, the main feature of all cases of ALS is the presence of large insoluble protein aggregates in the cytoplasm and nucleus of dying motor neurons. These neuronal cytoplasmic inclusions

(NCI) have been demonstrated to be positive for ubiquitin, and are more commonly found in the lower motor neurons, mostly observed as either filamentous skeins or compact round bodies[10]

The only available treatment for ALS is Riluzole, that modulates pre-synaptic glutamate release[11] and prolongs survival by two or three months. The lack of effective treatments reflects our poor understanding of the ethiopathogenesis of ALS[12]

1.1.2) The genetics of ALS: Sporadic vs. Familial

The vast majority of ALS cases present as sporadic (sALS), however ~10% of patients present an inherited familial form of the disease (fALS). Given the lack of knowledge regarding the pathological mechanism(s) behind ALS, studying this minority of inherited cases offers probably the best method to interrogate the mechanism of motor neuron degeneration.

The understanding of fALS pathogenesis began with the discovery of dominant causative mutations in the gene encoding a copper/zinc superoxide dismutase 1 (SOD1) in ~20% of familial ALS cases and ~1% of sporadic cases[13]. SOD1 is a ubiquitously expressed protein and its main function is to convert superoxide radicals to molecular oxygen and hydrogen peroxide. So far, more than 100 different mutations have been identified in cases of fALS[14].

For the last 20 years, most of the efforts done to gain an understanding of ALS pathogenesis have been focused on the SOD1-determined cases of fALS and SOD-1 based animal models.

Since the original discovery that SOD1 mutations cause fALS, pathogenic variants in several other genes have been associated with this disease.

Starting from 2008, several groups reported a series of dominant mutations in the *TARDBP* gene (encoding for a DNA-RNA binding protein, TDP-43) as causative of fALS [15-19]. Collectively these studies provided evidence that the aberrant form of TDP-43 can directly trigger neurodegeneration. To this day, 30 different mutations are now known in 22 unrelated families (~3% of

familial ALS cases) and in 29 sporadic cases of ALS (~1.5% of sporadic cases)[5].

Following the identification of TDP-43 mutations as genetic determinants of fALS, two separate groups reported that mutations in another DNA/RNA-binding protein called FUS (fused in sarcoma) or TLS (translocation in liposarcoma) are responsible for causing fALS [20,21]. Linkage in this particular region had already been reported, and crucial for the identification of FUS/TLS within it was the previous discoveries of fALS causative mutations in TDP-43, which is a DNA/RNA-binding protein. Vance and co-workers prioritized the sequencing of genes within the linkage region identified in a large family with fALS so as to target genes encoding DNA/RNA-binding proteins, leading to the identification of a dominant missense mutation (R521C) in the FUS/TLS gene. This result was then replicated analysing several other fALS cases, which lead to the identification of the same R521C mutation in four additional families, as well as two additional missense mutations in another four families.

More recently, another fALS-linked gene (responsible for a previously reported linkage on chromosome 9p21) was identified by two separate studies [22,23]. The particular genetic variant highlighted was a non-coding hexanucleotide repeat expansion within the promoter or first intron of the alternatively spliced C9ORF72 gene. Importantly, this expansion was reported to be a relatively common fALS causing genetic variants, particularly in the Finnish population, and it was estimated to account for 46 % of Finnish fALS cases and between 22.5 %[23] and 38 %[22] of all fALS cases worldwide[24].

1.2) Transactive Response DNA Binding Protein 43 (TDP-43)

1.2.1) TDP-43 Biology and Functions

In 2008 mutations on *Transactive Response Dna Binding Protein (TARDP)* were shown to be causative of some cases of fALS[15]. *TARDP* encodes for a

43 KDa protein that binds to DNA and RNA, first described in 1995 as a novel protein that regulates HIV-1 gene expression in human cells[25].

This gene is highly conserved throughout evolution, and is found in all higher eukaryotic species, including animal models *Drosophila Melanogaster, Xenopus Laevis,* and *Caenorhabditis Elegans*[26]. Human *Tardbp* is located in 1p36.22, and is constituted by 6 exons; the protein is encoded by the first 5 exons, and it is ubiquitously expressed, with a predominant nuclear localization. TDP-43 contains two RNA recognition motifs highly conserved among species, and a glycine rich C-terminal domain, typical of the heterogeneous nuclear ribonucleoprotein (hnRNP) family, to which TDP-43 belongs[27]. The C-terminal domain is a very important feature of this protein, for two reasons: first, its sequence varies considerably between species, reflecting species-specific functions; secondarily, all but one of the ALS causative mutations identified in Tardbp are located in this region[5].

TDP-43 is able to bind both mRNA and DNA, and although a clear consensus TDP-43 binding site in vivo has yet to be established, in early in vitro studies this protein seemed to preferentially bound RNAs via a GU dinucleotide repeat element [28]. Moreover, analyses of global TDP-43 binding sites showed that the most significant RNA binding occurred at either uninterrupted GU repeats[29] or a GU-rich motif interrupted by a single adenin[30].

This protein has been shown to play key roles in the regulation of gene transcription, pre-mRNA splicing, mRNA stability and transport[28]. Particularly, it has been reported that TDP-43 contributes to the splicing of the *cystic fibrosis transmembrane conductance regulator (CFTR)* gene, promoting exon skipping [31,32], and in the splicing of *Survival of Motor Neurons 2 (SMN2)* gene, promoting exon 7 inclusion [33].

TDP-43 has also been implicated to have a role in mitochondrial function, as abnormal expression of the mitochondria fission/fusion proteins MFN1 and Fis1 was observed in transgenic (Tg) mice constitutively expressing a human wild-type TDP-43 transgene driven by the mouse prion promoter [34].

A direct or indirect link between TDP-43 and mitochondria is also supported by the discovery that HDAC6, a downstream RNA target of TDP-43[35] has recently been implicated in mitophagy[36].

In 2012, Chiang and co-workers highlighted another role for TDP-43, by performing transcriptional profiling of TDP-43 deficient embryonic stem (ES) cells. Their study identified as a putative target of TDP-43 the RAB GTPase Tbc1d1, a gene linked to cellular metabolism and obesity[37].

Another TDP-43 role proposed recently is more directly linked to neuronal survival and neurodegeneration: Tollervey and colleagues showed that TDP-43 bound RNAs that encode proteins which regulate neuronal development and survival, and identified the noncoding RNAs MALAT1 and NEAT1 as disease relevant TDP-43 targets[38]. Although further studies are necessary to clarify the splicing regulatory role of this exciting class of noncoding RNAs in the survival and degeneration of neurons, direct binding of TDP-43 to a wide range of target RNAs relevant to neuronal survival suggests that TDP- 43 is involved in neuronal function and integrity in health and disease.

In the last 2 years, TDP-43 has been also shown to have a crucial role during development; two independent studies demonstrated that TDP-43 is essential during early embryonal stages, in particular for blastocyst implant and inner cell mass growth[27,39]. Sephton and co-workers in particular, demonstrated by in situ hybridization how TDP-43 is present throughout embryonic development and it is particularly expressed in the neuroepithelium and neural progenitors of the developing embryo[27]. Importantly this protein has been shown to relocate at the terminals of electrophysiologically active neurons[40].

Finally, several studies have reported that TDP-43 levels have particularly tight regulatory control mechanisms, to prevent cellular toxicity due variations in TDP-43 levels[41]. One such report increased TDP-43 expression in Tg mouse models or cultured cells led to a prominent reduction in endogenous TDP-43 levels [42-44] providing evidence that TDP-43 regulates

its expression via direct binding of the TDP-43 protein to its own 3'UTR sequence and contributes to TDP-43 mRNA instability and degradation.

Importantly, accumulating evidence indicates that TDP-43 has –amongst the other roles described – a key function in mRNA triage and stress-responsive RNA-associated factor. In particular, it has been demonstrated that exposure to oxidative stressors –such as zinc- leads to accumulation of insoluble TDP-43 aggregates in cultured cells[45]. More recently using a variety of cultured cells it has also been demonstrated that exposure to stress causes TDP-43 relocalisation to cytoplasmic foci called stress granules (SGs) [46-48]. SGs represent a cellular regulatory mechanism that triages stalled RNA regulation and sorting[49,50]. Other groups reported relocalisation of endogenous or ectopically expressed TDP-43 to SGs in human cell lines, NSC-34 cells (a motor neuron-like cell line) or cultured primary glia, in response to a variety of stresses including arsenite and sorbitol [48 51]. Although the descriptive nature of SG localization reveals a physical incorporation of TDP-43 within SGs, whether TDP-43 has an active role within SGs or a causal role in SG assembly remains uncertain.

1.2.2) TDP-43 Pathology, TDP Proteinopathy and the ALS-FTLD Spectrum

As described in the first part of this section, ALS is the most frequent form of motor neuron disease and the absence of available treatments is a reflection of our poor understanding of the ethiopathogenesis of this disease. A characteristic feature of degenerating neurons in ALS, and one of the most used pathological classification criteria, is the presence of cytoplasmic inclusions positive for ubiquitin (neuronal cytoplasmic inclusions, NCI). Interestingly, these NCIs are commonly found in another class of neurodegenerative disorders, termed Frontotemporal lobar degeneration (FTLD). FTLD is a focal, non-Alzheimer form of dementia, that can present either behavioural or aphasic symptoms [52 53] and is the second most frequent cause of presenile dementia[54].

Interestingly, besides the presence of NCIs, there is a degree of clinical overlap between dementia and ALS, demonstrated by the presence of cognitive and behavioural dysfunction in up to 50% of ALS patients[55,56]. These findings indicated for the first time that ALS and FTLD might represent two points in a spectrum of clinical phenotypes, related by common neuropathological mechanisms [57]. Further evidence for a clinical overlap between these two diseases is the presence of ALS cases displaying progressive aphasia [58 59] and frontotemporal atrophy [60].

Definitive evidence that ALS and FTLD are linked came in 2006, from a study by Neumann and colleagues. In this study the characterization of post-mortem samples presenting ubiquitin positive NCIs led to the identification of TDP-43 as the main component of pathological protein aggregates in 50% cases of FTLD-U (renamed as FTLD-TDP)[13] and in the vast majority of ALS cases (ALS-TDP) [61-63]. Besides the colocalisation of TDP-43 and ubiquitin in the pathological inclusions and specificity of TDP-43 immuno-reactivity for the NCI in these conditions these common pathology was also characterised by abnormal fragments of TDP-43 in post-mortem tissue, ubiquitination and hyperphosphorylation of TDP-43 and loss of the normal nuclear TDP-43 staining in cells harbouring NCIs[55].

These common pathological hallmarks confirm that ALS and FTLD are part of the same clinical manifestation spectrum and also provide a unifying pathology that allows the classification of both neurodegenerative disorders as "TDP proteinopathies".

In 2007 Mackenzie and colleagues demonstrated that even if SOD1 fALS has been extremely important in the understanding of ALS pathological mechanism, it might not represent the perfect model to obtain general insights on ALS mechanism: in their study they compared five different groups of patients (sporadic ALS, fALS with and without mutations in SOD1, and ALS with dementia) forming a cohort representative of the most common cases of ALS, and then analysed the presence of TDP-43 proteinopathy among the different groups. The results of this study demonstrated that SOD1 fALS is the only form of this disorder that does not

present ubiquitinated TDP-43 positive NCI cannot therefore be classified within the TDP proteinopathies [64]. This study indicated for the first time in a systematic way that studying of TDP-43 fALS cases has potentially a much wider relevance to our understanding of the vast majority of ALS cases.

1.2.3) Models of TDP-43 Proteinopathies

The role of mutated TDP-43 in the pathogenesis of ALS remain still unclear; however, in the last years several studies have shed some light on the mechanism of motor neuron toxicity in the presence of mutations on *Tardbp*.

In Vitro Models of TDP Proteinopathies

Since the original identification of TDP-43 as the component of the NCIs, several *in vitro* models have been established to elucidate the cellular pathways involved in TDP-43 toxicity and the mechanism of neurodegeneration. A number of different systems have been used, from immortalized cell lines such as HEK-293 cells and HeLa cells, to primary neuronal cultures and unicellular organisms such as yeasts.

In 2008 Winton and co-workers demonstrated that in the context of QBI-HEK 293A cells (an immortalized line of primary human embryonic kidney cells) the expression of a truncated form of TDP-43, lacking the nuclear localization sequence, was sufficient to disturb the nuclear localization of normal TDP-43, and to induce the formation of aggregate, sequestering the wild type form[44]. More recently Nishimura and co-workers, have conducted similar experiments on neuroblastoma cell lines, showing that impairment of the nuclear import of TDP-43 causes accumulations, suggestive of a mechanistic role for nuclear transport machinery in ALS and FTLD pathogenesis[65].

Immortalised cell lines have also been used by Igaz and co-workers in 2009 to show that the expression of C-terminal fragments of TDP-43 recapitulated features of TDP proteinopathies, with alteration of splicing

and accumulation of insoluble protein aggregates[66]. Interestingly, these studies demonstrated that it was possible to reproduce *in vitro* some of the aspects of the proteinopathies observed in patient, but they were not yet able to answer the question of possible mechanisms of aggregation. In the same year Johnson and collaborators demonstrated that TDP-43 is intrinsically aggregation prone, and mutations simply accelerate the aggregation process and increase the basal level of toxicity[67]; this particular study was conducted in a yeast model, and was crucial to highlight the behaviour of this protein in relation to specific mutations in the glycine rich domain and also to suggest that TDP-43 itself can initiate aggregate formation under certain conditions.

Another in vitro study published in the same year showed that in cultured neuroblastoma cells, the suppression of *Tardbp* expression induced cell death by disregulating three GTPase from the Rho family[68].

In vitro studies also indicated an important link between TDP-43 and cellular stress, as they demonstrated that this protein is part of the stress granules that are formed in response to certain adverse conditions in the cellular environment [46-48]. Interestingly, Cohen and colleagues showed that particularly redox signalling can promote TDP-43 cross-linking via direct cysteine oxidation, increasing the chances of insoluble aggregates formation [69].

Cellular models based on primary rodent neuronal cultures have also been particularly useful to understand TDP-43 toxicity. Amongst these, a system developed by Barmada and co-workers suggested that TDP-43 toxicity might be more directly linked to its localisation than to the formation of ubiquitinated aggregates[70].

In summary, several useful observations on the mechanisms involved in TDP-43 aggregation and toxicity have been derived from cellular models. However, these findings need to be further verified by both animal models and also by the development of further in vitro models, based on more relevant cell types.

Mouse models of TDP-43 proteinopathies

The first murine model developed to address the physiological role for TDP-43, were reported after 2009, and consisted mainly of *Tardbp* null mice. Because TDP-43 is an essential protein for embryonic development, in all instances embryonic lethality was observed, occurring between embryonic days 3.5 and 8.5 [27] [39]. Interestingly, heterozygous Tardbp null mice showed deficits in motor function, although without any displaying any apparent MN degeneration, suggesting that reductions in TDP-43 physiological levels are sufficient to cause a motor weakness phenotype [71]. To overcome the problems of total knockout mice a recent study developed a conditional Tardbp knockout mouse model, showing that postnatal deletion determines an array of different deficits. Interestingly, this study identified a role for TDP-43 in metabolism: in fact, amongst the identified problems caused by postnatal Tardbp deletion loss of body fat was noted. Moreover, these mice exhibited also a transcriptional profile consistent with what observed in metabolic dysfunction and obesity, and researchers were able to identify one of the crucial genes of this pathway, Tbc1d1, as a target of TDP-43 [37]. More recently, a study reported that specific deletion of Tardbp from the spinal cord MNs determines a motor deficit with pathological features similar to those observed in ALS[72]. As in many different diseases before TDP proteinopathies, deletion models can offer insight in the biological relevance of the studied protein in key cellular pathways, but there are limitations to the extent to which these knockout mice model the human pathology. For this reason the subsequent generation of animal models of TDP-43 toxicity was focused on creating appropriate transgenic mice. The following table present the list of transgenic mice reported in various study from 2009 till now, together with a brief description of the observed phenotypes.

Study	Transgene	Mutation	Promoter	Expression	Exp. Levels	Motor Impairment	Cytoplasmic TDP	Ubiq+ NCIs	Gliosis	TDP-43 Cleavage	Degeneration	Survival
Wegorzewska et al.2009	Flag tagged Human	A315T	PrP	Constitutive	Over expressed	Y	N	Y	Y	Y	MNs and Layer V cortex	154 days
Stallings et al. 2010	Human	WT	PrP	Constitutive	Over expressed	N	Y	N	Y	Y	N.R.	Normal
Stallings et al. 2010	Human	A315T	PrP	Constitutive	Over expressed	Y	Y	Y	Y	Y	N.R.	75 days
Xu et al. 2010	Human	WT	PrP	Constitutive	Over expressed	Y	Y	Y	Y	Y	Spinal cord	30-60 days
Zhou et al. 2010	Human	WT (minigene)	Endogenous	Constitutive	Constitutive	Y	Y	N	N	N	None	Normal
Zhou et al. 2010	Human	M337V	TRE (CAG-tTA)	Inducible (constitutive +10)	Over expressed	Y	Y	Y	Y	Y	MNs, Spinal cord neurons, hippocampus, cerebellum and cortex	up to 55 days depending on expression levels
Tian et al. 2011	Human	WT	CAG	Constitutive	Over expressed	N	N	N	N.R.	N.R.	Frontal cortex	N.R.
Xu et al. 2011	Human	M337V	PrP	Constitutive	Over expressed	Y	Y	N	Y	Y	N.R.	28 days
Wils et al. 2010	Human	WT	Thy1.2	Constitutive	Over expressed	Y	Y	Y	Y	Y	MNs, hippocampal neurons and Purkinje cells	up to 200 days depending on expression levels
Shan et al. 2010	Human	WT	Thy1.2	Constitutive	Over expressed	Y	N.R.	N	N.R.	N.R.	Spinal cord	Normal
Tsai et al. 2010	Mouse	WT	CaMKII	Constitutive	Over expressed	Y	Y	Y	Y	Y	Cortical neurons	495 days
Igaz et al. 2011	Human	WT	TRE (CaMKII-tTA)	Inducible (constitutive +28)	Over expressed	Y	N	Y	Y	N	hippocampal neurons and neocortex	N.R.
Igaz et al. 2011	Human	ΔNLS	TRE (CaMKII-tTA)	Inducible (constitutive +28)	Over expressed	Y	Y	Y	Y	N	Cevical spinal cord, hippocampal neurons neocortical neurons	N.R.

Four separate TDP-43 transgenic mice lines described in the table have been engineered to express the transgene under the control of the mouse prion protein (PrP) promoter which drives high expression in central nervous system. In particular, the mouse model generated by Wegorzewska and colleagues [73] overexpresses a flag-tagged mutant version of human TDP-43, and present a progressive motor dysfunction associated with weight loss, that cause the death of the animal by 5 months of age. Interestingly, even if the PrP promoter drives the transgene expression throughout all CNS areas, neurotoxicity is observed only in layer V cortical neurons and in spinal motor neurons.

However, Xu and colleagues reported similar results in their PrP-driven TDP-43 line overexpressing the wild-type human protein, with reduced body weight and motor impairment associated with spinal cord degeneration and reduced viability. These two studies indicated that the overexpression of either the wild-type or mutant versions of TDP-43 can induce a pathology in mice that presents several of the observed ALS characteristics (motor involvement, specific neurodegeneration, etc.). In this context, the study of more independently generated transgenic mice lines shed light on the differential toxicity of mutant and wild-type TDP-43. Stallings and co-workers reported that while at high expression levels there was no significant distinction between wild-type and mutant TDP-43 transgenic mice, at lower expression levels only the mutant TDP-43 expressing mice developed an observable pathology. Additional evidence supporting the idea of a differential toxicity between mutant and wild-type TDP-43 came from the analysis of transgenic rats, engineered to express a BAC-derived mini version of either M337V or wild-type TDP-43. Zhou and colleagues demonstrated that in this system the M337V mutant version of the protein was able to determine a observable motor deficit with associated specific neurodegeneration of spinal cord, cerebellum and cortex in transgenic rats. The same group also showed that postnatal expression of the mutant M337V-TDP-43 mini gene (using a inducible expression system) in rats caused MNs degeneration and progressive paralysis[74]. The same group

generated also a murine transgenic mouse model, that expresses either the mutant or wild-type TDP-43 under the control of the ubiquitous CAG promoter. This particular system confirmed what they already observed in the transgenic rats: the mutant version of the protein causes a significantly increased pathology compared to the mild deficits observed in wild-type overexpressing mice[75].

Another strategy to generate TDP-43 transgenic mice, adopted by some groups to overcome the overt embryonic and developmental toxicity of TDP-43 overexpression while maintaining a meaningful expression pattern, is to drive the transgene expression under the control of the Thy1 promoter, which ensure postnatal expression targeted in neurons.

Transgenic mice that express wild-type TDP-43 under control of the mouse Thy1 promoter, develop a dose- dependent degeneration and motor phenotype similar to what observed in PrP promoter transgenic lines [76,77]. In particular a dose-dependently influence the onset and rate of progression was observed by Wils and co-workers, while in the lines generated by Shan and colleagues the severity of the phenotypes correlates with the copy number of the transgene.

Another different strategy, used independently by two groups to generate transgenic murine models of TDP proteinopathies is to control the expression of TDP-43 with the Ca2+/calmodulin-dependent kinase II (CaMKII) promoter, which drives neuronal expression predominantly in the forebrain but not in the spinal cord. Interestingly, these mice develop progressive motor deficits with impairments in motor coordination, balance, and grip strength by six months of age [78]. Igaz and colleagues also reported that the CaMKII-mTDP-43 mice develop abnormal limb- clasping reflexes when suspended by their tails[43].

Several of the transgenic models presented above show several commonalities in the observed pathology, despite numerous variations in their design (i.e. selection of promoter driving transgene expression and, consequently, the regional expression, in the form of TDP-43 being expressed) and even in the species chosen for the model (mouse vs. rat).

Most of these consistently models show a motor pathology similar to what observed in ALS, but there are also several divergences in the pathological features they present.

One example of particular interest is the presence of TDP-43 positive ubiquitinated aggregates, which represents probably the most characteristic feature of TDP-43 proteinopathies. In the context of the Prp-promoter based models, Wegorzewska and colleagues observed ubiquitin-positive aggregates selectively in cortical layer V and spinal cord motor neurons, but in all cases these structures were TDP-43 negative[73]. Conversely, the mice generated by Stallings and co-workers present phosphorylated TDP-43 within ubiquitin-positive inclusions in late stage spinal cord motor neurons[79].

In general, TDP-43 immunopositive cytoplasmic inclusions are seldom observed when immunostaining of brain or spinal cord sections is carried out using the same phosphorylation-independent TDP-43 antibodies used to detect human pathology [34,43,73,75-77,79,80]. These observations would suggests that TDP-43 aggregates per se are not necessary for the development of a neurodegeneration dependent motor deficit, although this does not excludes that they might contribute to the overall toxicity. This concept is partially in contrast with what observed in the yeast model of TDP proteinopathies[81], where only the aggregates forming variants of the protein are shown to be toxic, but it finds support in the cellular system developed by Barmada and co-workers[70].

Another pathological hallmark of ALS and TDP proteinopathies in general is the change in localisation of TDP-43. In particular, in ALS patient samples it is possible to observe redistribution of TDP-43 from the nucleus to the cytoplasm, although it appears to be an early event in the pathogenesis of these disease [82], and eventually loss of nuclear TDP-43 staining[61].

Cytoplasmic TDP-43 staining is occasionally observed in some of the published transgenic murine models, but they mainly display a nuclear localization of the exogenous protein [77-80]. Similarly loss of nuclear TDP- 43

can be observed in selectively vulnerable neurons is observed prior to obvious signs of degeneration in some models [73,77,78].

In particular, Igaz and colleagues generated transgenic mice that inducibly overexpress, within the forebrain, human TDP-43 with a mutated nuclear localization signal (iTDP-43ΔNLS) using the CaMKII tetracycline-off inducible system [43].

An interesting observation that arose from the analysis of these transgenic models was the presence of mitochondrial abnormalities.

In particular, Xu and co-workers observed eosinophilic aggregates within the axons of spinal cord motor neurons in their transgenic model, that were revealed to be composed of abnormal clusters of mitochondria present, suggesting a causative link between overexpression of TDP-43 and mitochondrial dysfunction.

Shan and colleagues reported similar accumulations of mitochondria within the cytoplasm of motor neurons in their Thy1-drived TDP-43 transgenic[76].

Other Animal Models of TDP-proteinopathies

Besides the murine models described above, a number of other strategies have been used to model TDP proteinopathies. Since 2009 a number of groups published *Drosophila Melanogaster* based models that revealed particularly useful confirm several observation that emerged from the analysis of the murine models. Interestingly, most of the fruit fly models recapitulate the observations made in transgenic mice, and in particular the dose-dependent toxicity caused by overexpression of TDP-43 or its fruit-fly analogue TBPH [83].

For example, several Drosophila models support the hypothesis that TDP-43 toxicity also depends on its ability to bind RNA targets implying that the toxicity might be based on a "loss of function" mechanism [84,85] [86]. Moreover, some of the Drosophila models of TDP-43-pathologies described in this paper support the hypothesis that age-dependent degeneration can increase the TBPH/TDP-43 toxicity [87] [88]. However, even if several important information have been derived from analysis of these models

additional studies are required to understand how much of what learnt from *Drosophila* models can be generalized to humans[83].

Other species that have been used to model TDP-43 proteinopathies include *Danio Rerio,* the zebrafish and *Caenorhabditis elegans*, the flatworm . Examples include the study published in 2010 by Kabashi and collaborators, in which they demonstrated that disruption of *Tardbp* expression during development caused a motor phenotype. They also showed that the ectopic expression of human wild type TDP-43 was able to rescue this motor system abnormality, whereas expressing the human mutated form did not have any rescue effect [89]. More recently, both the zebrafish and C. elegans have been used to test compounds that might protect from TDP-43 and FUS neuronal toxicity [90].

Given that ultimately all these models need to be able to provide information useful to develop new therapeutic approaches for the human pathology, it is interesting to note that non human primates have started to be used in comparison to rodents to establish ALS and FTLD models. In particular, in 2012 a Japanese research published a study describing the analysis of a wild-type TDp-43 overexpressing *Macaca fascicularis* monkey. Their results showed that the primate model recapitulated several aspects of the human pathologies and also several molecular features observed in equivalent rodent models. The TDP-43 overexpressing primates presented a progressive motor pathology, accompanied by cytoplasmic TDP-43 localisation and loss of nuclear TDP-43 without any aggregates[91].

TDP-43 Proteinopathies: Proposed models of toxicity

Based on what observed in the in vitro and in vivo models published so far, it has not been possible to derive a consensus on the exact mechanism of TDP-43 toxicity. Some of the observations derived from these models seems to support a toxic gain of function mechanism, while other studies would suggest that a loss of TDP-43 function is responsible for the neurotoxicity observed.

TDP-43-mediated toxicity via toxic gain of function

The most distinctive molecular features of TDP-43 pathology are the cytoplasmic deposition of TDP-43 aggregates, the loss of nuclear TDP-43 and post-translational modifications such as phosphorylation and cleaved [61]. Similar to other protein-misfolding diseases, TDP-43-mediated toxicity may be the result, of a toxic gain of function from the aggregates. Traditionally, the toxic potential of protein aggregates is tested by overexpressing the protein of interest in animal models, however as reported in the previous section, in the transgenic mice analysed the presence of TDP-43^{+} accumulations in the cytoplasm of neurons (analogous to those observed in the post-mortem patients samples) is inconsistent between different lines, and constitutes a rare event. As an interesting example, Wegorzewska and colleagues observe ubiquitin-positive, but TDP-43-negative, aggregates[73]. In this particular mice however, as it is the case with most of the rodent model presented, it is possible to observe specific neurodegeneration and a motor phenotype consistent to that reported for ALS. This would suggest that toxicity can occur even in the absence of TDP-43 aggregation without the requirement for formation of cytoplasmic TDP-43 aggregates. This does not, however eliminate the possibility for a the cytotoxic potential of TDP-43 aggregates nor the possibility that their formation would enhance TDP-43-mediated neurodegeneration[92], shown with the yeast models. Moreover, overexpression of C-terminal fragments in vitro can cause aggregation of TDP-43 in several cell lines, ultimately leading to toxicity[66].

Therefore despite the evidence that TDP-43 aggregates might represent a important factor for cytotoxicity future studies will need to further investigate this question.

TDP-43-mediated toxicity via loss of function

Although the exact roles of TDP-43 remain largely unknown, a number of studies have indicated several cellular mechanisms that require TDP-43 function (see TDP-43 Functions above), like splicing, mRNA triage, mitochondrial stability and synaptic function. Given the observed loss of

nuclear TDP-43 observed in the disease, and considering that the formation of aggregates could further deplete the pool of functional TDP-43 available to participate to cellular functions, one of the proposed mechanism for TDP toxicity is the loss of function[41].

Most studies have so far concentrated on the nuclear properties of TDP-43 and its involvement in specific pre-mRNA splicing and transcription events, but it is in particular in the *Drosophila* models that the loss of function hypothesis find several supporting evidences. In fact, the depletion of the TDP-43 homologue causes synaptic toxicity and adversely affects motor neurone presynaptic terminals at neuromuscular junctions, ultimately determining deficits in locomotive behaviours and reduces life span [93]. Moreover, loss of TBPH decreases dendritic branching in *Drosophila* larvae, that is actively rescued by over-expressing either TBPH or human TDP-43[94]. Similar evidence can be obtained also by neuroblastoma lines based studies, as reported above[68].

1.3) Astrocytes

Astrocytes (collectively known as astroglia) are specialized glial cells present in the entire central nervous system (CNS), that out-number neurons by over fivefold, accounting for the majority of the raw cellular mass of the brain and spinal cord[95]. These cells were originally identified as the CNS "connective tissue", have been regarded for decades as passive support cells in the brain, affording structural and metabolic support to neurons. In recent years however, it has become clear that astrocytes are key players in the regulation of the brain microenvironment, in particular as regards neurotransmitter and ionic homeostasis, metabolic support of neurons, regulation of energy metabolism, synaptic transmission and neuronal excitability, synaptic generation, detoxification, free-radical scavenging, metal sequestration, development and maintenance of the blood-brain barrier, guidance of neuronal migration and immune function[96].

1.3.1) Gliogenesis

All three major cell types, neurons, astrocytes and oligodendrocytes, in the central nervous system (CNS) are generated from multipotent self-renewing Neural stem cells (NSCs) [97]. However, during CNS development the differentiation of NSCs into the three different lineages is precisely regulated both spatially and temporally. In particular early gestation NSCs do not present multipotentiality and differentiate exclusively into neurons until mid-gestation; they then gradually begin to display multi- potentiality and differentiate into glial cells during late gestation, after most of the neuronal networks have already been established [98]. This specific timing mechanism in NSCs fate determination is controlled by extracellular cues, as cytokine signalling[98], and transcriptional states [99] but also by intracellular programs, in particular epigenetic gene regulation [100] [101,102].

Extracellular Cues

Many secreted protein have been reported to play a role in the induction of gliogenesis. In particular, it has been know for over a decade that JAK-STAT pathway regulates the induction of astroglial differentiation and specification[103,104]. The JAK-STAT pathway is activated by leukaemia inhibitory factor (LIF), a member of IL-6 interleukin family, through the heterodimeric receptor LIFRβ and gp130, and can in turn significantly induce astroglial differentiation. Evidence in support of this include the results of gene knock-outs for LIF, LIFRβ, gp130 or STAT3[105-107] showing impaired astrocyte differentiation in vivo, suggesting that JAK-STAT signalling contributes to astrogliogenesis in the developing CNS gene knock-outs of LIF, LIFRβ, gp130 or STAT3 results in impaired astrocyte progenitors pool generation and ultimately impaired astrogliogenesis[105-107]. Interestingly, it has been also demonstrated that it is the activity of EGFR that controls the competence of NPC to interpret LIF signalling as a astrocyte induced in vivo[108]. }.

Bone morphogenetic proteins (BMPs) are a family of pleiotropic cytokines active in many tissues (including the CNS) that belongs to the transforming

growth factor-β (TGFβ) superfamily[109]. It has been recently shown that BMPs can induce astrocyte differentiation by forming complexes between STATs and BMP-activated transcription factor Smads, bridged by the transcriptional coactivators, p300/CBP[110].

Several growth factors have also been shown to have an important role in the determination of gliogenesis onset, and in particular epidermal growth factor (EGF) and fibroblast growth factor 2 (FGF2) play a key role in the determination of neural progenitors potency.

FGF2 in particular is a widely used mitogen to expand neural stem cells in vitro, and its role in the maintenance of neural stem cells in developing brain has been demonstrated previously[111]. FGF signalling has many roles during development, but it exerts its function in a context dependent manner, as it has been previously shown with an analysis of different FGF receptors and their influence over self-renewal and differentiation of neural progenitors[112].

Previous studies have demonstrated that in the developing mouse brain it is possible to isolate different populations of progenitors in neurosphere formation assays, using either FGF2 or EGF [113,114]. A later study from the van der Kooy group demonstrated that FGF-responsive stem cells divide symmetrically between E11 and E14, and then switch to asymmetrical cell divisions between E14 and E17; at the same time EGF-responsive progenitors arise from asymmetric division of the FGF-responsive pool of stem cells, hence mainly at E14 [115]. These results are in line with previous studies reporting that between E13 and E16 in the developing mouse brain there is a change in responsiveness to EGF-family ligands, reflecting a increased level of expression of EGFR[116,117]. Interestingly this timing coincide with the late onset gliogenesis during development, when neural progenitors acquire the potency to generate astrocytes and other glial cells trough several mechanism (one example is the demethylation of GFAP promoter, after E14 [118]). Moreover, it has been demonstrated by Sanalkumar and co-workers, that in vitro neuronal versus glial specification in ES derived NPCs is largely determined during their proliferation trough

exposure to either FGF2 or EGF[119]. Moreover, this study clearly demonstrates that EGF-responsive NPC in vitro are capable of generating 6-fold more GFAP+ cells than their FGF-responsive counterparts.

Transcription factors

Transcription factors have also been shown to play an important role in determining the ability of NSCs to differentiate into astrocytes. In particular neurogenic basic helix-loop-helix (bHLH) transcription factors Neurogenein1 and Neurogenin2 have been shown to regulate astrocyte differentiation during early neural development by competitively binding to p300/CBP-Activated Smad complexes, preventing their binding to activated STAT3. Preventing STAT3-Smad complexes to form, this mechanism restrict astrocyte differentiation in NSCs, which are only capable of generating neurons under the influence of high-level neurogenic bHLH during the neurogenic period [99].

Intracellular Programmes

In addition to these extracellular cues and transcription factors, astrogliogenesis fine timing is also highly dependent on the epigenetic regulations in NSCs, in particular the regulation of CpG methylation state [100]. In NSCs during the waves of neurogenesis a CpG dinucleotide within a STAT-binding element (TTC CGA GAA) in the gene promoter of the astrocytic marker glial fibrillary acidic protein (GFAP) is highly methylated, preventing the binding of activated STAT3-Smad complexes and thus preventing astroglial gene expression [118]. As an effect of this regulatory mechanism, neural progenitors at mid-gestation are not able to express *GFAP* even when stimulated by STAT-activating IL-6 family cytokines. As gestation proceeds, the STAT-binding site becomes gradually demethylated in NSCs, enabling them to express *GFAP* in response to LIF stimulation [100].

Gliogenesis in vitro

Generally proliferation and propagation of NPC in vitro is maintained by FGF2 and EGF, for both monolayer NPC cultures[120-123] and neurospheres[124-126]. FGF2 in particular is a widely used mitogen to expand neural stem cells in vitro, and its role in the maintenance of neural stem cells in developing brain has been demonstrated previously[111]. FGF signalling has many roles during development, but it exerts its function in a context dependent manner, as it has been previously shown with an analysis of different FGF receptors and their influence over self-renewal and differentiation of neural progenitors[112].

Previous studies have demonstrated that in developing mouse brain it is possible to isolate different populations of progenitors in neurosphere formation assays, using either FGF2 or EGF [113,114]. A later study from the van der Kooy group demonstrated that FGF-responsive stem cells divide symmetrically between E11 and E14, and then switch to asymmetrical cell divisions between E14 and E17; at the same time EGF-responsive progenitors arise from asymmetric division of the FGF-responsive pool of stem cells, hence mainly at E14 [115]. These results are in line with previous studies reporting that between E13 and E16 in the developing mouse brain there is a change in responsiveness to EGF-family ligands, reflecting a increased level of expression of EGFR[116,117]. Interesting this timing coincide with the late onset gliogenesis during development, when neural progenitors acquire the potency to generate astrocytes and other glial cells trough several mechanism (one example is the demethylation of GFAP promoter, after E14 [118]). Moreover, it has been demonstrated by Sanalkumar and co-workers, that in vitro neuronal versus glial specification in ES derived NPCs is largely determined during their proliferation trough exposure to either FGF2 or EGF[119]. Moreover, this study clearly demonstrates that EGF-responsive NPC in vitro are capable of generating 6-fold more GFAP+ cells than their FGF-responsive counterparts.

There is therefore an increasing body of information pointing to the possibility to increase the efficiency of gliogenesis in vitro by culturing the NPC in EGF alone.

1.3.2) Functions

Although astrocytes have a key role in several different functions within the CNS, their role is essentially to maintain homeostasis and ensure the continuity of function and cellular health for the neuronal networks. In order to perform this role, astroglial cells express numerous receptors that enable them to respond to neurotransmitters, neuropeptides, growth factors, cytokines, small molecules and toxins; not only enabling them to participate in signal processing, but also to sense any changes in the extracellular environment [127,128].

Astrocytes are able to secrete a variety of neurotrophic factors essential for the proliferation, survival and maturation of committed neuroblasts [129], including nerve growth factor (NGF), brain-derived neurotrophic factor (BDNF), glia-derived neurotrophic factor (GDNF), ciliary neurotrophic factor (CNTF), glia-derived nexin (protease nexin-1) and epidermal growth factor (EGF) [128 130].

Astrocytes can also control neuronal health more directly, by regulating the production of synapses and taking part in synaptic transmission.

In particular, it has been shown that astrocytes can promote the formation and stabilisation of synapses in CNS neurons and are able to control synaptic modulating synaptic activity [131-134].

Moreover, in the last decade the term “Tripartite synapse” has been proposed, to properly describe the bidirectional communication between neurons and astrocytes [135]. In fact, astrocytes are able to express many neurotransmitter receptors which are stimulated during synaptic activity and can initiate calcium signalling within the astrocytes[135] In conditions of a high calcium concentration, increased release of neurotransmitters such as glutamate, D-serine and also ATP is observed, [128,129,136].

Astrocytes also have a direct contact with neurons via gap-junction channels that allow direct electrical and biochemical communication and support astrocytic key functions, such as shuttle of metabolic substrates and spatial K^+ buffering [129] [137] [138]. Finally, astrocytes are also involved in synaptic elimination via the reduction of synaptic contacts [96,135].

Moreover, astrocytes are responsible for re-uptaking the excess glutamate at the synaptic cleft, thus preventing excitotoxicity [127].

Astrocytes play also a role in CNS metabolisms, as they are able to release molecular mediators that influence the blood flow [139] and represent the principal storage sites of glycogen granules in the CNS.

Another role of astroglial cells is the production of cytokines in response to certain CNS stimuli, including tumour necrosis factor-a (TNF-a), interleukin-1b (IL- 1b) and TGF- β [96].

In response to several diverse forms of CNS injury, astroglial cells can undergo a morphological and transcriptional transformation referred to as reactive astrocytosis or astrogliosis. Reactive astrogliosis is normally associated with increased production of the intermediate filaments glial GFAP, vimentin and nestin, together with astrocyte proliferation, hypertrophy and cellular process extension [140] [141] is observed. Reactive astrogliosis entails a radical change in astrocytes properties, including a loss in some essential functions (i.e. glutamate uptake, increased inflammation due to loss of astrocytes barrier functions) and also the gain of some detrimental effects (i.e. inhibition of axonal regeneration, increase inflammation via cytokines production, production of reactive oxygen species)[95]

1.4) Astrocytes In Disease and Neurodegeneration

1.4.1) Non-Cell Autonomy in Neurodegenerative Diseases

Astroglial cells are –as presented above- responsible for maintaining the environment in which neuronal populations survive and function. However,

as observed in reactive astrogliosis, astrocytes can also contribute to the generation of neuronal toxicity, following an injury or during disease.

Interestingly, the classic view of neurotoxicity is based upon the idea that specific neuronal populations are progressively exposed to toxic insults—for example, in dominantly inherited disease, accumulation of a toxic mutant protein or toxic by-products of a mutant enzyme. Over time, this increasing burden of neurotoxic insults combined with aging is able to overcome the neuron's defensive mechanisms, triggering degeneration and neuronal death[142]. Initially this process was thought to be largely cell autonomous: that is, a situation in which the toxicity causing neuronal death is directly caused by a loss of function or gain of toxic function within the cellular machinery of the neuron itself, independent of other cell types that interact with the affected neurons[2].

In recent years, thanks to multiple evidence coming from animal models of diverse human neurodegenerative diseases, including ALS, spinocerebellar ataxia (SCA), Huntington's disease (HD), Multiple System Atrophy (MSA) and Parkinson's disease (PD), this view of the neurotoxicity in neurodegenerative diseases has been radically changed to include the contribution of cell types other than the degenerating neurons themselves. Non-cell autonomous mechanisms in neurodegenerative disease are now an important area of research, and provide an explanation for the ethiopathogenesis of several neurodegenerative disorders, termed Non Cell Autonomous Neurodegenerative Diseases (NCA-ND). The concept behind NCA-ND is that the overall neurodegeneration observed is strongly influenced by toxicity or mutant protein expression in both neuronal and non-neuronal cells in the vicinity of the vulnerable neurons, as oligodendrocytes [143] [144], and especially astrocytes [145] [146-148], with evidences also from the study of multiple sclerosis (MS).

In general it is possible to conceive three different mechanisms of non-cell-autonomous toxicity/degeneration[2]:

- Toxicity within the affected neurons induces damaging responses from glia that are not otherwise directly involved in the pathology

(as an example, a mutant protein is specifically produced in neurons, and progressive neurodegeneration triggers reactive astrogliosis that in turn increases inflammation)

- Glial cells produce mutant proteins or another toxicity mediator, that determines a loss of normal glial function, amplifying initial cell-autonomous damage to the vulnerable neurons
- Mutant proteins or other toxicity mediators directly and exclusively produced within the glial cells determines a loss of function or a toxic gain of function, thus becoming a primary source of neurotoxicity, independent of cell autonomous toxicity within the neurons at risk.

Interestingly, the latter two possibilities present a link between diseases previously thought to be of primary neuronal origin (as SCA and HD) and those that are of known primary glial origin, accompanied by secondary neurodegeneration (as Multiple Sclerosis, MS).

1.4.2) Astrocytes, ALS and the question of Cell-Autonomy

In recent years accumulating evidence from different experimental systems has suggested that astrocytes might have an important role to play in ALS pathogenesis. The first evidence for an potential non-cell autonomous effect in ALS came from a study in 2006 reporting that in a SOD1-fALS murine model the deletion of mutant SOD1 from cells other than the MNs did not change the onset of symptoms but it significantly slowed the progression[1]. These results where further refined in another study from the same authors, published two years later, reporting that the progression of symptoms in SOD1-fALS animal models was not due to mutant SOD1 expressed in either MNs or oligodendrocytes, leaving as the "prime suspects" astrocytes and microglial cells. The astrocytes carrying SOD1 mutations were then identified as responsible for the progression of the disease in the murine model used[149,150]. These findings were then replicated *in vitro* by a series of studies that used either primary astrocytes derived from SOD1-overexpressing mouse models in coculture with either WT or mutant SOD1

murine motor neurons. This in vitro platform confirmed that astrocytes carrying mutant copies of SOD1 are toxic to the cocultured MNs [147]. The same non-cell autonomous toxicity was observed independently in two studies that used human ES derived MNs cocultured with primary SOD1 murine astrocytes [151,152].

Further support to the idea of an astrocyte involvement in ALS comes also from an increasing body of pathological studies on post-mortem patient material. Several studies have reported findings suggesting that an underlying astroglial pathology is not limited to SOD1 cases but is also a common theme in other/unrelated cases of ALS. One examples of this is the presence of gliosis in ALS patients observed in ventral horns of the spinal cord, extending beyond the regions of MN loss[153,154]. Furthermore in some animal models astrogliosis develops at pre-clinical stages of the disease, prior to any MN loss, suggesting that gliosis might not be exclusively a secondary reparative response[155].

Collectively these studies highlight the need to better understand the nature of astroglial involvement in ALS. However, as previously observed in this section, fALS cased –on which models the totality of this cell-autonomy studies are based- cannot be classified as a TDP proteinopathy, while that is the case for all other case of ALS and for half of the FTLD cases. For this reason it is of extreme importance to clarify whether the reported SOD1 astrocytes non –cell autonomous toxicity mechanism is present also in TDP proteinopathies.

1.5) Induced pluripotent Stem Cells and in vitro modelling

The lack of appropriate treatments for ALS is a reflection of the lack of understanding of its pathological mechanisms and molecular causes. As seen in the previous sections of this literature review, a number of models have been established to study ALS and TDP proteinopathies, and although they will continue to produce key insights into the disease mechanism, they present also several limitations. The most obvious of such problems is that most models are based on the overexpression of either human or murine

mutant versions of the disease protein, and most of them present levels of expression several times higher than the biological levels present in the patients. Moreover, although a major causative protein has been identified, for most cases the disease present as a sporadic form, probably determined by a combination of toxic insults and genetic background prone to vulnerability (both of which are at present beyond the level of understanding available for ALS). Also, the pathology observed in animal models is sometimes considerably different from what observed in patients (*see TDP Proteinopathies Models*).

Human cellular models of diseases could potentially overcome some of these limitations, and an important step in this direction has been the introduction of embryonic stem cells based models, as described for SOD1- in vitro models [151,152].

Human embryonic stem cells are isolated from the inner cells mass of blastocyst stage embryos which can be further differentiated into all three germ layers (ectoderm, mesoderm, and endoderm) [156]. Embryonic stem cell based approaches to obtain human cells in vitro have been successfully established in the last decade, to the point that at present a wide variety of developmentally relevant paradigms can be applied to hESC cultures to generate specific human cell types. As a particular example, a number of studies reported successful generation of human MNs in vitro starting from hESCs[157-160].

Although hESCs provide a source of human cellular material to perform neurodevelopmental and neurofunctional studies, to establish a model of a dominant genetic disorder it is still necessary to perform genetic modifications or rely on overexpression techniques, as most of the commonly available hESC lines do not have disease specific mutations.

To derive disease-specific hESCs lines, there are essentially two conventional methods:

- Rederivation by isolating of single blastomere from morula stage embryos which are entered into pre-implantation genetic diagnostic program

- Derivation of hESCs by somatic cell nuclear transfer (SCNT) [7].

The first option present both practical problems (availability and cost of screening) and in some cases legal and ethical issues [161].

The second alternative is an based on the nucleus from the somatic donor cells transplanted into the enucleated oocytes by micromanipulator[162]. However, the success rate of hESC establishment from SCNT is considerably low and technically demanding.

In 2007 Takahashi et al. published a new methodology (i.e. *reprogramming*) that allowed to overcome these issues. This study described hoe pluripotent cells could be derived from somatic cells by the forcing the expression of key pluripotent transcription factors identified in hESCs (OCT4, c-MYC, SOX2, and KLF4); these "reprogrammed" cells were named induced pluripotent stem cells (iPSCs) [163] [164]. The advantage of iPSC cells over other in vitro approaches is that the reprogrammed cells present the same genetic alterations present in the original somatic cells, including obviously the dominant genetic mutations, but –even more importantly- also including the genetic background on which the inherited disease develop, open the door to the possibility of "patient-specific disease modelling".

In general, human iPSCs and ESCs display several similar properties, such as their morphology, self-renewal, differentiation capacity, cell surface antigens, and gene expression profile [165] Both show high expression of telomerase reverse transcriptase as well as the stage specific embryonic antigens (SSEAs), as SSEA-3, SSEA-4, TRA-1-60and TRA-1-81. More importantly iPSCs could be differentiated into all three germ layers, following the same protocols used to differentiated hESCs.

Importantly, new methodologies have been published, allowing to produce iPSC lines from not just fibroblasts but also a wide variety of other somatic cell types, such as mesenchymal stem cells, umbilical cord blood, and T-cell lymphocyte.

For diseases such as ALS, the reprogramming of somatic cells from nervous disorder patients provides a unique opportunity to generate disease-harbouring pluripotent cells that can be differentiated into neural cells for

studying disease development, shed light on specific molecular mechanisms and investigate their involvement in disease pathogenesis.

Several in vitro disease models based on patient-derived iPSC lines have been successfully established in the last years and some of them have been hugely influential in understanding the molecular mechanisms of the modelled disease. In particular iPSC-based models have been established not only for monogenic disease such as HD[166], familial dysautonomia [167], spinal muscular atrophy (SMA) [168], but also for multifactorial disorders such as PD [169,170] and neurodevelopmental disorders such as fragile-X syndrome [171].

Aims of the Project

Aim I:

The first aim of this project is to establish a patient-derived iPSC based platform to study the consequences of TDP proteinopathies-causing mutations on motor neurones and astrocytes. To accomplish this specific protocols will be optimised to generate functional populations of astrocytes and motor neurones, and the consequences of TDP-43 mutations will addressed by biochemical, molecular and survival studies.

Aim II:

Use the established platform to answer the question of cell autonomy in TDP-43 proteinopathy. In particular, the experiments will be focused on:

- Determining whether the TDP-43 mutation causes cell-autonomous toxicity in motor neurones.
- Determining whether the TDP-43 mutation causes cell-autonomous toxicity in astrocytes populations.
- Determining whether the TDP-43 mutation carrying astrocytes exert a non-cell autonomous toxic effect on motor neurones, affecting either progression of the symptoms as shown for SOD1 fALS.

Chapter 2: Materials and Methods

2.1) Generation and Characterisation of iPSC Lines

2.1.1) Reprogramming

Fibroblasts from a normal male (56 y old; CRL- 2465; ATCC), a normal female (40 y old; CRL-2524; ATCC), and from a 56-y-old male carrying the M337V TDP-43 mutation were reprogrammed using integrating retroviral vectors encoding for Sox2, Oct4, c-Myc and Klf-4 as previously described[172].

From the reprogramming experiments, four iPSC lines were generated: two independent clonal lines derived from the patient with the M337V TDP-43 mutation [M337V-1 and M337V-2], one line from the age-matched male control fibroblast [CTRL-1] and one from the age-matched female control fibroblasts [CTRL-2].

2.1.2) Assay for Teratoma Formation.

To perform the teratoma formation experiments, iPSC were harvested, washed once with DMEM/F12, and mixed with Matrigel (BD Biosciences). A total of 10^6 cells were injected intra musculus into immune-compromised NSG mice. Teratomas formation was confirmed within 6 to 8 weeks post injection. Paraffin fixed sections were stained with Masson trichromatic for histological determinations.

2.1.3) PCR and Quantitative PCR (qPCR).

Cells were harvested at confluence using Accutase (Sigma) and RNA was isolated from the samples with RNeasy kit (Qiagen) following the manufacturer's instructions. DNA contaminations were removed by the treatment with DNA-Free (Ambion). cDNA synthesis was performed by using 1 μg of total RNA with the First Strand cDNA Synthesis Kit (Roche) or the DyNAmo cDNA Synthesis Kit (New England Biolabs) in a 20- to 25-

μL volume. Real-time qPCR reactions were set up in triplicates with the Brilliant II SYBR Green QPCR Master Mix (Stratagene) or Applied Biosystems TaqMan Assays and run on an iCycler System (Bio-Rad). Primer sequences are provided in Primers Table.

2.1.4) Bisulfite Sequencing.

Bisulfite genomic DNA sample treatment and processing were performed as previously described[173] with a primer pair designed to target bp 2136 to 1721 of the Oct4 promoter (forward: 5′-GGATGTTATTAAGATGAAGATAGTTGG- 3′; reverse: 5′-CCTAAACTCCCCTTCAAAATCTATT-3′). Bisulfite conversion efficiency of non-CpG cytosines ranged from 85% to 99% for all individual clones for each sample.

2.1.5) iPSC Culturing:

Once established the iPSC lines were propagated as colonies on a layer of irradiated mouse fibroblasts, and passage 1:3 when confluent using the enzyme Collagenase I (R&D). Feeder based iPSC cultures were maintained for up to passage 60 *in vitro* and samples were cryopreserved regularly. Pluripotent colonies on feeders were cultured with *KSR-F10 Medium*.

Before starting any experiment, iPSC lines were transited from feeder culture conditions to feeder free cultures, by plating the colonies on Matrigel coated plates and maintaining them in *mTSER 1 medium* (Stem Cell Technologies).

2.2) Generation and Characterisation of Motor Neurones from iPSC Lines

2.2.1) Neural Conversion

Feeder free cultures were used for neural conversion protocol 4 to 6 days after passaging. Neural conversion of iPSC lines was obtained by dual SMAD inhibition, as described by Chambers and collaborators[1],

supplementing CDM medium[174] with N-acetyl cysteine (NAC, Sigma) 1mM, SB431542 (Tocris) 10 μM and Dorsomorphin (Tocris) 2 μM. During neural conversion the medium was changed every 48h, and the treatment was prolonged for 6-7 days. After the end of the neural conversion phase the clusters of newly formed NSCs were lifted with mechanical dissociation coupled with collagenase treatment, and then cultured in suspension in CDM for 24 hours. The NSCs clusters were then plated on laminin coated plates in NSCR Base medium supplemented with 5 ng/mL FGF2, changing the medium every 48 hours for 4-5 days, until neural rosettes structures formed. Neural rosettes were then manually dissociated using a 19G needle and used for the patterning phase.

2.2.2) MNs induction Protocol:

After enzymatic dissociation, neurospheres were formed and caudalised in suspension in Phase II Medium for 7–12 days, according to the iPSC Line. For the monolayer based MN differentiation caudalised neurospheres were then dissociated with Accutase (Sigma) and plated down on coverslips coated with laminin (Sigma) and fibronectin (Sigma) in Phase III Medium. to generate MN precursors. Replated MN precursors were switched to MN Maturation medium and cultured for 3–6 wk. For the sphere based MN differentiation caudalised neurospheres were then cultured in Phase III Medium for 7-9 days and finally switched to MN Maturation medium for 2-4 weeks before checking the HB9 induction with immunostaining.

Dissociation of neurospheres after the maturation phase was performed using Papain Dissociation System (Worthington Biochemical). For each experiment a sample containing 5-20 spheres (according to experiment type) was taken from the original culture. Each sample was washed three times in D-PBS (Life Technologies) before being treated with 500 μL of Papain/DNAseI dissociation solution (reconstituted in HBSS according to manufactured instructions) for 1 hour at 37º C. After a successful dissociation treatment with papain, the neurospheres appeared less compact and with a visibly increased size (more noticeable with larger diameter

neurospheres). Single cells suspensions were obtained by pipetting 10-20 times the papain-treated neurospheres with a p1000 tip. The cell suspension was then pellet at 1.2 rcf for 3 minutes, and the pellets re-suspended in 300 µL of Inhibitor/DNAseI solution (reconstituted in HBSS according to manufactured instructions). To eliminate the remaining debris and un-dissociated neurospheres the cell suspensions were carefully layered on top of 1 mL of undiluted Ovomucoid inhibitor Solution (reconstituted in HBSS according to manufactured instructions). After 5 minutes incubation at room temperature the debris and neurospheres precipitate to the bottom of the tube, while the single cells remain in the top layer, which can be collected and then centrifuged at 1.2 rcf for 3 minutes. The single cells can then be re-suspended in MN Maturation Medium and plated according to experimental needs.

2.2.3) Electrophysiology

Whole cell patch-clamp recordings were made at room temperature using an Axopatch-1C amplifier. Coverslips containing iPSC-derived neurons are transferred to a recording chamber perfused with an acsf containing: 152 NaCl, 2.8 KCl, 10 HEPES, 2 $CaCl_2$, 10 glucose pH 7.3 (320–330 mOsm).

Patch pipettes were filled with an internal solution containing (in mM): 155 K-gluconate, 2 $MgCl_2$, 10 Na-HEPES, 10 Na-PiCreatine, 2 Mg_2-ATP and 0.3 Na_3-GTP, pH 7.3 (300 mOsm).

For the recording of whole-cell AMPA- and NMDA-evoked currents the external solution was supplemented with picrotoxin (50 µM) and strychnine (20 µM). Whole cells currents were recorded in voltage clamp in response to bath application of NMDA(100uM) and Glycine (50uM), AMPA (50uM) and GABA(100uM).

Spontaneous excitatory post synaptic currents (EPSCs) in voltage-clamp where induced by application of the GABA receptor antagonist Picrotoxin(50uM) along with the potassium channel blocker 4-AP. This spontaneous activity was recorded in (1mM) Mg^{2+} and was blocked the AMPA receptor antagonist CNQX(5uM).

2.2.4) Neuromuscular Junction Assay:

Mouse myoblast line C2C12 was cultures in DMEM 4.5 Glucose (GIBCO) supplemented with 20% FBS (Hyclone - Thermo Scientific) and 1% P/S (GIBCO). Once the culture reached ≅70 % density the medium was changed to DMED 4.5 Glucose supplemented with 2% Horse Serum (Invitrogen), 1% GlutaMax (GIBCO) and 1% P/S (GIBCO). Neurospheres at the end of the patterning phase were seeded on the C2C12 after observing fused myofibers (3-5 days from medium change). For the visualisation of the acetylcholine receptors clustering we use α-Bungarotoxin conjugated with Alexa 555 (Invitrogen) at a concentration of 1:500, during the staining procedure described above.

2.3) Generation and Characterisation of Astrocytes from iPSC Lines.

2.3.1) EL Conversion protocol Protocol:

Generation of neurospheres from iPSC lines and their patterning to acquire motor neuron progenitor identity were performed as described above. The patterned neurospheres for the EL conversion were collected from cultures that have been maintained for 2 weeks in maturation phase of the MN induction protocol. The selected neurospheres were mechanically chopped at the beginning of the enrichment phase and cultured in NSCR EL20 medium for 2–4 weeks (depending on the size of the chopped spheres). After enrichment, the spheres were then propagated in NSCR EF20 medium and passaged mechanically by chopping them every 2 weeks. After the EL conversion the neurospheres were maintained in cultures for up to 20 months and used to establish monolayer progenitors cultures.

Samples from each iPSC lines used in this study containing ≃100 EL converted neurospheres were taken for cryopreservation after the establishment of the cultures and then regularly every 6 months. Each sample was re-suspended in NSCR base medium containing 10% DMSO (Sigma) and then stored within a iso-pentane based cryopreservation unit at

-80º C overnight, to be then transported to the main liquid nitrogen tanks for long-term cryopreservation.

2.3.2) Generation of Astrocyte Progenitors Cells (APCs) cultures:

Monolayer APCs cultures were obtained by dissociating the EL converted spheres with the Papain Dissociation System (Worthington Biochemical). For each experiment a sample containing 10-30 spheres (according to the size) was taken from the original culture. Each sample was washed three times in D-PBS (Life Technologies) before being treated with 500 µL of Papain/DNAseI dissociation solution (reconstituted in HBSS according to manufactured instructions) for 1 hour at 37º C. After a successful dissociation treatment with papain, the neurospheres appeared less compact and with a visibly increased size (more noticeable with larger diameter neurospheres). Single cells suspensions were obtained by pipetting 10-20 times the papain-treated neurospheres with a p1000 tip. The cell suspension was then pellet at 1.2 rcf for 3 minutes, and the pellets re-suspended in 300 µL of Inhibitor/DNAseI solution (reconstituted in HBSS according to manufactured instructions). To eliminate the remaining debris and un-dissociated neurospheres the cell suspensions were carefully layered on top of 1 mL of undiluted Ovomucoid inhibitor Solution (reconstituted in HBSS according to manufactured instructions). After 5 minutes incubation at room temperature the debris and neurospheres precipitate to the bottom of the tube, while the single cells remain in the top layer, which can be collected and then centrifuged at 1.2 rcf for 3 minutes. The single cells can then be re-suspended in NSCR base medium to be counted and plated on Matrigel (BD Biosciences, 1:80 dilution)-coated plates at a density of 10^4 cells/cm^2. These cultures usually reach confluence within a week and are considered the initial passage for the APC monolayers.

The monolayer APC cultures were propagated in NSCR EF20 medium and passaged when confluent using Accutase (Sigma) [split ratio 1:2-1:3].

2.3.3) Astrocyte Generation:

To obtain differentiated astrocytes from APC monolayers, confluent cultures were passaged 1:3 as described above on a Matrigel coated plate and the day after their medium was changed to *AstroMED* medium containing 10 ng/mL CNTF (R&D). The differentiating cells were maintained for 14 days with 75% medium change every 48 hours. Once differentiated, astrocytes were detached and re-plated on a suitable substrate/plate according to the experimental needs.

2.3.4) Astrocytes Functional Characterisation:

Glutamate Uptake Assay

Differentiated astrocytes were plated on Matrigel-coated 96-well plates at a density of $2x10^4$ cells per well and cultured in *AstroMED-CNTF* for an additional 7 days. During the assay, astrocytes were exposed to phenol free HBSS (Invitrogen) containing 100 µM L-Glu; samples from the cultures were taken after 30, 60 and 120 minutes. The concentrations of L-Glu in the samples were determined using the Amplite Fluorimetric Glutamic Acid Assay Kit (ATT Bioquest), following the manufacture's instructions.

Fluorescence intensity was then measured on a FluoSTAR Optima plate Reader (BMG Labtech).

As negative controls for the assay L-Glu HBSS supplemented with 2 mM L-trans-pyrrolidine-2,4-dicarboxylic acid (Sigma) or 100 µM L-Glu HBSS without sodium (Biosera) were used, both were assayed at 120 min.

To obtain an indirect estimate of number of cells per well CyQuant Cell Proliferation Assay (Invitrogen) was used as indicated by the manufacturer, and the quantification of fluorescent signal was performed on FluoSTAR Optima plate Reader (BMG Labtech). The raw CyQuant data were processed by subtracting the background calculated on an empty plate with the same coating as the plates used in the glutamate uptake assay. The data were then normalized by the CyQuant value of CTRL-1 iPSC-derived

astrocytes. The processed CyQuant data were used to normalize the glutamate uptake assay data.

Data obtained during the Glutamate uptake assay were analysed with the 1-way Anova and Bonferroni post-test or with 2-way Anova. Results from the mutant lines (M337V-1 and M337V-2) and from the control lines (CTRL-1 and CTRL-2) were pooled together to be presented in the figures.

Synaptogenesis Assay

For quantification of synapse formation, differentiating neurons derived from Control iPSC and hESC (H9) were plated either in isolation (as described above for MN cultures) or on a layer of iPSC-derived differentiated astrocytes. The coculture were maintained for 3 weeks in the same medium used for isolated neuronal cultures (*NSCR Neurons* or *MNs Maturation Med*) and then analysed by immunostaining for synaptic proteins [Synapsin I (SynI) in the preliminary experiment, SynaptophysisnI (PSY) and PSD-95 in the following experiment] and the neuronal marker β-3 tubulin. The average number of $SynI^+$ or PSY^+/$PSD\text{-}95^+$ positive puncta per 30 μm axonal segment was calculated on five different fields for every condition, analysing three biological replicates. The average number of puncta in equivalent isolated cultures of neurons was used as a normalizer. Results from the mutant lines (M337V-1 and M337V-2) and from the control lines (CTRL-1 and CTRL-2) were pooled to be presented in the figures, and analysed using 1-way Anova with Bonferroni post-test.

Calcium Waves.

Differentiated astrocytes cultures were incubated in HBSS containing 5 μM Fluo-4AM dye (Invitrogen) for 1 h at 37ºC according to manufacturer instructions. Cultures were then washed three times in HBSS solution and left for an additional 30 minutes at 37ºC to allow complete de-esterification of the dye. At this point, 50 μM 2-APB (Calbiochem) was added to the negative control. For mechanical stimulation, a suspension of 200-μm diameter glass beads in HBSS was applied to the cells during imaging.

ATP-evoked calcium responses were obtained by local application of a 5mM ATP solution (Sigma). Imaging was performed at 1fps on a Zeiss Axiovision microscope with incubation chamber at 37ºC.

2.4) TDP-43 transfections and over-expression analysis in astrocytes

2.4.1) Transfections

For this experiments 2 weeks old differentiated astrocytes cultures were plated in a 96-well Matrigel coated plate, at a density of $3x10^4$ cells/well and then transfected with pGW1-eGFP and either pGW1-^{WT}TDP43:mApple pGW1-^{M337V}TDP43:mApple, using LIPO-2000 (Invitrogen) transfecting reagents. Transfections were performed using 0.5 µL of LIPO-2000 reagent for every transfected well, and 0.5 µg DNA per plasmid per well. Astrocytes were incubated with the transfecting reagents and DNA for 45 minutes at 37ºC and then their medium was changed to fresh *AstroMED-CNTF*.

2.4.2) Imaging

Live-Imaging started 24 hours after transfection, on a Zeiss Axiovision microscope with incubation chamber at 37ºC.

2.4.3) Expression Levels Analysis

Images of transfected astrocytes were analysed with ImageJ64 and original ImageJ plug-ins written in Jython. The eGFP images were used to determine a ROI around the astrocytes to be analysed; the same ROIs were then used to calculate area, raw integrated density (RawInt) and background levels on both eGFP and TDP43:mApple images. Relative TDP43:mApple expression levels were calculated by normalizing background-subtracted RawInt of the red channel to that of the green channel. Arbitrary expression units (x) were derived by normalizing the relative expression level of each cell to the average value for each group (WT and M337V). These arbitrary units were used to stratify the transfected astrocytes into six groups with increasing relative expression (A= below 0.65x, B=between 0.66x and

0.81x, C=between 0.82x and 0.97x, D=between 0.98x and 1.14x, E=between 1.15x and 1.30x, F=above 1.30x). The astrocytes were scored using the following criteria: cells with TDP43:mApple localized in the nucleus were assigned to the *nuclear* group; cells that presented TDP43:mApple in both nucleus and cytoplasm or cytoplasm alone were assigned to the *cytoplasmatic* group.

2.5) Astrocytes-Motor Neurones Cocultures

For cocultures experiments 2 weeks old neurospheres from the maturation phase were dissociated using papain (as described for MNs) and plated on a layer of differentiated astrocytes at a density of $7.5x10^4$ cells per well of a 96 well plate. Astrocytes for the cocultures were plated on Matrigel coated 96 well plates after differentiation at a density of $2.5x10^4$ cells per well of a 96 well plate. The cocultures were maintained in MN Maturation Medium.

2.6) Molecular Analysis in differentiated cultures

2.6.1) Quantitative RT-PCR

Differentiated cultures were detached using Accutase (Sigma), and RNA was isolated using the RNeasy kit (Qiagen), following the manufacturer's instructions. The Turbo DNA-Free kit (Invitrogen) was used to eliminate genomic DNA contaminations. Synthesis of cDNA was performed using 0.5 μ g of total RNA with the DyNAmo cDNA Synthesis Kit (Thermo Scientific) in a 20 μ L volume. Real-time qPCR reactions were performed in triplicate using the DyNAmo Flash SYBR Green qPCR kit (Thermo Scientific) and examined on a CFX96 System (Bio-Rad). Relative expression levels were calculated by the 2DDCt method with β-actin as the reference gene.

2.6.2) Western Blots

Differentiated cultures (at the end of the maturation phase for MNs and after 14 days of differentiation for astrocytes) were harvested using Accutase and lysed in cold RIPA buffer (50 mM Tris-HCl pH 7.4, 150 mM NaCl, 1% Triton x-100, 1% sodium deoxycholate, 0.1% SDS, 1 mM EDTA). To isolate the detergent-soluble fraction the lysates were centrifuged at 15,700 × g for 30 minutes at 4°C and the supernatant was collected. Subsequently, the detergent-insoluble fraction on the remaining part of the samples was extracted using an equal volume of urea buffer {7 M urea, 2 M thiourea, 4% (wt/vol) 3-[(3-cholamidopropyl)dimethylammonio]-1-propanesulfonate (CHAPS), 30 mM Tris (pH 8.5), after an additional RIPA buffer wash to minimize the carryover contamination from the soluble fraction. To eliminate genomic DNA samples were sonicated three times for 10 seconds in a water bath, and centrifuged again at 100,000 × g for 30 min at 22°C. Fresh protease inhibitors [complete Mini (Roche) and 1 mM PMSF] were added to all buffers. Soluble protein concentrations were determined by a BCA protein assay (Pierce). 12% SDS/PAGE gels were loaded with 15 μg of protein for each sample on transferred after complete resolution on PVDF membranes. For the insoluble fraction, an equivalent sample volume was analysed. The PVDF membranes were blocked in Western Blocker Solution (Sigma) and incubated in primary antibody overnight at 4°C. Proteins were detected with horseradish peroxidase–conjugated secondary antibodies, and blots were developed with Amersham ECL Plus and Hyperfilm (GE Healthcare). Semiquantitative densitometric analysis of western blots was performed with ImageJ, using β-actin as a loading control for the soluble fraction and Ponceau S staining for the detergent-resistant fraction.

2.6.3) Immunofluorescence and Densitometry Analysis

Cultures were fixed for immune-labelling with 2% paraformaldehyde, and then permeabilised with 0.2% Triton X-100 (Sigma) at room temperature, and blocked in 3% goat serum (DAKO). Incubation with primary and secondary (Alexa Fluor dyes; Invitrogen) antibodies was performed at room

temperature for 1 hour and 30 minutes respectively, with three PBS washes between each phase. The nuclei were counterstained with DAPI (Sigma) after the secondary antibody incubation. Images were acquired using either a Zeiss Observer microscope or a Zeiss LSM 780 microscope laser-aided confocal microscope (both running ZEN vers. 1.4, Zeiss), according to the experimental needs.

Densitometric analysis on TDP-43 astrocytes immunostaining immunostaining was performed using ImageJ64 (vers. 1.4.4.0): the DAPI channel was converted into a thresholded binary mask from which regions of interests (ROIs) were defined, and nuclear TDP-43 signals were measured in these ROIs. Cytoplasmic TDP-43 signals were measured by subtracting the binary mask from the TDP-43 channel, and the average signal intensity normalized by the number of astrocytes on the field.

Densitometric analysis on TDP-43 in MNs cocultures with astrocytes was performed using the same software packages described above. ROIs were designed around SMI-32^{+} neurons that resided in a field with minimal presence of GFAP^{+} astrocytic protrusion within the focal plane considered, and then used to measure TDP-43 signal intensity. Results are presented as normalized on the same genotypes neurons cocultured on WT astrocytes.

2.7) Survival Analysis by longitudinal microscopy

2.7.1) Transfections

MNs Transfections.

Neurospheres were patterned to MN identity using the sphere-based protocol described above. Samples for the survival analysis were collected from the main neurospheres cultures after 2-4 weeks in the MN Maturation phase. Dissociation was performed using Papain Dissociation Kit (Worthington) as described above; after obtaining a single cell suspension we performed electroporation using the NEON electroporation system (Invitrogen). Electroporation were performed using three 1300 mV pulses, each 10 ms in length. Electro orated cells were then plated at a density of

75x10^3 per well in a 96 well plate coated with poly-Ornithine and Laminin. To identify the MNs for survival analysis a reported plasmid expressing eGFP under the control of HB9 promotorial element was used (developed in Steve Goldmann Lab and kindly donated[175]).

Astrocytes Transfections.

Differentiated astrocytes were plated in a 96-well Matrigel coated plate, at a density of $3x10^4$ cells/well and then transfected with pGW1-mApple, using LIPO-2000 (Invitrogen) transfecting reagents. Transfections were performed using 0.5 µL of LIPO-2000 reagent for every transfected well, and 0.5 µg DNA per plasmid per well. Astrocytes were incubated with the transfecting reagents and DNA for 45 minutes at 37ºC and then their medium was changed to fresh *AstroMED-CNTF*.

2.7.2) Imaging Set-up

Live-Imaging started on the cultures 24 hours after the transfections, and was performed daily for consecutive days. At the first time-point for each plate, the central position within the analysed wells was identified and saved within a virtual reference frame based on a physical feature of the plate (generally one of the markings), adopted as point of origin. This allowed to re-image every day the exact same position within the transfected wells.

All imaging necessary for the survival analysis experiment was performed either on a Zeiss Axiovision microscope at the MRC Centre for Regenerative Medicine in Edinburgh, or on a custom robotic microscope system (described in Barmada, S.J. et al. *Journal of Neuroscience* 2010) at the Gladstone Institute, San Francisco CA.

2.7.3) Data Analysis

The images acquired during the survival analysis experiments were analysed using ImageJ built-in cell counter macros and original programs

written with MatLab. Cell death was determined by cell membrane rupture, blebbing, or loss of GFP fluorescence.

The data collected for survival analysis was analysed using R software (www.r-project.org) and the freely available survival analysis scripts library associated.

The Kaplan-Meier (KM) estimator was used to establish the survival in the different groups (as called by the `survfit()` function) and then cumulative risk of death curves were plotted (based on the KM fit, as called by the `survfit()` function parameter `fun="cumhaz"`) to analyse the difference in survival between the various lines. Statistical significance of differences between groups was determined with log-rank test. Cox proportional hazards analysis was used to determine the influence of the M337V iPSC background on the risk of death of Motor neurons and astrocytes in culture.

Results were pooled together using a unified analysis (*Simple Survival*) when coming from the same batches of transfections/electroporation; otherwise, experiments performed in different days with different reagents batches were analysed using stratified analysis (*Stratified Survival*).

2.8) Cell Culture Media

NSCR Base Medium: AdDMEM/F12 with 1% N2 supplement and 0.1% B27 Supplement, 1% nonessential amino acids, 1% penicillin/streptomycin, 1% GlutaMAX solution (all from Invitrogen)

NSCR EF20 Medium: NSCR Base Medium supplemented with 20 ng/mL FGF-2 (PeproTech) and 20 ng/mL EGF (R&D Systems).

NSCR EL20 Medium: NSCR Base Medium supplemented with 20 ng/mL LIF (Sigma) and 20 ng/mL EGF (R&D Systems).

AstroMED-CNTF: Neurobasal with 0.2% B27 Supplement, 1% nonessential amino acids, 1% penicillin/streptomycin, 1% GlutaMAX solution (all from Invitrogen), 10 ng/mL CNTF (R&D Systems).

NSCR Neuron Medium: AdDMEM/F12 with 1% N2 supplement and 0.5% B27 Supplement, 1% nonessential amino acids, 1% penicillin/streptomycin, 0.5% GlutaMAX solution (all from Invitrogen), 0.1 μM retinoic acid (R&D Systems); 20 ng/mL BDNF (R&D Systems) and 20 ng/mL GDNF (R&D Systems) were added after the first week of differentiation.

Phase I Medium: CDM medium[174] supplemented with N-acetyl cysteine (NAC, Sigma) 1mM, SB431542 (Tocris) 10 μM and Dorsomorphin (Tocris) 2 μM.

Phase II Medium: NSCR Base Medium supplemented with 0.1 μM retinoic acid and 5 ng/mL FGF2.

Phase III Medium: NSCR Base Medium supplemented with 0.1 μM retinoic acid, 1 μM purmorphamine (Calbiochem) and 5 ng/mL FGF2.

MN Maturation Medium: NSCR Base Medium supplemented with 0.01 μM retinoic acid (R&D Systems), 0.1 μM purmorphamine (Calbiochem), 20 ng/mL BDNF (R&D Systems) and 20 ng/mL GDNF (R&D Systems).

2.9) Antibodies

Antibody	Host	Company	Dilution
TDP-43 C-Term	*Rabbit (poly)*	*Cell Signalling*	*1:100*
TDP-43 mono	*Mouse (mono)*	*Abnova*	*1:500*
SMI-32	*Mouse (mono)*	*Covance*	*1:1000*
ChAT	*Goat (poly)*	*Millipore*	*1:350*
β-3 Tub	*Mouse (mono)*	*Sigma*	*1:1000*
HB9	*Mouse (mono)*	*DHSB*	*1:250*
Olig2	*Rabbit (poly)*	*Millipore*	*1:300*
Pax6	*Mouse (mono)*	*DHSB*	*1:250*
Sox2	*Mouse (mono)*	*Millipore*	*1:250*
Sox1	*Rabbit (poly)*	*Millipore*	*1:200*
Nestin	*Mouse (mono)*	*Millipore*	*1:500*
Synapsin I	*Mouse (mono)*	*Millipore*	*1:250*
Vimentin	*Mouse (mono)*	*Millipore*	*1:500*
NFIA	*Rabbit (poly)*	*Abcam*	*1:250*
GFAP	*Rabbit (poly)*	*DAKO*	*1:500*
GFAP-cy3	*Mouse (mono)*	*Sigma*	*1:500*
S100B	*Rabbit (poly)*	*DAKO*	*1:500*
EAAT1	*Rabbit (poly)*	*Novus*	*1:200*
PSD-95	*Rabbit (poly)*	*Cell Signalling*	*1:200*
Synaptophysin I	*Mouse (mono)*	*Millipore*	*1:200*

2.10) Primers

Gene	Forward (5'-3')	Reverse (5'-3')
B-actin	GTTACAGGAAGTCCC TTGCCATCC	CACCTCCCCTGTGT GGACTTGGG
TDP-43	CGGCCTAGCGGGAA AAGTAAAAGA	AGCACCGTCCCAT CGTCTT
HDAC6	TCGCTGCGTGTCCTT TCAG	CCCTCATTCATGTA CTGGGTTG
S100B	TGGCCCTCATCGACG TTTTC	CAGTGTTTCCATGA CTTTGTCCA
GFAP	ATCGAGAAGGTTCGC TTCCTG	TGTTGGCGGTGAG TTGATCG
Oct4	GTACTCCTCGGTCCC TTTCC	CAAAAACCCTGGCA CAAACT
Nanog	AATACCTCAGCCTCC AGCAGATG	TGCGTCACACCATT GCTATTCTTC
Sox1	GGAAACACAATCGCT GAACC	ATTATTTTGCCCGT TTTCCC
Hoxb4	GTGAGCACGGTAAA CCCCAAT	CGAGCGGATCTTG GTGTTG
Nkx6.1	CACACGAGACCCACT TTTTCC	CCCAACGAATAGG CCAAACG
Olig2	GGACAAGCTAGGAG GCAGTG	ATGGCGATGTTGA GGTCGTG
TDP-43	CGGCCTAGCGGGAA AAGTAAAAGA	AGCACCGTCCCAT CGTCTT
HDAC6	TCGCTGCGTGTCCTT TCAG	CCCTCATTCATGTA CTGGGTTG
Pax6	ATGTGTGAGTAAAAT TCTGGGCA	GCTTACAACTTCTG GAGTCGCTA
TERT	AACCTTCCTCAGCTA TGCCC	GTTTGCGACGCAT GTTCCTC
Rex1	AACGGGCAAAGACA AGACAC	GCTGACAGGTTCTA TTTCCGC
Nestin	GGCGCACCTCAAGA TGTCC	CTTGGGGTCCTGA AAGCTG
HPRT	AATTATGGACAGGAC TGAACGTCTTGCT	TCCAGCAGGTCAG CAAAGAATTTATAG C

2.11) R Analysis Commands

Command	Function	Procedure
library(survival)	*Load the survival library*	*General*
source("{file path}")	*Load the survival source database*	*General*
datafile <- read.csv("{file path}")	*Load the datasheet*	*General*
test.data <- data.frame(time=datafile${variable1}, event=datafile${variable2}, group=as.factor(datafile${variable3}))	*Analyse the data associating the time and occurrence of a binary event, based on groups*	*Simple Survival*
kmfit.by.group <- survfit(Surv(time, as.logical(event)) ~ group, data=test.data)	*Fit the K-M model by group*	*Simple Survival*
lrtest <- survdiff(Surv(time, as.logical(event)) ~ group, data=test.data)	*Defines the terms for the likelihood ratio (LR) test by group*	*Simple Survival*
lrtest	*Show the LR test results, indicating groups used and n. numbers*	*Simple Survival*
plot(kmfit.by.group, fun="cumhaz", main="{title of the graph}", xlab="{axis title}", ylab="{axis title}", col=c("{color1}", "{color2}" ...), lty=c({line type1}, {line type2}...))	*Plots the cumulative hazard curves by applying the Kaplan-Meier Analysis to the groups*	*Simple Survival*
legend(list(x={legend_position_x}, y={legend_position_y}), legend=c("{group1}", "{group2}" ...), col=c("{color1}", "{color2}" ...), lty=c({line type1}, {line type2}...))	*Add a legend to the Graph:*	*Simple Survival*
coxfit <- coxph(Surv(time, as.logical(event)) ~ group , data=test.data)	*Statistical Analysis with the Cox Proportional model*	*Simple Survival*
summary(coxfit)	*Show the Statistical Analysis results*	*Simple Survival*
test.data <- data.frame(time=datafile$"{variable1}", event=datafile$"{variable2}", group=as.factor(datafile$"{variable3}"), expt=datafile$"{stratifying_variable}")	*Analyse the data associating the time and occurrence of a binary event, based on groups but stratified by a variable (ex. Date)*	*Stratified Survival*
kmfit.by.group <- survfit(Surv(time, as.logical(event)) ~ group +*strata*(expt), data=test.data)	*Fit the K-M model by group stratified by a certain variable*	*Stratified Survival*
coxfit <- coxph(Surv(time, as.logical(event)) ~ group +strata(expt), data=test.data)	*Statistical Analysis with the Cox Proportional model*	*Stratified Survival*
survfit(coxfit)	*Show the Statistical Analysis results*	*Stratified Survival*
plot(survfit(coxfit), fun="cumhaz", main="{title of the graph}", xlab="{axis title}", ylab="{axis title}", col=c("{color1}", "{color2}" ...), lty=c({line type1}, {line type2}...))	*Plots the cumulative hazard curves extrapolated by the Cox Proportional Analysis stratified by a variable*	*Stratified Survival*

Note: characters in {...} represent the input variables/groups/data paths specific for every experiments

Chapter 3: Generation of Motor Neurones and Astrocytes from iPSC Lines

3.1) Characterisation and Validation of the iPSC lines

At the beginning of this project, a number of pluripotent cell lines cultures had already been established (all listed in Table 2). The iPSC lines were generated in George Q. Daley's lab in 2009 using a 4 factor reprogramming strategy (Oct-4, Sox2, Klf4 and c-Myc). Lines M337V-1 and M337V-2 represent two clonal lines generated from fALS patient derived fibroblasts carrying the M337V mutation on *TARDBP*. Lines CTRL-1 and CTRL-2 were generated from male and female control fibroblasts respectively, and they represent the major controls used in this project. As an additional control for the behaviour of iPSC lines and their derivatives, cultures from human embryonic stem cells (hESC), H9 and Shef-4 were established and used in several optimization experiments.

The purpose of this initial stage was to determine whether the iPSC lines were completely reprogrammed and therefore constituted a suitable source of materials for this project. The iPSC lines used in this study were validated using a set of established criteria including expression profile of pluripotency markers, efficiency of reprogramming, karyotype analysis and stability over long-term culture. M337V and CTRL lines were maintained in culture for over 40 passages on both MEF feeders or as feeder free culture **(Fig. 1B & C)** and demonstrated long-term culture stability. They also presented a normal 46 XY karyotype **(Fig. 1D**, *karyotype analysis performed by J. Fletcher, in Ian Wilmot's lab***)** and them retained the expression of pluripotency markers such as OCT4, TRA1-60 and SOX2 **(Fig 1E & 1F)**. The fALS iPSC and control lines were regularly genotyped by direct sequencing of single nucleotide change causing the M337V switch, in order exclude cross contamination between mutant and wild-type cultures at the pluripotent stage **(Fig. 1G)**. To assess the efficiency of the

reprogramming process on the iPSC lines, bisulphite sequencing of one fragment of OCT4 promoter was undertaken **(Fig. 1H**, *bisulphite sequencing performed by Dr. B.Bilican***)**, which revealed a methylation pattern similar to established human ES lines.

Figure 1. Establishment of iPSCs from patient fibroblasts. (A) Primary dermal fibroblast cultures were established from a punch biopsy belonging to a fALS TDP-43 ALS patient. (B) Cultures formed tightly packed human ES-like colonies after lentiviral reprogramming with OCT4, SOX2, KLF4, and c-MYC, when plated on a layer of MEF. (C) Reprogrammed colonies remained pluripotent and self-renewing when cultured in feeder-free conditions. (D) Reprogrammed iPSC presented a normal karyotype [46 XY, representative image from M337V-1 shown]. (E-F) Immunohistochemical characterization of feeder-free patient iPSCs for the pluripotency markers OCT4, Tra-1-60, and SOX2. (G) Direct sequencing confirmed the M337V mutation in TDP-43 in patient-derived iPSCs. (H) Bisulphite sequencing analysis of the OCT4 promoter in M337V iPSCs and hESC line H9s. All results are from M337V iPSC clone 2 (M337V-2) and are representative of what iPSC clone M337V-1 and Control IPSC lines.

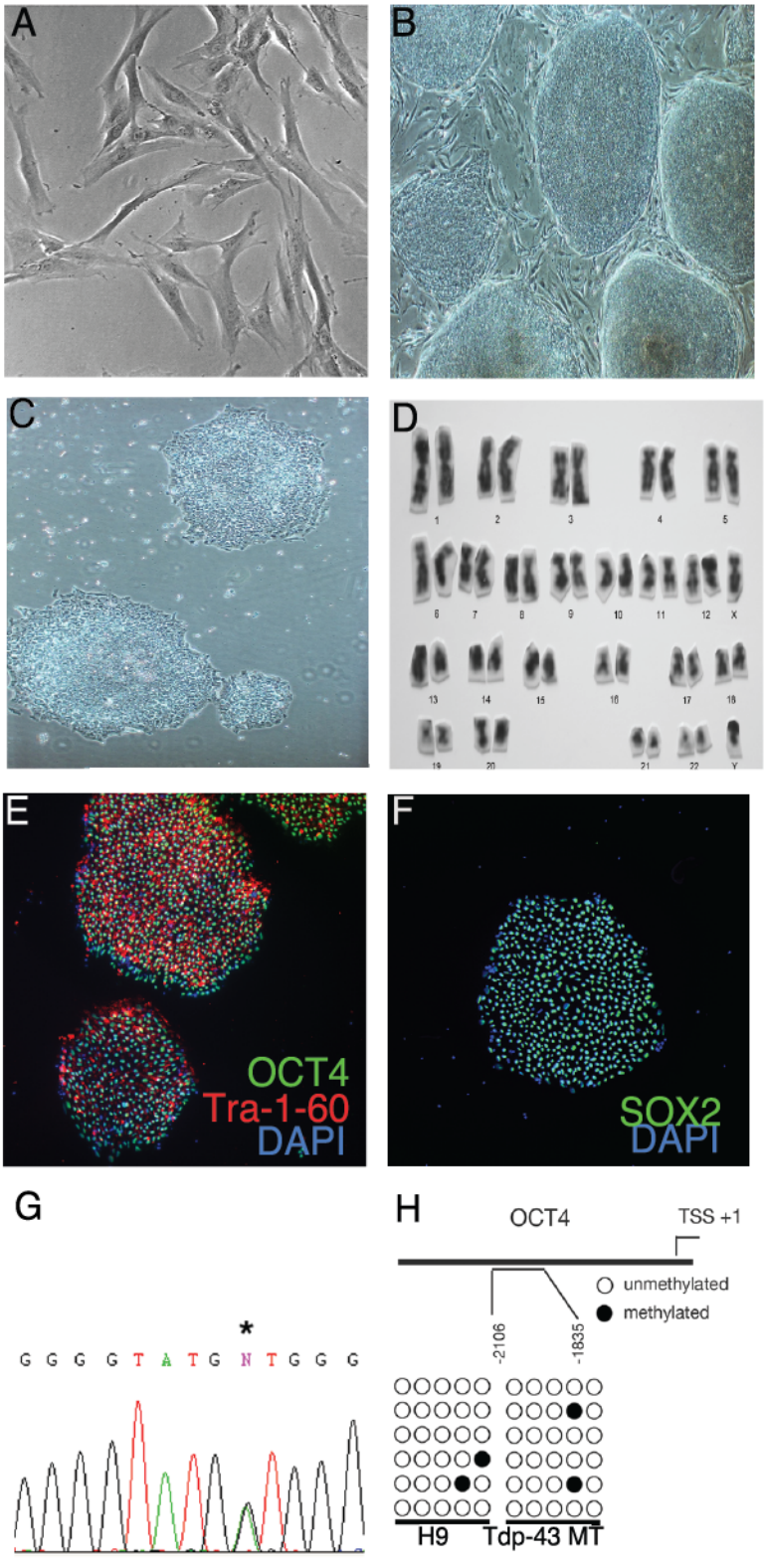
A
B
C
D
E
OCT4
Tra-1-60
DAPI
F
SOX2
DAPI
G
G G G G T A T G N T G G G
H
OCT4
TSS +1
unmethylated
methylated
-2106
-1835
H9
Tdp-43 MT

All iPSC lines used in this study showed silencing of the exogenous reprogramming factors and activation of endogenous OCT4, SOX2, c-Myc and KLF4 **(Fig. 2A,** *assay performed by Dr. G.Sullivan***)**; moreover, they also had comparable total expression levels of OCT4, SOX2, c-MYC, and KLF-4 as verified by qPCR with probes specific for endogenous and exogenous reprogramming factors **(Fig. 2B)**. The ability of these lines to generate all three germ layers was further assessed by performing a teratoma formation assay **(Fig. 2C**, *teratoma formation assay performed by Dr. G.Sullivan***)**.

Table 1:

Pluripotent Cell Lines used in this Study

Name	***Karyotype***	***Sex***	***Origin***	***Mutation***
M337V-1 (31D1)	Normal (46)	XY	Patient fibroblasts	M337V on *TARDBP*
M337V-2 (31D3)	Normal (46)	XY	Patient fibroblasts	M337V on *TARDBP*
CTRL-1 (33D9)	Normal (46)	XY	Control fibroblasts	none
CTRL-2 (34D6)	Normal (46)	XX	Control fibroblasts	none
H9 (WA09)	Normal (46)	XX	Donated I.V.F. blastocyst	none
Shef-4	Normal (46)	XY	Donated I.V.F. blastocyst	none

Figure 2. Validation of patient-derived iPSCs. (A) RT-PCR analysis showing the activation of endogenous loci and silencing of transgenic expression of the four reprogramming factors [OCT4, SOX2, KLF4, and c-MYC] in M337V-2 and control iPSCs. (B) Quantitative RT-PCR (qRT-PCR) analysis of total expression levels of NANOG in M337V and WT iPSCs and hESC lines H1, Shef4, and Shef6. Values are mean ± SEM. (C) After transplantation, all iPSCs generated teratomas displaying immature/mature neural tissue (ectoderm), chondrocytes (endoderm), and gut and sebaceous gland (mesoderm). Representative fields for iPSCs M337V-2 and control 2 (Cont-2) are shown.

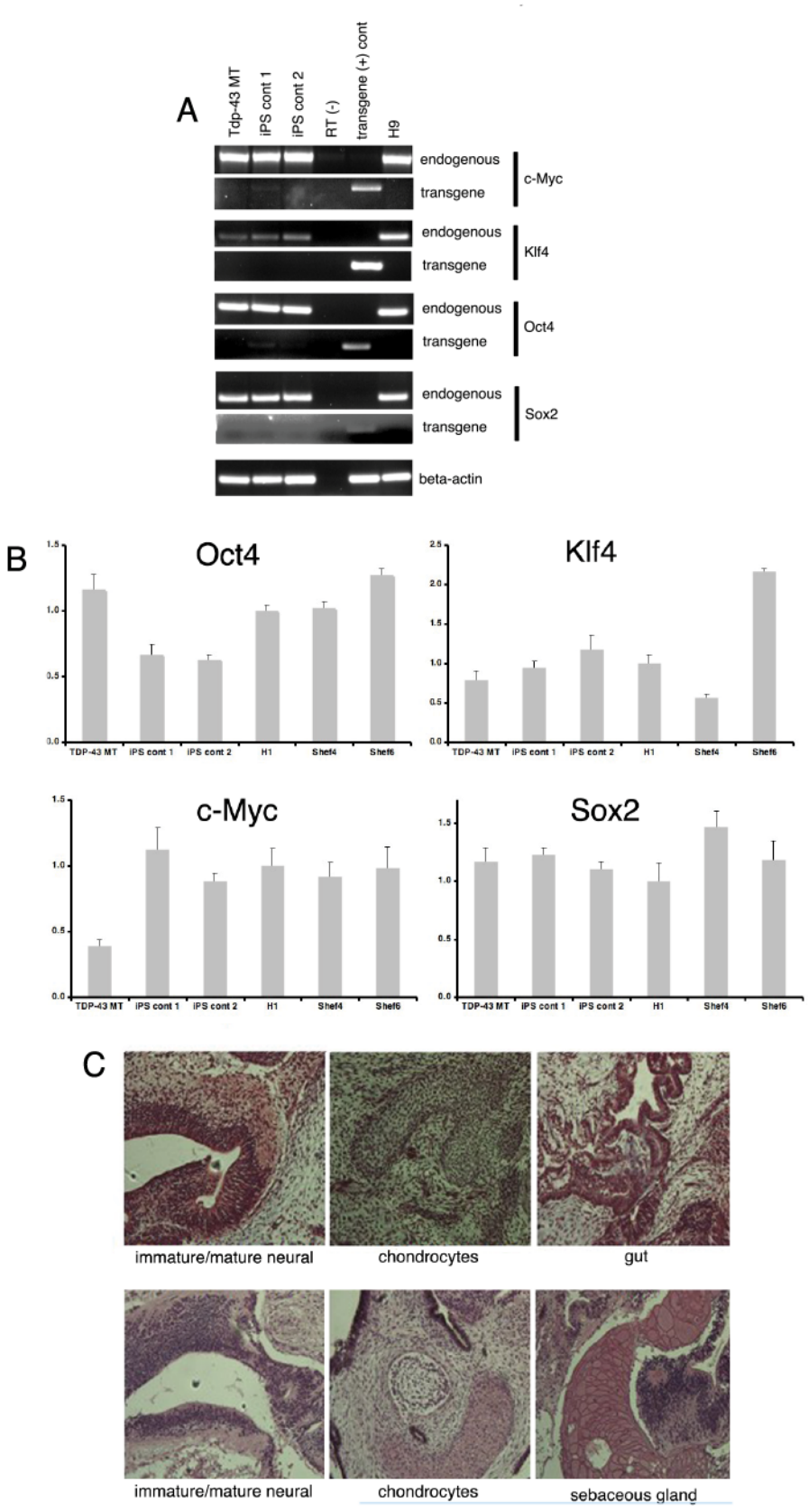
A
Tdp-43 MT
iPS cont 1
iPS cont 2
RT (-)
transgene (+) cont
H9
endogenous
transgene
c-Myc
Klf4
Oct4
Sox2
beta-actin
B
Oct4
Klf4
c-Myc
Sox2
TDP-43 MT
IPS cont 1
IPS cont 2
H1
Shef4
Shef6
C
immature/mature neural
chondrocytes
gut
sebaceous gland

3.2) Generation of Motor Neurones from iPSC Lines

To establish a motor neurone (MN) generation protocol we started from recapitulating the developmental process that leads *in vivo* to MN specification [176,177], taking as example already published protocols for the generation of human spinal neurons [157,158,178].

The protocol established for MN specification and differentiation **(Fig. 3)** encompasses three general phases that mimic the *in vivo* developmental process. Over a period of 6-12 weeks this protocol generates functional MNs from iPSC cells, passing through:

(1) *Neural conversion* of iPSCs, resulting in neural stem cells (NSCs) populations.

(2) *Patterning* phase that specifies the correct positional identity in NSCs, converting them to regionalised motor neuron progenitors (pMN).

(3) *Maturation* phase that allows the regionalised progenitors to differentiate into mature MNs.

Figure 3: Motor Neurons Generation Protocol. The protocol established for the generation of MNs from iPSC lines is composed of three independent phases that recapitulate the developmental processes taking place *in vivo*. The first phase consists of the neural conversion of pluripotent cells by dual smad inhibition, prolonged for the first week of treatment, followed by a patterning phase with retinoid signalling and hedgehog signalling for 2 weeks. The final step of the protocol consists of a maturation phase, in which a supportive medium with neurotrophic factors and without mitogens allows the patterned neuroblasts to generate MNs during the course of 4-8 weeks.

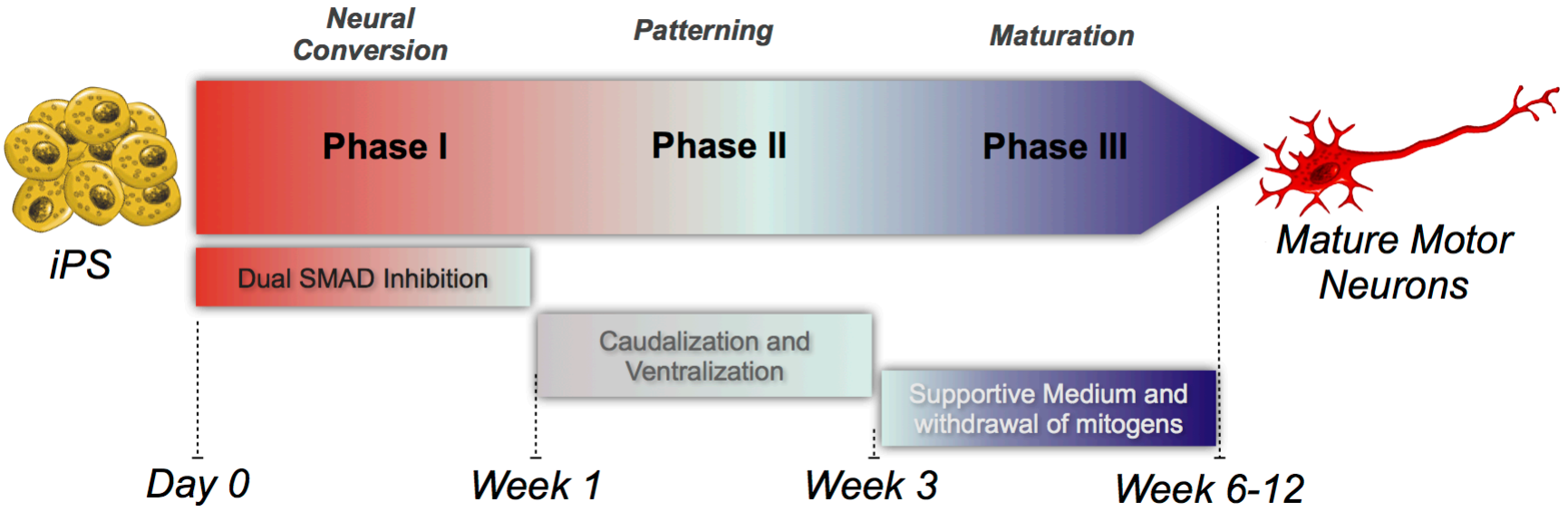
Neural Conversion
Patterning
Maturation
Phase I
Phase II
Phase III
iPS
Mature Motor Neurons
Dual SMAD Inhibition
Caudalization and Ventralization
Supportive Medium and withdrawal of mitogens
Day 0
Week 1
Week 3
Week 6-12

3.2.1) Neural Conversion

As previously shown in several developmental studies based in Xenopus embryos and in mice [179-182], the BMP pathway inhibition plays an important role in neural fate determination and it has been already used to promote the conversion of cultured pluripotent cells to neural progenitors [183]. To develop the neural conversion phase for this protocol the dual SMAD signalling inhibition methodology, as published by Chambers and co-workers in 2009[184] was taken as a starting point and optimised. To begin the neural conversion phase feeder free iPSC or hESC cultures were exposed to a chemically defined medium (CDM) containing SB431542, a compound that inhibits the Active/TGFβ pathways, and dorsomorphine, an analogue of Noggin, to inhibit BMP signalling (Phase I Medium; *see M&M)*. Half of the medium was replaced every 48 hours for a period of 7 days. During this conversion phase pluripotent cell colonies change their attachment properties, as they shift their identity towards the neural lineage, and can be easily detached as small clumps after seven days of dual SMAD inhibition by treatment with collagenase. The spheroids obtained by lifting the colonies are cultured in suspension overnight in CDM and plated the following day on laminin. Once plated on laminin, the neurospheres were left in culture for a period of 3 - 5 days in FGF2 containing medium, until they formed recognisable "neural rosettes" (Fig. 4A), organised structures formed by a high concentration of neuroepithelial precursors, positive for the human early neuroepithelium marker Pax6 (Fig. 4B-C). These neural rosettes were manually isolated from the rest of the plated neurosphere-colony and then cultured in suspension to form new neurospheres. The efficiency of neural conversion was calculated by staining selected neurospheres for the neural progenitor cytoskeletal filament Nestin and the transcription factor Sox1 **(Fig. 4C & 4D)**; both M337V and Control iPSC lines presented a high (90-95%) neural conversion efficiency, showing a behaviour similar to the hESC line H9 **(Fig. 4E)**.

Figure 4: Neural Conversion Efficiency. (A) When played on laminin at the end of the neuralisation protocol, colonies formed tridimensionally coherent structures known as "neural rosettes". (B-C) Neural rosette from iPSC lines present a high concentration of Pax6+ cells within the radially organized structures, as expected from previous reports. [B shows representative rosette from Control iPSC line, C shows representative rosette from M337V Lines]. (D-E) After rosettes selection cells were stained for Nestin (green) and Sox1 (red) to determine the efficiency of neural induction/selection; representative fields at both 63x (D) and 20x (E) magnification are shown from M337V iPSC-derived neurospheres. (F) Quantification of 5 independent fields for each line after neural induction; percentage of double labelling was comparable between the three cell lines used [M337V, 91.9 ± 0.8 % ; CTRL 93.3 ± 2.6 %; hESC (H9) 96.4 ± 3.5 %]

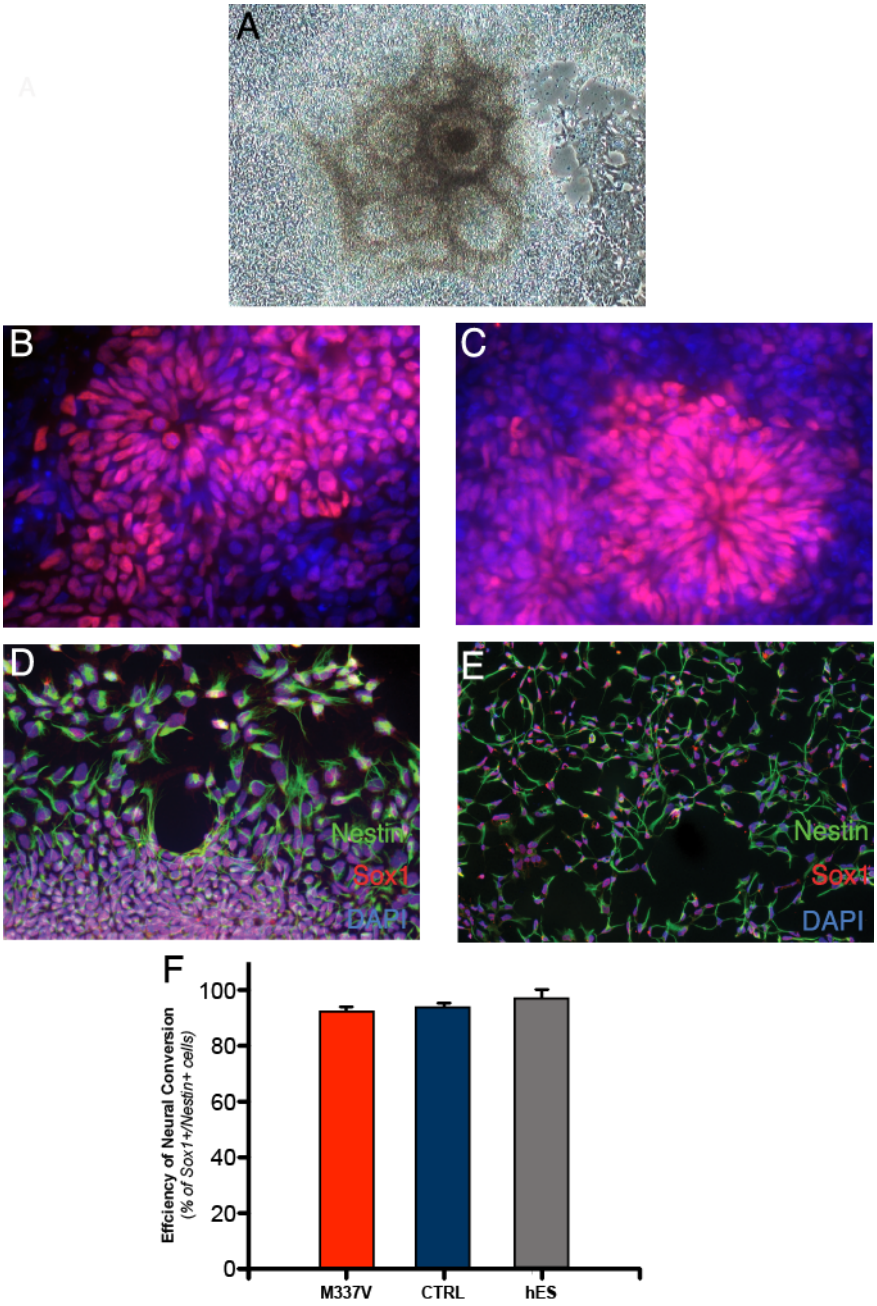
A
B
C
D
Nestin
Sox1
DAPI
E
Nestin
Sox1
DAPI
F
Effciency of Neural Conversion
(% of Sox1+/Nestin+ cells)
100
80
60
40
20
0
M337V
CTRL
hES

3.2.2) Patterning and Induction of Motor Neurones progenitors

Following neuralisation neural stem cells (NSCs) formed tight clusters of cells. Importantly, at this stage of the process, the clusters of NSCs have a poor attachment to the substrate compared to the original iPSC colonies. Taking advantage of this variability in attachment the clusters of NSCs were detached from the plate using a combination of enzymatic and mechanical dissociation treatment. The clusters were then cultured in suspension overnight to form neurospheres, which are then taken through the patterning phase to specify a regional identity suitable for the generation of MNs. MNs arise from the pMN domain in the spinal cord, which represents the second most ventral population of the spinal cord **(Fig. 5A)** after the p3 interneurons progenitors domain. For this reason the principal signals needed for the specification of the pMN identity are retinoic acid (RA), whose gradient determines the antero-posterior identity in the neural tube, and sonic hedgehog (SHH) signalling generated from the floor plate, the gradient of which determines the acquisition of ventral identities **(Fig. 5B)**.

Figure 5: Schematic representation of the developing neural tube. (A) Spinal cord positional identities are established during the elongation of the neural tube, thanks to a gradient of retinoic acid (RA), which influence the expression of the Hox positional identity genes. Spinal cord progenitors are specified posteriorly to the hindbrain, from r7 downwards, and are therefore characterised by the expression of the Hox4 family. (B) The roof plate (RP) and floor plate (FP) in the developing neural tube are the sources of BMP and Hedgehog signalling, determinants for dorso-ventral identity specification. The pMN domain represents the second most ventral progenitor population of the spinal cord, after the p3 interneurons progenitors.

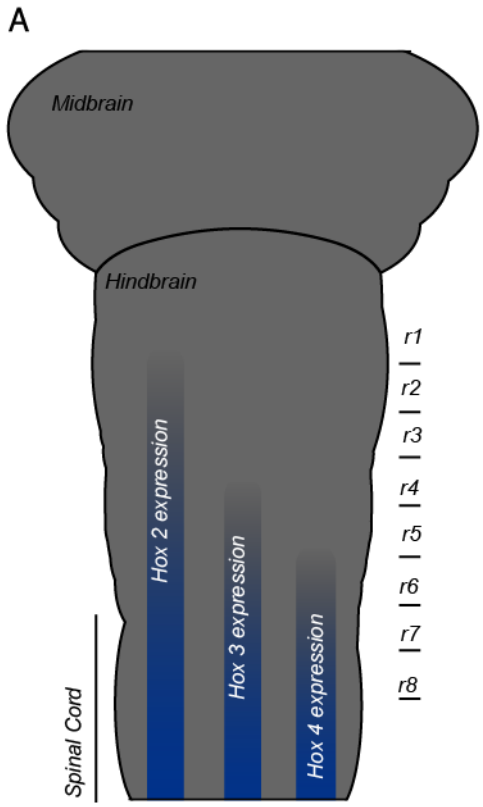
A
Midbrain
Hindbrain
r1
r2
r3
r4
r5
r6
r7
r8
Hox 2 expression
Hox 3 expression
Hox 4 expression
Spinal Cord

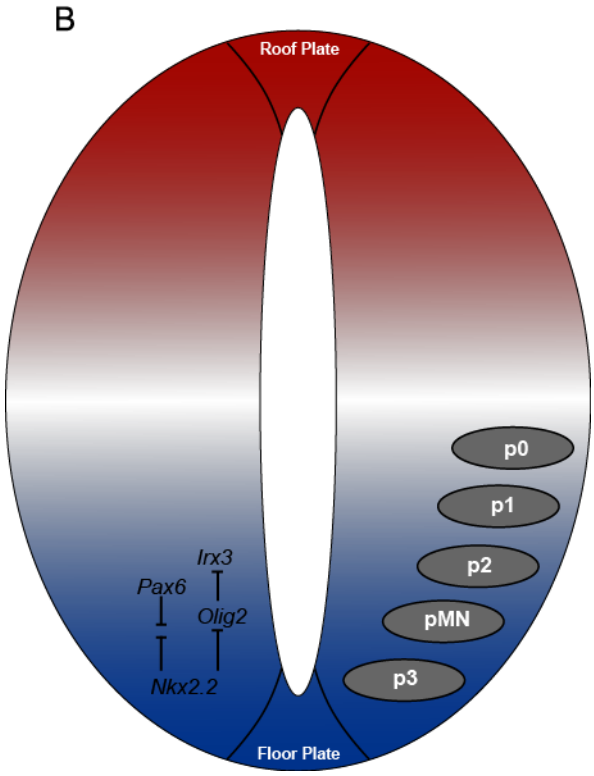
B
Roof Plate
p0
p1
p2
pMN
p3
Irx3
Pax6
Olig2
Nkx2.2
Floor Plate

In order to mimic the patterning of the neural tube *in vivo* the regional specification phase of the neurospheres was decided trough a caudalisation phase (first 7-9 days) in which the neurospheres are exposed to retinoic acid to acquire a caudal identity, and a second phase in which puromorphamine (an analogue of Sonic Hedgehog) is introduced in the culture to induce ventralisation.

Readouts for determining the efficiency of pMN specification included expression analysis for the homeobox gene HoxB4 **(Fig. 6A)**, expressed from rhombomere 7 to more caudal portions of the neural tube, were Pax6 and Olig2, two factors expressed in the pMN that are necessary for MN progenitor specification [185].

All lines exposed to the patterning protocol homogeneously expressed HoxB4 **(Fig. 6A)**, indicating that exposure to RA efficiently induced the specification of caudal identity. Both M337V and control iPSC lines responded to the patterning phase with comparable efficiency, and their performance was similar to he's cells exposed to the same protocol. In particular, no significant difference was observed in the percentage of cells expressing Pax6 or Sox2, a neural progenitor marker at the end of the patterning phase **(Fig. 6B-D)**. Moreover, all lines showed comparable levels of Olig2 induction, as measured with double immunolabelling with antibodies against Nestin and Olig2 **(Fig. 6E & 7F)**. Patterning of the neurospheres resulted in the induction of an $Olig2^{+}/Nestin^{+}$ pMN progenitor identity in ≈30% (variable between lines) of the NSCs used.

Figure 6: Generation of Motor Neuron Progenitors. (A) At the end of the casualization phase, after exposure to RA, the neural progenitors in culture exhibited a uniform expression of the positional identity gene HoxB4. (B) Representative image of immunostaining for Pax6 and Sox2 from M337V iPSC lines. (C) Quantification of cells positive for the neural stem cell marker Sox2 after the patterning phase showed that all lines present a comparable induction efficiency [M337V 79.45% ± 2.9 SEM; CTRL 65.69% ± 6.5 SEM; hESC (H9) 78.40% ± 2. SEM] (D) Quantification of cells positive for Pax6 after the patterning phase showed that iPSC lines present a comparable induction efficiency, although there is a difference in induction efficiency when compared to he's cells [M337V 52.38% ± 2.03 SEM; CTRL 51.65% ± 4.06 SEM; hESC (H9) 67.68% ± 23.35]. (E) Representative image of immunostaining fro the pMN domain marker Olig2 from M337V iPSC lines. (F) Quantification of cells positive for Olig2 after the patterning phase showed that all lines used present an equivalent induction of pMN identity in culture [M337V 29.44% ± 4.43 SEM; CTRL 33.81% ± 3.46 SEM; hESC (H9) 23.40% ± 4.25]

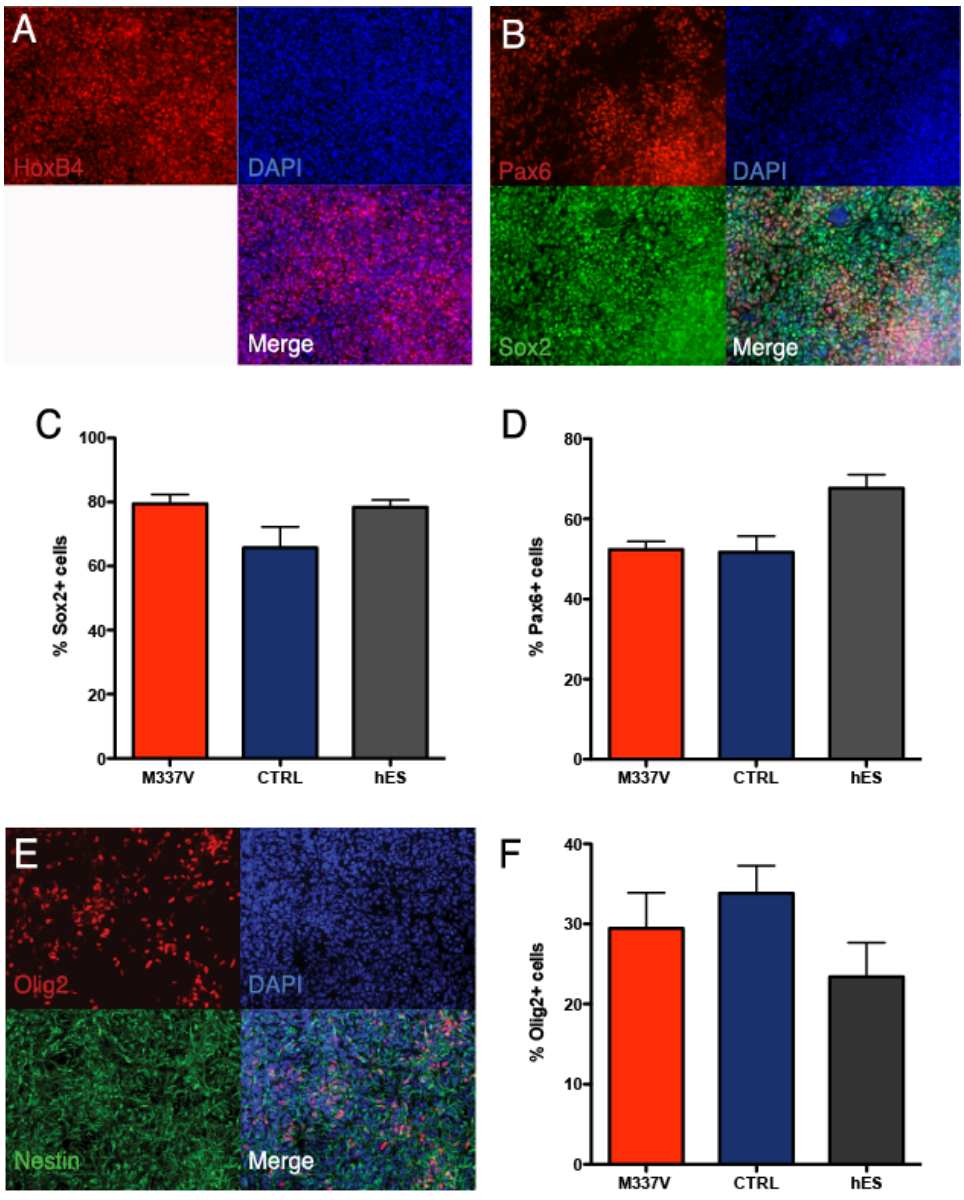
A
HoxB4
DAPI
Merge
B
Pax6
DAPI
Sox2
Merge
C
% Sox2+ cells
100
80
60
40
20
0
M337V
CTRL
hES
D
% Pax6+ cells
80
60
40
20
0
M337V
CTRL
hES
E
Olig2
DAPI
Nestin
Merge
F
% Olig2+ cells
40
30
20
10
0
M337V
CTRL
hES

3.2.3) Establishment of pMN Maturation Protocol in both neurospheres and monolayer

The neurosphere-based system described so far has many practical advantages: it is a robust and scalable system and allows for a easy transportation of the cellular material even over long distances. However, the maturation of the specified MNs in the neurospheres present specific challenges related to the inaccessibility of most cell bodies and in general the difficulty in assessing the cellular morphology. In particular, assessment by immunocytochemistry and immunofluorescence becomes particularly challenging when MNs are differentiated within the neurospheres, and this can result in an unreliable quantification of the protocol's efficiency. For this reasons the maturation phase of the MN protocol was optimised using both a neurosphere-based system and a transition to a monolayer culture.

After the patterning phase the pMN Olig2/Nestin progenitors can be taken further into the differentiation protocol by plating them on laminin/fibronectin[186] coated coverslips for the maturation phase. The differentiation of the progenitors was induced by removing mitogens (FGF2 in particular) from the culture media, which results in the neuroblasts exiting the cell cycle and starting to generate post-mitotic neurons, as demonstrated by the extending neurites on the surface of the coverslips **(Fig. 7A)**. The vast majority of neuroblasts and maturing neurons tend to remain within the neurosphere **(Fig. 7B)**, which makes extremely difficult to study the behaviour and localisation of TDP-43 in the neurons, since almost all cell bodies reside inside the sphere.

To overcome this problem a protocol to enzymatically dissociate the patterned neurospheres was established and optimised. After the regional specification the neurospheres were dissociated using Accutase, and the resulting progenitors were plated as a monolayer at high density **(Fig. 7C)**. The differentiation in this monolayer cultures was induced using the same mitogen free medium used in the neurosphere-based protocol. The monolayer culture was permissive for MN specification and maturation, as demonstrated by the differentiation of plated progenitors into $Isl1^{+}$ neurons

(Fig. 7D) and allowed analysis of cell bodies as well as identification of each cell's neurites and axon.

Figure 7: Comparison between standard sphere-based and monolayer MN maturation protocol . Plating neurospheres at the end of the patterning phase (A) results in enhanced neurites outgrowth but limited migration of the cell bodies out of the sphere (B); the monolayer patterning/maturation protocol (C) allows to analyse the ultrastructure of motor neurons (D), and therefore facilitate the analysis of TDP-43 localization

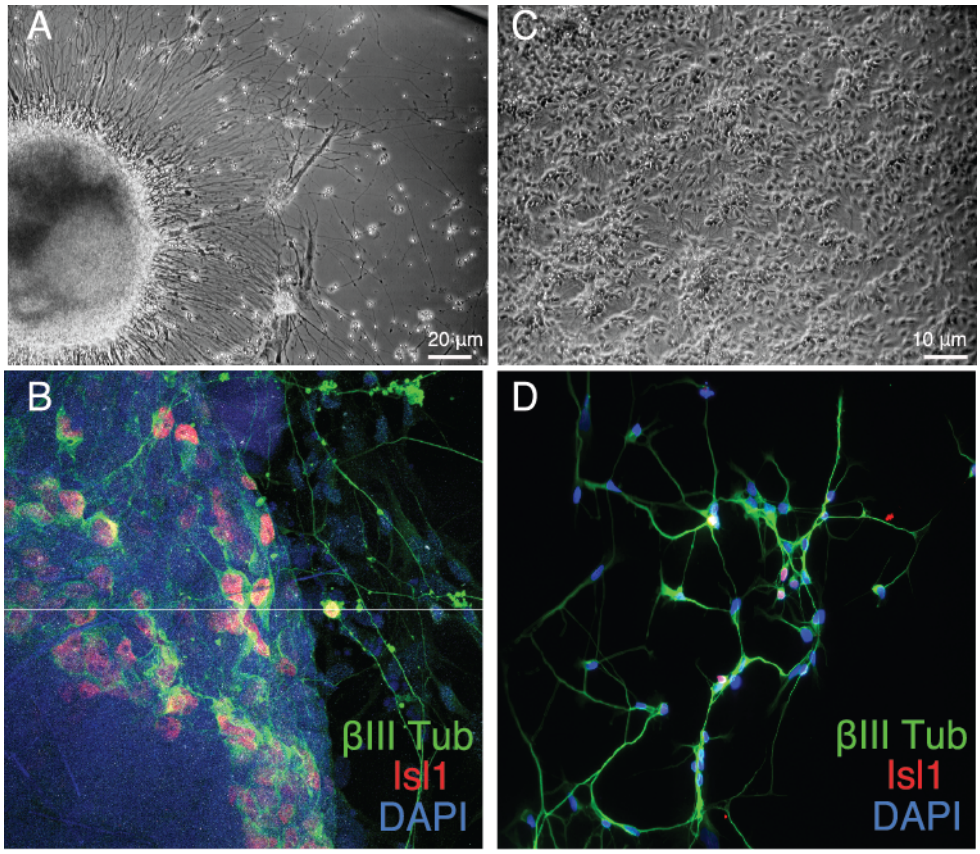
A
20 µm
C
10 µm
B
βIII Tub
Isl1
DAPI
D
βIII Tub
Isl1
DAPI

3.2.4) Motor neurones maturation phase

Patterned MN progenitors were plated on laminin/fibronectin-coated coverslips for a period of 3-6 weeks to differentiate into motor neurons. To allow the development of MNs, the culture medium was modified by withdrawing mitogens (FGF2 in particular) and supplementing it with supportive factors (in particular ascorbic acid and forskolin [187]), NAC[188], neurotrophic factors GDNF and BDNF. Initial stages of MN differentiation in culture were assessed by co-immunolabelling using antibodies against the transcription factor HB9 (Mnr2) that can be used as a post-mitotic MN marker[189], and βIII tubulin (Fig. 8A) or co-labelling with Hb9 and SMI-32 (an antibody directed against a non-phosphorylated epitope of neurofilament heavy chains used to identify mature motor neurons in the spinal cord[190]) later on during MN maturation (Fig. 8B). We then wanted to measure the efficiency of MN generation in order to exclude differences in the way the iPSC TDP M337V line and the control line responded to the protocol (Fig. 8C): quantification of the percentage of cells that expressed HB9 over three independent differentiation experiments revealed that the M337V mutation does not determine a difference in the MN generation efficiency *in vitro*.

At the end of the maturation phase expression of ChAT (choline acetyltransferase) a marker of cholinergic neurons, (Fig 8D), and synapsin I (Fig. 8E) was observed, indicating that both iPSC lines can generate cultures with a functional profile comparable with that of mature MNs in response to the same protocol.

Figure 8: Maturation of iPSC-derived Motor Neuron in vitro. (A) After 4-6 weeks in culture the patterned neural progenitors give rise to MNs positive for the specific Marker HB9. (B) As maturation proceeds MNs in culture acquire co-positivity for HB9 and the neurofilament marker SMI-32, used *in vivo* to identify spinal MNs (C) Quantification of neurons positive for the MN specific marker HB9 after the maturation phase showed that the iPSC lines present a comparable MN induction efficiency [M337V 79.45% ± 2.9 SEM; CTRL 65.69% ± 6.5 SEM; hESC (H9) 78.40% ± 2.] (D) Quantification of cells positive for Pax6 after the patterning phase showed that iPSC lines present a comparable induction efficiency, although there is a difference in induction efficiency when compared to he's cells [M337V 50.72% ± 6.36 SEM; CTRL 53.17% ± 10.56 SEM]. (E) Representative image of immunostaining fro the MN functional marker Chat from M337V iPSC lines, showing that maturation of MNs in vitro proceeded towards the expression of more mature markers. (F) Representative image of immunostaining for Synapsin I from M337V iPSC lines.

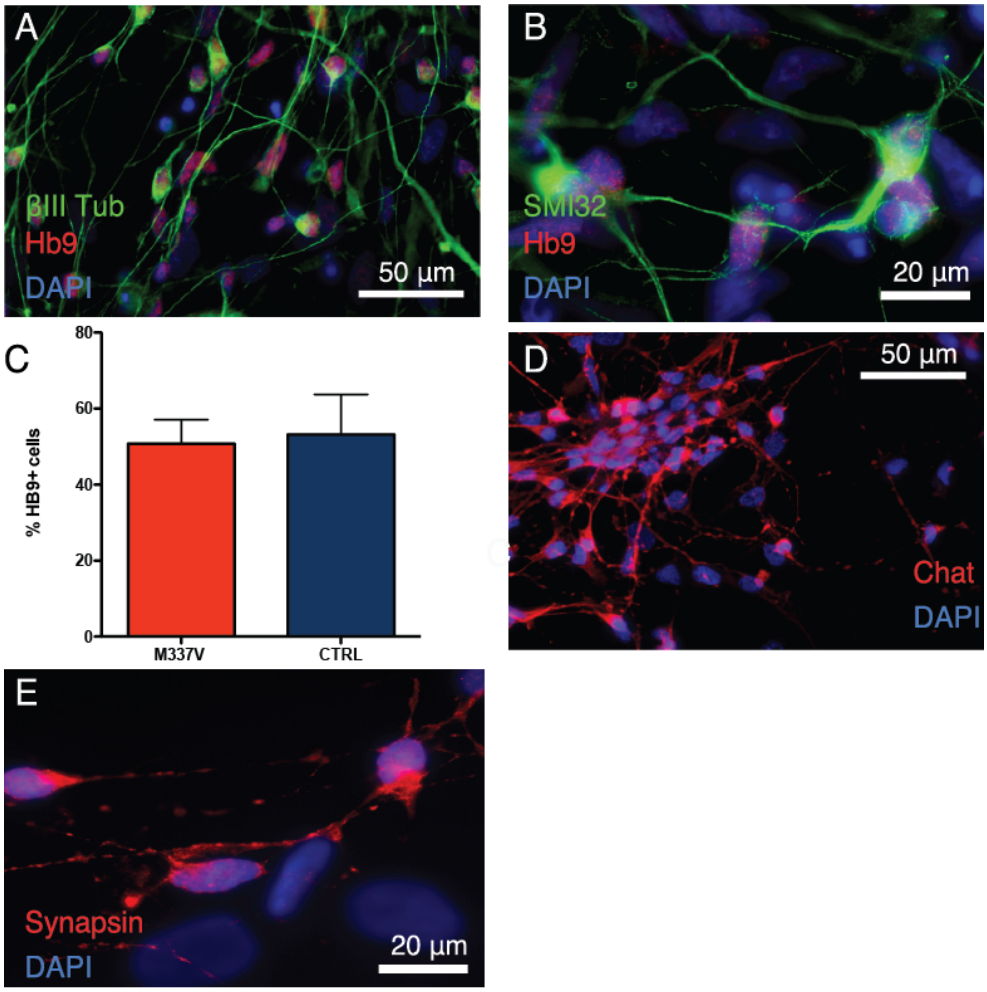
A
βIII Tub
Hb9
DAPI
50 µm
B
SMI32
Hb9
DAPI
20 µm
C
% HB9+ cells
80
60
40
20
0
M337V
CTRL
D
50 µm
Chat
DAPI
E
Synapsin
DAPI
20 µm

3.2.5) Electrophysiology and NMJ Assay

In order to be able to properly model the pathology of ALS *in vitro* the MNs generated with this protocol need not only to stain for pMN specific markers but also to have measurable functional properties comparable to *in vivo* MNs. We decided to concentrate our functional characterization on their ability to form neuromuscular junctions (NMJs) *in vitro* and on their electrophysiological properties. In order to asses whether the iPSC-derived MNs lines are capable of forming NMJ *in vitro* an assay established to test their ability to form putative neuromuscular contact points when cocultured with fused murine myofibers[191]. To perform this assay differentiating precursors (before the HB9 expression could be detected in the culture) were plated on a layer of already fused C2C12 cells, and kept in culture using the MN maturation medium for a period of 1-2 weeks. The readout of this experiment was detection of α1 nicotinic acetylcholine receptor clustering on the myofibers, a typical phenomenon observed *in vivo* at the contact points between axonal growth cones and skeletal myofibers, using Alexa-555 conjugated α-Bungarotoxin, which is a specific inhibitor of nicotinic acetylcholine receptors. Both iPSC lines were able to generate NMJ-like structures during this assay **(Fig. 9A)**. Furthermore the electrophysiological activity of functional motor neurons was indicated by repetitive firing of action potentials and receptor responsiveness, (**Fig. 9C** *performed by Clare Puddifoot in David Wyllie's lab*). Whole-cell patch-clamp recordings of $ChAT^+$ TDP-43 M337V iPSC-derived MNs demonstrated tetrodotoxin-sensitive, repetitive firing of action potentials **(Fig. 9D)**. Furthermore, in 10-week old cultures, spontaneous excitatory post-synaptic currents were also observed (Fig. 9E). Currents evoked in response to bath application of NMDA, AMPA and GABA suggested the expression of the two glutamatergic excitatory neurotransmitter receptors as well as the $GABA_A$ receptor (Fig. 9F&G). These results are consistent with the functional maturation profile of hESC- and iPSC-derived neurons and indicate that M337V iPSC-derived MNs are electrophysiologically active.

Figure 9: Functional Characterisation of iPSC-derived Motor Neuron in vitro. (A) Representative image of cocultures of maturing MNs differentiating murine myofibers (derived from C2C12 line), stained for SMI-32 and the nicotinic receptor antagonist α-Bungarotoxin. At the point of contact between MN neurites and fused myofibers it is possible to observe clustering of the nicotinic receptors. (B) Representative image of MN used for electrophysiological recordings, filled with LucY+ dye during the recordings and post-stained with the MN marker Chat (C-D) Current–clamp traces showed tetrodotoxin-sensitive action potentials in response to injection of depolarizing current in M337V (C) and WT (D) MNs. (E) Sample traces of spontaneous miniature EPSCs recorded from an M337V culture. All miniature EPSC events were blocked with CNQX. (F) (E) Examples of whole-cell currents recorded from ChAT+ M337V iPSC-derived MNs in response to bath application of NMDA (100 μM) plus glycine (50 μM), AMPA (50 μM), or GABA (100 μM). (G) As in E but illustrating recordings from Control iPSC-derived MNs.

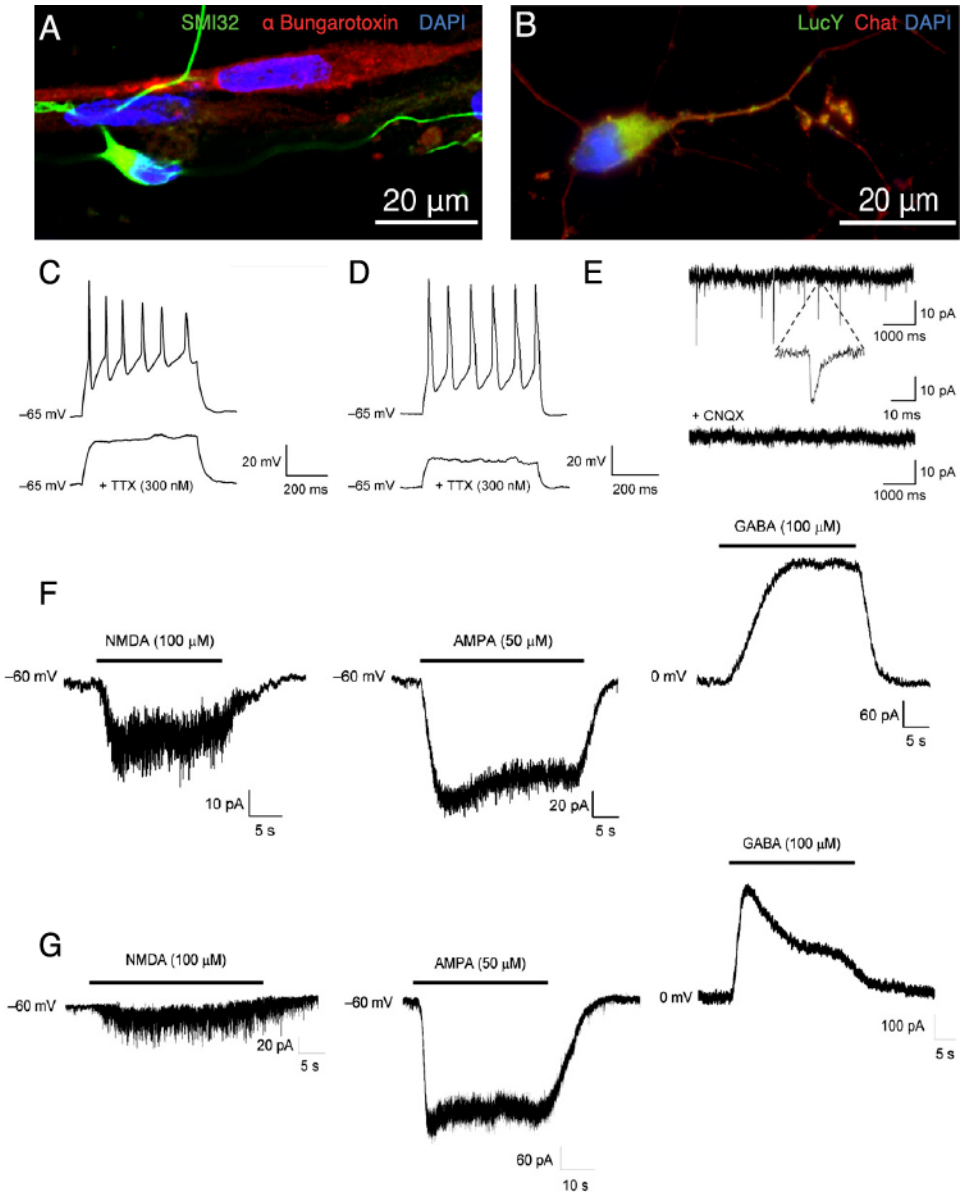
A
SMI32
α Bungarotoxin
DAPI
20 µm
B
LucY
Chat
DAPI
20 µm
C
–65 mV
–65 mV
+ TTX (300 nM)
20 mV
200 ms
D
–65 mV
–65 mV
+ TTX (300 nM)
20 mV
200 ms
E
10 pA
1000 ms
10 pA
10 ms
+ CNQX
10 pA
1000 ms
F
NMDA (100 µM)
–60 mV
10 pA
5 s
AMPA (50 µM)
–60 mV
20 pA
5 s
GABA (100 µM)
0 mV
60 pA
5 s
G
NMDA (100 µM)
–60 mV
20 pA
5 s
AMPA (50 µM)
–60 mV
60 pA
10 s
GABA (100 µM)
0 mV
100 pA
5 s

3.3) Generation of Astrocytes from iPSC Lines

In order to study the effect of M337V mutation on the astrocytes and in turn the role of mutations on the disease phenotype, it was necessary to optimize a scalable protocol to efficiently specify glial phenotypes in our cultures. Moreover, in order to asses whether the presence of the mutation had any functional consequences on the astrocytes – and in turn on the disease phenotype - the glial populations used in this part of the study needed to present a functional profile comparable to *in vivo* astrocytes.

As discussed previously (see *Introduction, chapter on Gliogenesis*) the mammalian central nervous system develops in a precisely organized temporal and spatial sequence of events. Early neural progenitors are incapable of generating astrocytes, and gliogenic potential is acquired over time during development at the expense of the ability to give rise to neurons.

In recent years a number of different protocols have been developed to generate astrocytes from human pluripotent cells, trying to reproduce this neuronal- to glial- fate specification potency switch with different approaches[124,192-194]. These methodologies differ in degrees of efficiency, purity and functional characterization of the differentiated cells, but can be divided into two main categories based on the approach used to induce the gliogenic switch:

- Some methodologies rely on the ***use of serum*** in the culture media to induce astroglial specification in the cultured progenitors. The use of animal serum (normally festal calf serum, FCS) and TGF-β has been historically very widely used in the differentiation and culture of astroglial cells *in vitro* [195], given their ability to induce the expression of astrocytes lineage specific markers in cultured neural progenitors[196]. This approach has been used in a recently published iPSC-disease modelling study for Huntington's Disease (HD) [192]. The downside of using serum-containing media is the fact that serum itself is a non-chemically defined xenon component, and it presents issue in terms of possibilities of translation and reproducibility.

- Protocols that rely on ***prolonged time in culture*** to achieve the gliogenic potential switch *in vitro*. As described previously (*see Introduction, chapter on Gliogenesis*) a number of studies reported that cultured neural progenitors do not give rise to significant number of astrocytes within the first weeks of culture [120,121,193]. It is known that prolonged propagation of neural progenitors *in vitro* leads to decreased neurogenic potential and progressively increasing ability to differentiate into GFAP+ cells, and several groups have taken advantage of this mechanism to generate astrocytes from human progenitors[124,193,194]. The use of this particular approach has a limitation in that the efficiency of astrocytes differentiation and the purity of the culture are dependent on time spent in culture. Emdad and colleagues reported that in a adherent NPCs system, by 5 weeks there is a significant number of cells expressing GFAP (≃70%), but at the same time a consistent number of cells still express neuronal markers (TuJ1, ≃40%)[193]. Similar results were obtained with suspension NPC cultures in the Zhang lab, but they were also able to obtain efficiently highly enriched astroglial cultures by prolonging the time in culture from 90 to 180 days[124].

To fulfil the aims of this project one needs to be able to obtain highly enriched astroglial populations from iPSC-derived NPCs in a chemically defined culture environment. However, at the same time we sought to decrease the time needed to specify the astroglial lineage *in vitro*. Moreover, we wanted to be able to produce astrocytes populations from the same progenitors used to generate our MN cultures, in order to be able to compare directly the different phenotypes in the two cell types without any bias due to differences in the neural conversion or patterning phase.

To accomplish this, it was necessary to optimize a methodology that relies on the application of pro-gliogenic signals during propagation of suspended NPCs cultures to accelerate the neurogenic-gliogenic switch.

3.3.1) Optimization of gliogenic conversion phase

The optimization of the NPC gliogenic conversion phase started by examining the prolonged propagation based protocols described in the previous section, focusing on which elements could be manipulated to accelerate and enhance the acquisition of glial fate specification potency. Generally proliferation and propagation of NPC in vitro is maintained by FGF2 and EGF, for both monolayer NPC cultures[120-123] and neurospheres[124-126].

As see in the introduction, responsiveness of neural precursors to either FGF2 or EGF is directly linked to their gliogenic potential. Moreover, several studies have convincingly demonstrated that activation of JAK-STAT pathways by members of the IL-6 family plays a key role in determine the acquisition on neurogenic potential, indicating LIF as one of the most important pro-gliogenic factors *in vivo* as well as in cultured progenitors (*see Introduction, chapter on Gliogenesis*).

Interestingly, it has been also demonstrated that it is the activity of EGFR that control the competence of NPC to interpret LIF signalling as an astroglial-fate inducer i*n vivo*[108].

Against this background it was decided to modify the classical *prolonged culture* approach to specify glial identities in vitro by withdrawing FGF2 and culturing the cells in the presence of EGF and LIF. The aim of this culture modification is to obtain a reliable –and short timed- "conversion phase" in which the population of cultured NPC homogeneously shifts its identity towards astroglial fate.

To test the validity of this approach, it was first tested on hESC derived NPCs.

H9-derived neurospheres where derived as in the previous sections of this chapter. After the neural conversion phase, samples were divided into two different populations: one propagated in FGF2 and EGF containing medium (EF), the other to be expanded in EGF and LIF containing medium (EL). The identity of the NPC in the neurospheres from the different groups was

assessed by plating them on Matrigel-coated plates and performing immunostaining for NESTIN and GFAP after 24 to 48 hours (according to attachment efficiency). After 2 weeks of treatment the EL population already presented a noticeable increase in the amount of GFAP+ cells and processes migrating out of the landed neurospheres (**Fig 10 A&B**).

At this point, a quantification of the number of spheres presenting the majority of cells positive for GFAP or Nestin was performed within the samples, in order to assess whether the treatment was having a positive effect not only on a single-spheres basis but also on a population level, independent of inter-spheres variation in size and composition. The results show that the EL treatment does not affect the expression of NESTIN in the spheres population after either 1 week or 2 weeks of treatment (**Fig. 10C**). However, the EL treatment combined with propagation had a significant effect in increasing the amount of GFAP+ cells in the neurospheres over the course of 2 weeks, compared to equivalent cultured propagated in EF (**Fig. 10D**). The EL treatment was then tested on unpatterned iPSC-derived neurospheres, showing that by 4 weeks in EL propagation all neurospheres in the culture (regardless of their size) homogeneously expressed GFAP. The EL conversion test was carried out on both M337V and CTRL iPSC derived neurospheres, obtaining similar results (**Fig. 10 E&F**).

These results demonstrate that it is possible to increase the rate of gliogenic switch in cultured NPC by withdrawing FGF signalling and actively supporting the process with co-application EGF and LIF. Neurospheres that have been trough the EL-based conversion are then labelled as 'astrospheres.' The next necessary step for this protocol was a suitable neurosphere dissociation system, to obtain single cells population to plate for following differentiation and analysis. The dissociation system was optimized starting from a commercially available kit designed to obtain viable populations of single cells from rodent brain explants, based on the combined action of Papain and DNAseI (*Papain Dissociation Kit, see Materials & Methods*).

After optimization of volumes and enzymes concentration, with this particular enzymatic approach it was possible to successfully dissociate the neurospheres after 4 weeks of propagation in EL conditions, obtaining a viable population of single cells to be plated in monolayer for differentiation and characterization.

The differentiation potential of the EL neurospheres-derived monolayer cultures was then tested by withdrawal of mitogens and application of factors known to promote astroglial differentiation in NPCs, in particular: ciliary neurotrophic factor (CNTF), bone morphogenic protein-4 (BMP4), LIF, co-application of BMP4 and LIF and a basal medium containing only general cell supportive factors (as B27 supplement) [107,197,198] (**Fig. 10G**).

Interestingly, all conditions tested gave rise to high percentages of $GFAP^+$ cells within the differentiated population. The application of pro-gliogenic factors increases the efficiency of differentiation (61% ± 7.63 SEM in B27 only, compared to the average effect of all the pro-gliogenic factors combined of 87.5% ± 6.17 SEM). Moreover, amongst the different factors tested, CNTF was the most effective at promoting the induction of GFAP+ cells after 14 days of differentiation compared to the others (CNTF 89.3% ± 2.7 SEM, BMP4 85.3% ± 7.3 SEM, LIF 88.7% ± 5.02 SEM, BMP4/LIF 86.6% ± 9.6 SEM). Also, CNTF treated cultures gave rise to homogeneously GFAP+ monolayer on Matrigel coated plates after 14 days, without displaying any overgrowth of the cultured cells or any attachment problems. Other pro-gliogenic factors tested (particularly BMP4/LIF combination) were less reliable in terms of maintaining a perfectly attached monolayer of cells at the end of the differentiation.

Given that the aim of this part of the project is to model the glial counterpart of the already generated spinal MNs, the following part of the project was focused on the generation astrocytes populations using this methodology starting from neurospheres that have been through the MN patterning phase (*see above*) and proven to generate efficiently HB9+/SMI-32+ cells.

Figure 10: Optimization of Glial conversion phase in vitro. (A-B) he's-derived neurospheres were cultured for 2 weeks with either EGF/LIF medium (EL) or EGF/FGF2 medium (EF), and then plated on Matrigel to perform immunostaining for GFAP and Nestin. (C) Immunofluorescence profiling of the plated neurospheres populations based on the diffusion of Nestin positivity within the spheres shows that at both time-point considered the EL and EF population are equivalent. [EF week1 97.55% ± 1.41 SEM; EF week2 93.23% ± 1.41 SEM; EL week1 89.90% ± 4.25 SEM; EL week2 96.15% ± 3.85 SEM;] (D) Immunofluorescence profiling of the plated neurospheres populations based on the diffusion of GFAP positivity within the spheres shows that at both time-point considered the EL population presented a significantly increased number of spheres homogeneously positive for GFAP+, compared to the EF population [EF week1 19.05% ± 4.22 SEM; EF week2 36.95% ± 1.75 SEM; EL week1 74.13% ± 6.69 SEM; EL week2 94.60% ± 3.19 SEM; *** for p<0,001, 2-way ANOVA]. (E-F) After 4 weeks of EL conversion treatment both Control (E) and M337V (F) iPSC-derived neurospheres presented diffuse and homogeneous positivity for GFAP within the spheres. (G) Quantification of GFAP+ cells after single cells dissociation and 14 days differentiation with different morphogens [CNTF 89.3% ± 2.7 SEM, BMP4 85.3% ± 7.3 SEM, LIF 88.7% ± 5.02 SEM, BMP4/LIF 86.6% ± 9.6 SEM]

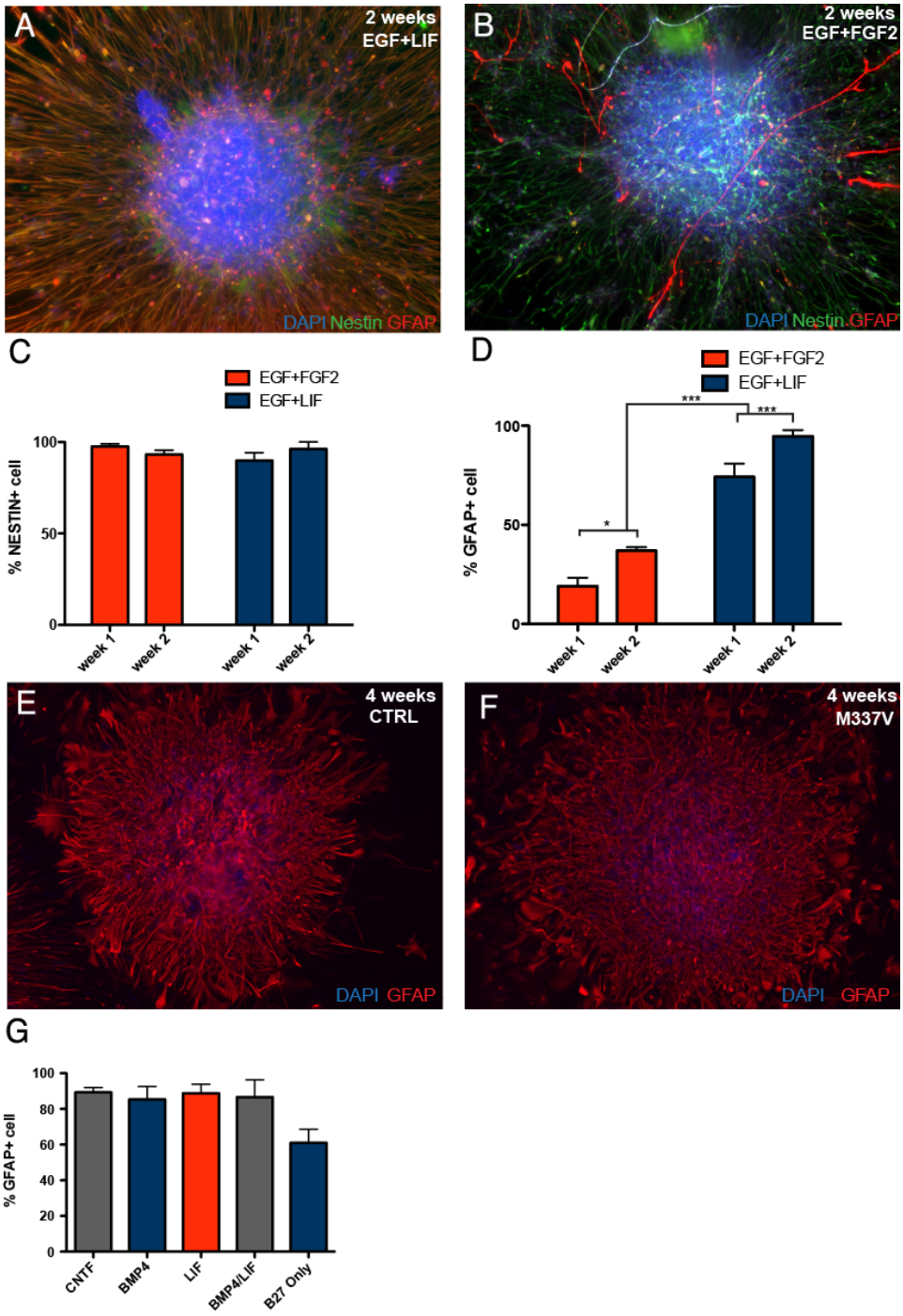
A
2 weeks
EGF+LIF
DAPI Nestin GFAP
B
2 weeks
EGF+FGF2
DAPI Nestin GFAP
C
EGF+FGF2
EGF+LIF
% NESTIN+ cell
100
50
0
week 1
week 2
week 1
week 2
D
EGF+FGF2
EGF+LIF
***
***
*
% GFAP+ cell
100
50
0
week 1
week 2
week 1
week 2
E
4 weeks
CTRL
DAPI GFAP
F
4 weeks
M337V
DAPI GFAP
G
% GFAP+ cell
100
80
60
40
20
0
CNTF
BMP4
LIF
BMP4/LIF
B27 Only

3.3.2) Generation of astrocytes from patterned iPSC-derived NPCs

Building on the results presented on the previous paragraph a time-efficient and scalable "conversion phase" based on the EL protocol was optimized to be used specifically on iPSC-derived MN patterned neurospheres (*see MN protocol above*) **(Fig.11A).**

Neurospheres from two clones of the TDP-43 M337V iPSC line and two control (CTRL) iPSC lines were used for this phase of the project. Immediately after the end of their MN maturation phase, the neurospheres were mechanically chopped to expand their numbers and then switched to their EL-based conversion phase for a period of 4 to 6 weeks (depending on lines, spheres size, etc.). To maximize the number of astrospheres after the EL conversion, cultures were then switched back to EGF- and FGF2-containing expansion medium. Once a suitable number of astrospheres from each iPSC line was obtained they were dissociated to generate monolayer cultures for differentiation and characterization.

The resulting populations were positive for vimentin and nuclear factor 1A (NFIA), two markers of astrocyte progenitor cells (APCs) [199,200]**(Fig. 11B)**, and could be propagated as a monolayer culture with EGF and FGF2 for several passaged in culture.

Consistent with what has been described for APCs *in vivo* and *in vitro*, less than 30% of cells in early passage APC cultures were positive for the astrocytic marker glial fibrillary acidic protein (GFAP) during proliferation. However, subsequent differentiation over 14 days in the presence of CNTF increased the proportion of GFAP positive cells to over 90% **(Fig. 11C)**.

Consistent with the results obtained from the optimization of the EL conversion phase, after two weeks of differentiation the vast majority of the cells co-expressed the astrocytic markers GFAP and S100β **(Fig. 11D)**. Moreover, less than 2% of cells were positive for the neuronal marker βIII tubulin **(Fig. 11D&E)**, confirming the efficiency of this protocol in generating highly enriched APC populations.

The efficiency of astrocytes generation between M337V and CTRL iPSC

lines was compared, to determine whether the mutation has any effects on gliogenic fate specification. No difference was observed in the efficiency of astrocyte differentiation between iPSC lines **(Fig. 11F)**.

Figure 11 Generation of astrocytes from iPSC lines. (A) iPSC-derived neurospheres were enriched for APCs by culturing in EGF/LIF-containing medium for 2–4 weeks and then expanded in EGF/FGF2-containing medium. To obtain monolayer cultures, enriched neurospheres were dissociated using papain and differentiated with CNTF. (B) APCs in monolayer cultures maintained a homogenous identity and morphology, featuring a high percentage of cells positive for the glial progenitors markers Vimentin [85.6% ± 2.9 SEM] and NFIA [79.8% ± 1.9 SEM] (scale bar = 100 μm). (C) APC present 24.6%± 2.61 SEM cells positive for GFAP during proliferation in EGF and FGF2; this percentage increases rapidly during the first 7 days of CNTF differentiation [84.9%± 0.53 SEM] reaching a peak after 14 days [90.8% ± 1.13 SEM] (D) Differentiation of monolayer APCs for 14 days in CNTF results in a population of astrocytes positive for GFAP [90.6% ± 0.7 SEM] and S100β [91.9% ± 1.9 SEM] (panels represent the same field, scale bar = 25 μm). A few neurons were found in the differentiated cultures [1.7% ±0.4 SEM]. (E) Representative field for a differentiated iPSC-derived astrocytes after 14 days of CNTF differentiation, labelled for GFAP (red) and TuJ1 (green), showing that the protocol gives rise to highly enriched astrocytes cultures. (F) M337V and control iPSC lines showed comparable numbers of GFAP-positive cells post-differentiation [M337V 92.25% ±0.97; WT 91.36% ±1.0 SEM].

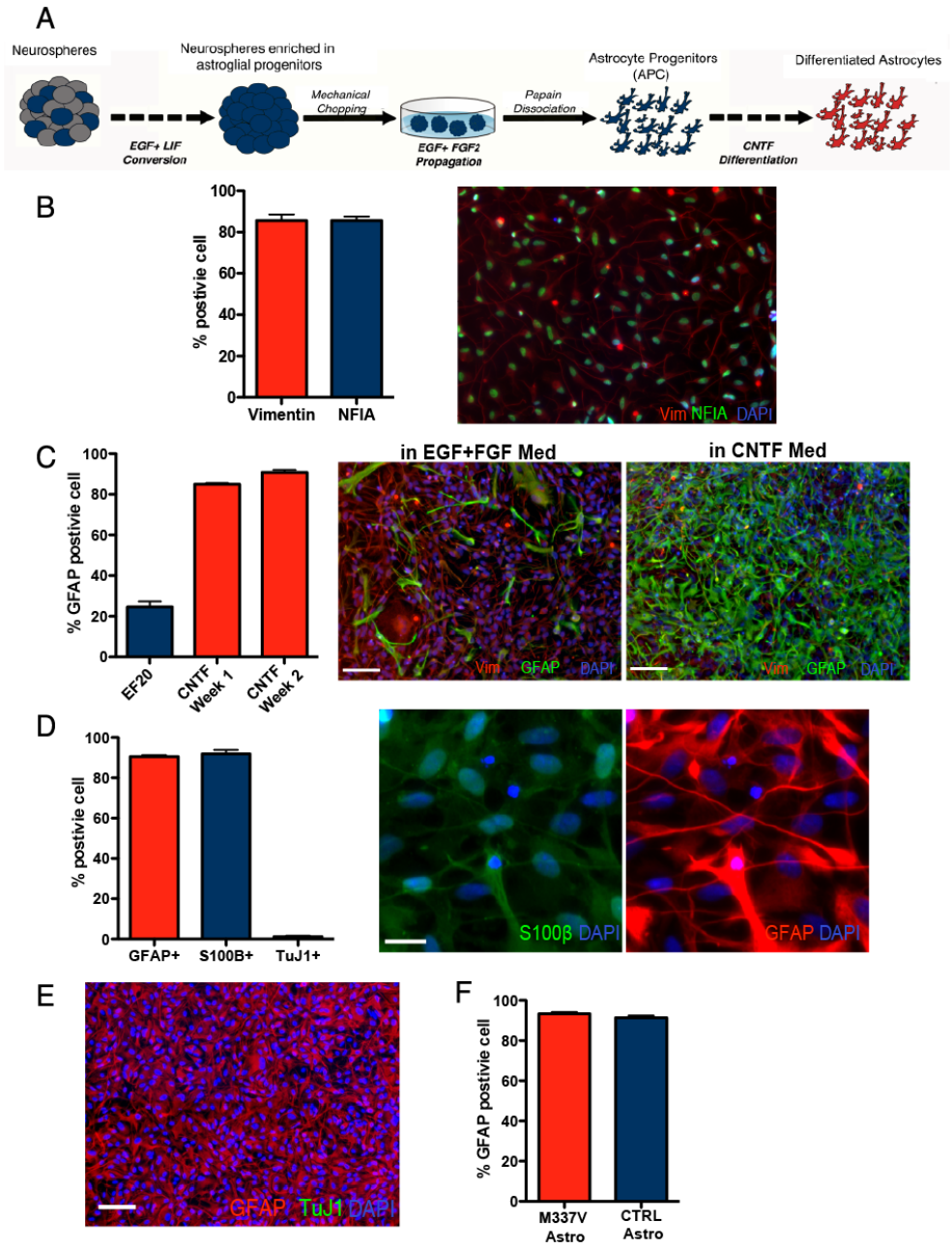
A
Neurospheres
Neurospheres enriched in astroglial progenitors
Mechanical Chopping
Astrocyte Progenitors (APC)
Differentiated Astrocytes
EGF+ LIF Conversion
EGF+ FGF2 Propagation
Papain Dissociation
CNTF Differentiation
B
% postivie cell
Vimentin
NFIA
Vim NFIA DAPI
C
% GFAP postivie cell
EF20
CNTF Week 1
CNTF Week 2
in EGF+FGF Med
in CNTF Med
Vim GFAP DAPI
D
% postivie cell
GFAP+
S100B+
TuJ1+
S100β DAPI
GFAP DAPI
E
GFAP TuJ1 DAPI
F
% GFAP postivie cell
M337V Astro
CTRL Astro

3.3.3) Functional Characterization of iPSC-derived Astrocytes

In order to successfully model the astroglial component of TDP-43 fALS, it is of utmost importance that the cells generated to perform the modelling experiments not only present an expression profile compatible with *bona fide* astrocytes, but they also an appropriate functional profile. We decided to test our GFAP+/S100β+ cells for three distinct functional properties:

- Ability to uptake L-Glutamate
- Ability to promote Synapses formation
- Ability to propagate Calcium Waves

Glutamate Uptake Assay:

The Glutamate uptake assay is based on measuring the concentration of a known solution of L-glutamate added to the culture medium in which the astrocytes are cultured, repeating the measurements at regular intervals (**Fig. 12A**). The detection system used is an enzymatic reaction that couples the interaction between L-glutamic acid and NADP to produce NADPH, which is specifically recognized by a fluorescent NADPH sensor and recycled back to NADP. A red florescence signal proportional to the amount NADPH produced is generated during the reaction and measured with an automated plate reader.

We first tested whether the differentiated astrocytes expressed members the metabotropic glutamate transporters (EAAT) family. Differentiated astrocytes derived from both genetic backgrounds were positive for the metabotropic glutamate transporter EAAT1 (**Fig. 12B**).

Moreover, the astrocytes generated through the optimized protocol were able to uptake L-Glutamate from the medium in a time-dependent fashion (**Fig. 12C**). L-Glutamate uptake was blocked by the glutamate transporter inhibitor L-trans-pyrrolidine-2,4-dicarboxylic acid (PDC) or by removing sodium from the medium, consistent with the action of EAAT1.

Interestingly no significant difference was detected in the l-glutamate clearance rate between M337V and CTRL iPSC-derived astrocytes (**Fig. 12**

D , CTRL 0.447µM/min ± 0.4 SEM; M337V 0.428µM/min ± 0.7 SEM) or in the total amount of L-glutamate cleared from the medium after the experiment with or without EAAT-inhibition (**Fig.12E**).

Taken together these results suggests that the astrocytes generated from either mutant or wild-type iPSC lines with this novel protocol display the ability to successfully clear excesses of excitatory amino acids from the culture. Implications are that the presence of the M337V mutation does not seem to have a detrimental effect on this particular astrocyte function, or at least an effect that could be measured under the present experimental conditions.

Figure 12: Functional characterization of iPSC-derived astrocytes I (Glutamate Uptake). (A) Schematic representation of L-glutamate uptake assay on iPSC-derived astrocytes. (B) Representative field of immunolabelling for glutamate transporter EAAT-1 and GFAP in differentiated iPSC-derived astrocytes cultures (panels represent the same field, scale bar = 100 μm). (C) L-Glutamate uptake assay on iPSC-derived astrocytes: iPSC-derived astrocytes cleared L-glutamate in a time-dependent fashion (*** for $p<0.01$, 1-way ANOVA). The uptake was abolished by either the absence of sodium or the presence of 2 mM PDC [both negative controls were run for 120 min]. (D) M337V iPSC-derived astrocytes did not show a significant difference in glutamate clearance rate, compared to control astrocytes (1-way ANOVA, $p>0.05$ for all times considered). (E) Glutamate uptake fold increase: M337V and CTRL astrocytes are able to clear over 75% of L-glutamate from the medium in 120 min, and uptake is inhibited equally by PDC. No significant difference was observed between the groups.

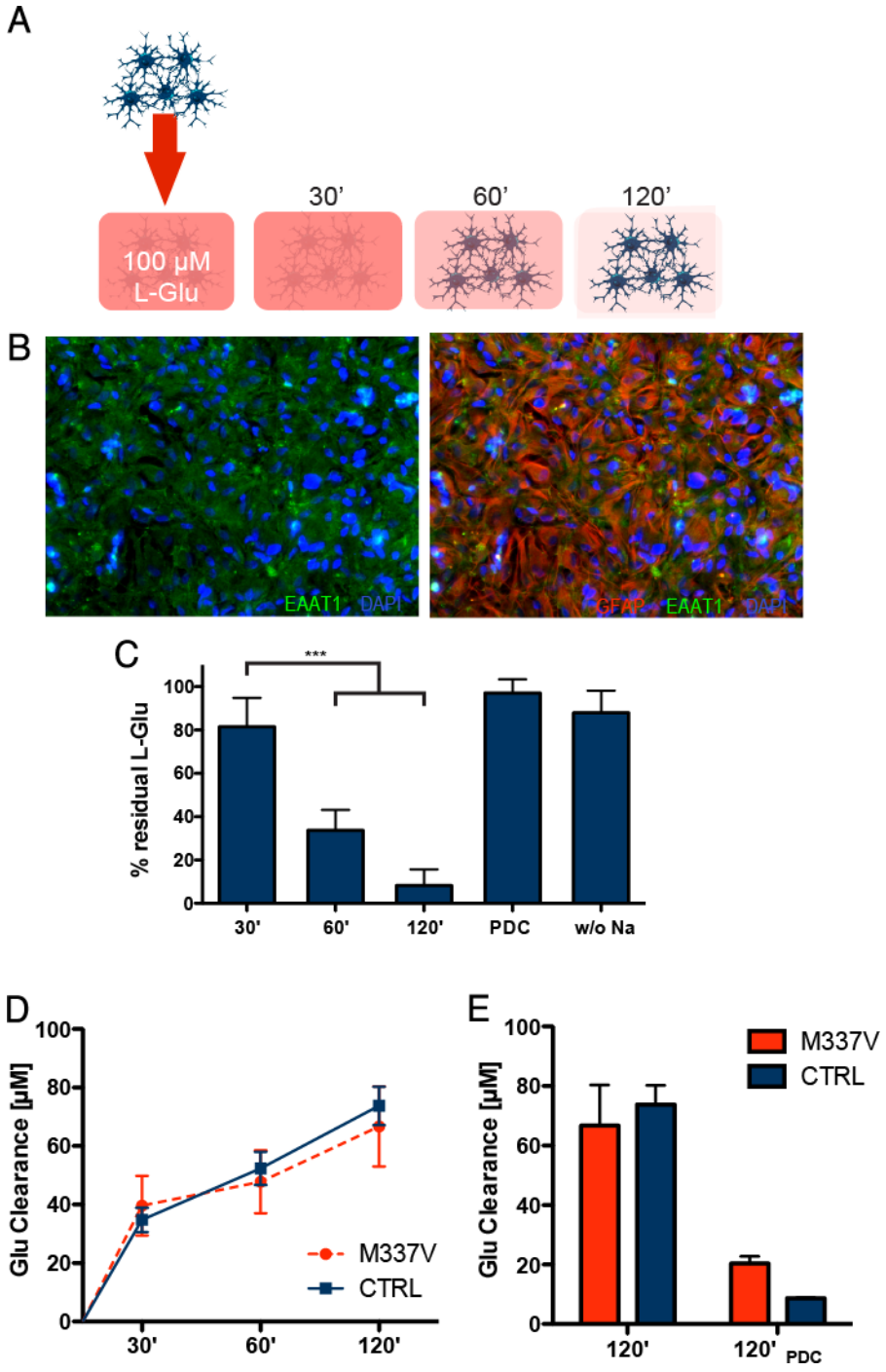
A
100 µM
L-Glu
30'
60'
120'
B
EAAT1
DAPI
GFAP
EAAT1
DAPI
C
***
% residual L-Glu
100
80
60
40
20
0
30'
60'
120'
PDC
w/o Na
D
Glu Clearance [µM]
100
80
60
40
20
0
30'
60'
120'
M337V
CTRL
E
Glu Clearance [µM]
100
80
60
40
20
0
120'
120' PDC
M337V
CTRL

Synaptogenesis Assay:

To measure the ability of the iPSC-derived astrocytes to promote the formation of synapses, we devised a simple assay on coculturing differentiating neurons on a monolayer of astrocytes for three weeks and quantifying the number of vesicle positive for synaptic components in the neurites of the patterned neurons **(Fig. 13A).**

An initial test, modelled on the data presented by Krencik and colleagues [124], was performed using neurons derived from hESC-derived (H9) adherent neural progenitors patterned to obtain a ventral-spinal cord identity [120]. At first the experiment was focused on confirming that iPSC-derived astrocytes behaved similarly to hESC-derived astrocytes in their ability to promote synaptic puncta formation, the differentiating neurons were plated either in isolation or in coculture with H9 astrocytes and control iPSC-derived astrocytes. After three weeks the cultures were analysed by immunostaining for the pre-synaptic vesicle marker Synapsin I [SYN] **(Fig. 13B)**, and the average number of SYN+ puncta per neurite was quantified. Results show that both hESC- and iPSC-derived were equally able to upregulate by 2-fold the number of synaptic puncta compared to isolated neuronal cultures (Neurons 1.00 ± 0.08 SEM, Coculture hESC 2.48 ± 0.36 SEM, Coculture WT 2.15 ± 0.11)**(Fig. 13C).** Moreover, in a separate replicate of this experiment it was possible to prove that M337V iPSC-derived astrocytes performed similarly to control astrocytes in this particular assay **(Fig. 13D)**.

These initial experiments provide evidence that the ability to promote synapses formation does not seem to be impaired by the M337V mutation in astrocytes. To be able to draw a definitive conclusion on the synaptogenesis ability of the iPSC-derived astrocytes it was necessary to measure not only their ability to promote the formation of synaptic puncta [defined by immunostaining for a pre-synaptic markers, such as SYN] but also the ability to promote the formation of mature synapses, defined as co-localisation of pre- and post-synaptic markers in the cocultured neurons.

For this reason astrocytes from either control or mutant iPSC lines were cocultured with differentiating control iPSC-derived ventral-spinal cord

patterned neurons for a period of three weeks. Cultures where then stained with antibodies against the presynaptic protein Synaptophysin I (PSY) and the post-synaptic protein PSD-95, in order to quantify the number of mature synapses in coculture conditions compared with the same neurons plated in isolation **(Fig. 13E)**. Our results showed that mutant astrocytes promoted the formation of PSY+/PSD-95+ mature synapses similarly to control astrocytes **(Fig. 13F)**. Moreover, replicates of the synaptogenesis assay performed using equivalent neurons derived from the M337V iPSC lines revealed that mutant astrocytes perform similarly to control in promoting formation of synapses, regardless of the genotype of the cocultured neurons **(Fig. 13G).**

In conclusion, the results presented in this section suggest that the presence of the M337V mutation in astrocytes does not affect negatively their ability to promote the formation of synaptic puncta and mature synapses in cocultured neurons.

Figure 13: Functional characterization of iPSC-derived astrocytes I (Synaptogenesis). (A) Schematic representation of Synaptogenesis assay on iPSC-derived astrocytes. (B) Representative field of immunolabelling for GFAP and Synapsin I in cocultures between iPSC-derived astrocytes cultures and differentiating patterned neurons (panel on top represent isolated neuronal, cultures, panel at the bottom represent neurons cocultured with astrocytes). (C) iPSC-derived astrocytes presented a behaviour comparable to hESC (H9) derived astrocytes, and significantly promoted formation of synaptic puncta [Neurons 1.00 ± 0.08 SEM, Coculture hESC 2.48 ± 0.36 SEM, Coculture WT 2.15 ± 0.11; *** $p<0.01$, 1-way ANOVA]. The increase in synaptogenesis was measured by scoring the average number of SYN+ puncta in 30-µm neurite segments. (D) Both genotypes of iPSC-derived astrocytes were equally able to promote formation of synaptic puncta (quantification as described in C) [Coculture M337V 1.91 ± 0.08 SEM; Coculture WT 2.134 ± 0.12 SEM; Neurons 1.000 ± 0.09 SEM]. (E) Representative immunofluorescence panels from synaptogenesis assay; image shows representative neurite segment used for analysis, stained with TuJ1 (blue), PSY (red) and PSD-95 (green), scale bar=15 µm. (F) iPSC-derived astrocytes significantly promoted formation of mature synapses when cocultured with differentiating neurons (*** $p<0.01$, 1-way ANOVA). The increase in synaptogenesis was measured by scoring the number of PSY+/PSD-95+ puncta in 30-µm neurite segments. [Coculture M337V 2.351 ±0.17 SEM; Coculture WT 2.595 ±0.12 SEM; Neurons 1.000 ± 0.08 SEM]. No significant difference was observed in the behaviour of M337V or CTRL iPSC-derived astrocytes. (G) Synaptogenesis assay with M337V or WT patterned neurons revealed that astrocyte promotion of synapse formation was independent from the genotype of cocultured neurons, and that M337V astrocytes do not exert a negative effect on synaptic formation, even to mutant neurons. [M337V Neurons on WT Astro 0.897 ±0.04 SEM; M337V Neurons on M337V Astro 0.980 ±0.03 SEM; WT Neurons on WT Astro 0.996±0.01 SEM; WT Neurons on M337V Astro 1.007 ±0.02 SEM].

Data presented in this figure represent the average of three independent experiments, each with two clones of M337V (M337V-1 & M337V-2) iPSC and two independent CTRL lines (CTRL-1 & CTRL -2); data from different lines were pooled for graphical presentation.

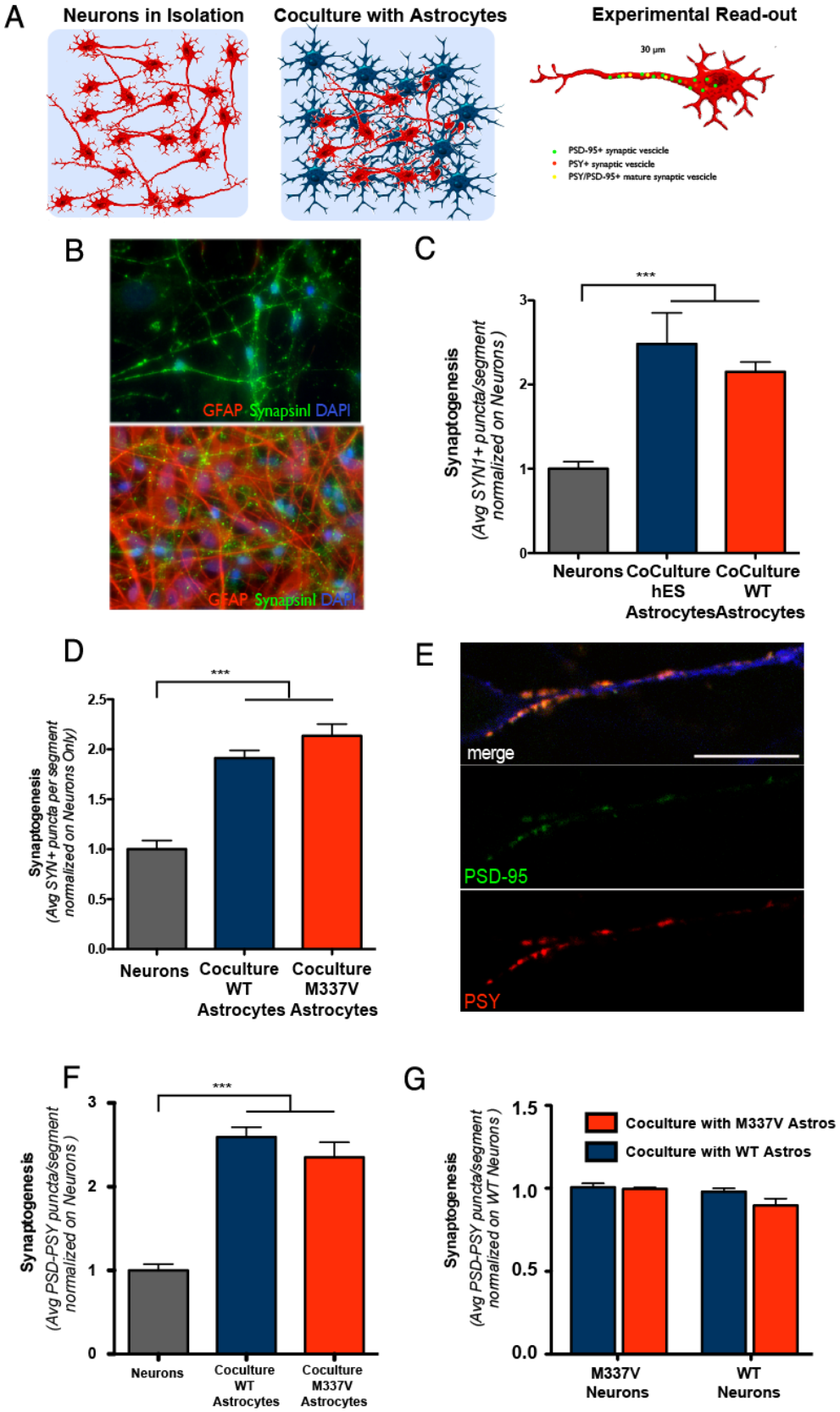
A
Neurons in Isolation
Coculture with Astrocytes
Experimental Read-out
30 µm
PSD-95+ synaptic vesicle
PSY+ synaptic vesicle
PSY/PSD-95+ mature synaptic vesicle
B
GFAP Synapsinl DAPI
GFAP Synapsinl DAPI
C
***
Synaptogenesis
(Avg SYN1+ puncta/segment normalized on Neurons)
Neurons
CoCulture hES Astrocytes
CoCulture WT Astrocytes
D
***
Synaptogenesis
(Avg SYN+ puncta per segment normalized on Neurons Only)
Neurons
Coculture WT Astrocytes
Coculture M337V Astrocytes
E
merge
PSD-95
PSY
F
***
Synaptogenesis
(Avg PSD-PSY puncta/segment normalized on Neurons)
Neurons
Coculture WT Astrocytes
Coculture M337V Astrocytes
G
Coculture with M337V Astros
Coculture with WT Astros
Synaptogenesis
(Avg PSD-PSY puncta/segment normalized on WT Neurons)
M337V Neurons
WT Neurons

Calcium Waves Assay:

Astrocytes are able to respond to a variety of stimuli (mechanical, electrical and chemical) by increasing the free intracellular concentration of calcium[201,202]. This rapid increase in calcium can rapidly spread from one stimulated cell to the neighbouring astrocytes, in a directional fashion, thus creating a "wave" of synchronous responses.

It is possible to visualize the uncomplexed cytoplasmic calcium ions in astrocytes by using a fluorescent dye that reacts to their presence. The Fura class dyes in particular[203], are a family of polyamino-carboxylic acids with can be used as ratiometric fluorescent dyes, thanks to their ability to bind uncomplexed calcium. Moreover, it is possible to convert Fura compounds to acetoxymethyl esters (AM) versions, to grant them the ability to pass the cell membrane, which greatly simplify the experimental design of this assay. For these experiments a commercially available membrane permeable dye, Fura-4AM was used. Astrocytes for these calcium waves tests were differentiated in CNTF for 14 days and then plated on matrigel-coated 6well plates. Before the experiment, astrocytes cultures were loaded with Fura-4AM in a HBSS solution.

The first test was focused on the ability of the iPSC-derived astrocytes to propagate intercellular calcium waves upon mechanical stimulation. To generate obtain a focal stimulation a glass micro-beads with a diameter of 200μm was dropped on the astrocytes within the field of illumination **(Fig. 14A).** Both genotypes astrocytes exhibited the potential to propagate calcium waves from the area of stimulation to neighbouring cells in a time dependent fashion (**Fig. 14B, Supplementary Video 1**).

One of the mechanism that astrocytes use to propagate the intracellular increase of calcium is the release of ATP, which in turn activates IP3 pathway in neighbouring cells allowing them to both release calcium from intracellular depots and release ATP in the extracellular space to support the spread of calcium response [204,205]. For this reasons it was also necessary to test whether iPSC-derived astrocytes were able to respond predictably to ATP focal application. For this reason the experiment previously described

was repeated, substituting the mechanical stimulus with the local application of a concentrated ATP solution (Fig. 14C). Again, calcium waves were elicited upon ATP stimulation (Fig. 14D, **Supplementary Video 2**), in both M337V and Control iPSC-derived cultures. This ATP-evoked increase in cytosolic calcium was abolished by application of 2-APB, an inhibitor of IP3- dependent calcium release [205](Fig. 14E, **Supplementary Video 3**).

Figure 14: Functional characterization of iPSC-derived astrocytes I (Calcium Waves). (A) Schematic representation of Calcium Waves mechanical stimulation on iPSC-derived astrocytes. (B) Representative time-lapse images (extracted from Supplementary Video 1) showing that iPSC-derived astrocytes are able to generate intercellular calcium waves upon mechanical stimulation. Annotations represent time in seconds from stimulus application. (C) Schematic representation of Calcium Waves ATP stimulation on iPSC-derived astrocytes. (D) Local application of ATP was able to promote increase in intracellular calcium in iPSC-derived astrocytes, consistently whit what described for calcium waves in vivo. (E) ATP-evoked increase in calcium concentration was abolished in the presence of 2-APB. Bright-field image demonstrated that astrocytes used in this particular test were healthy.

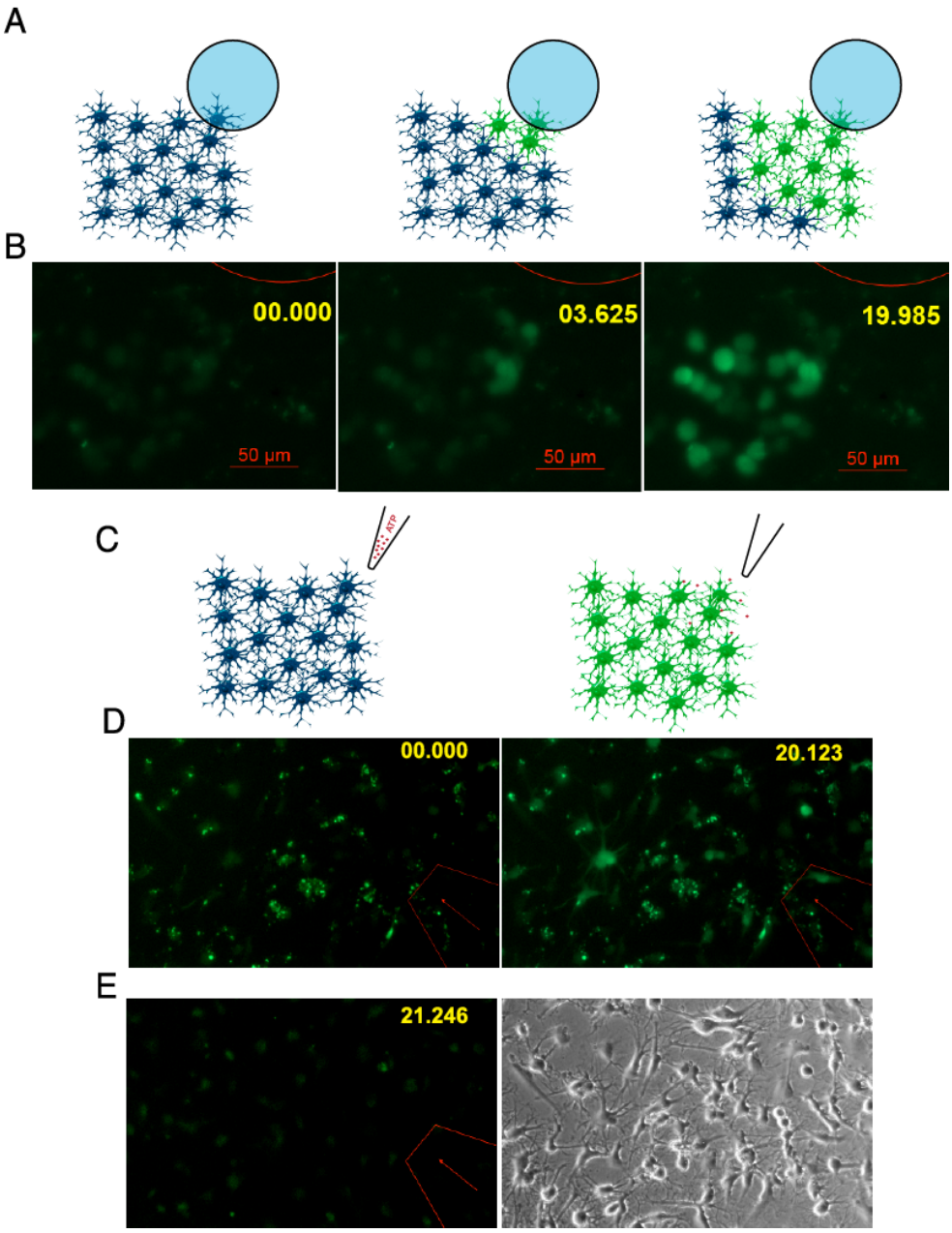
A
B
00.000
50 µm
03.625
50 µm
19.985
50 µm
C
ATP
D
00.000
20.123
E
21.246

3.4) Conclusions

The first and most important step of an *in vitro* disease-modelling project is the ability to generate reliably the appropriate cellular types.

The results presented in this chapter show by transporting developmental biology observation in vitro it has been possible to optimise two protocols that give rise reliably and efficiently to motor neurones and astrocytes starting from patient-derived iPSC lines. Moreover we have been able to functionally characterise the differentiated cells and prove that they present a functional profile comparable to what is described for their *in vivo* counterparts.

Interestingly no significant difference was observed in the functional profile of either motor neurones or astrocytes derived from the M337V iPSC lines compared to Control iPSC, indicating that the presence of the mutation does not *per se* affect negatively the generation of functional neurones or glia.

Chapter 4: Phenotype Analysis in isolated cultures

As described in the introduction chapters, TDP-43 is the major component of the ubiquitinated protein aggregates found in ALS and FTLD pathological human samples. During the development of these pathologies, TDP-43 presents specific changes in localisation and biochemical profile, that constitute the typical phenotype described for TDP-proteinopathies[206]. In particular TDP-43 localisation is drastically changed during pathology. While normally this protein resides mainly in the nucleus, shuttling transitorily to the cytoplasm to mediate aspects of RNA metabolism[15,28], in pathological samples TDP-43 is accumulated in the cytoplasm, sometimes with complete depletion of the nuclear TDP pool in affected neurons. Also, TDP-43 aggregates are observable during the pathology in the cytoplasm.
From a biochemical point of view, TDP-43 during the disease frequently accumulates in the detergent resistant fraction, presenting also cleavage into 35 and 25 kDa fragments and phosphorylation[61,206]. These changes in TDP-43 biochemistry and localisation constitute a "pathological signature" of TDP proteinopathies.

After the protocols to generate functional MNs and astrocytes from iPSC lines, presented in Chapter3, were tested and optimised, we proceeded to analyse the localisation and biochemical signature of TDP-43 in the differentiated cells in isolation, in order to determine whether the iPSC-based model reproduces the described disease phenotype.

4.1) Expression and Biochemistry of TDP-43 in iPSC-derived Motor Neurones

Before analysing the biochemical profile of TDP-43 in differentiated MN cultures, it was necessary to determine whether the expression levels of its mRNA, *TARDBP gene*, were significantly modified in the M337V genetic background.

For this reason the gene expression levels of TDP-43 in the MN cultures was analysed. Quantitative RT-PCR on RNA extracted from mature cultures revealed that expression levels of *TARDBP*, or *HDAC6* (a transcriptional target of TDP-43 itself [85]) do not vary significantly between the M337V and Control iPSC-derived MNs **(Fig. 15 A-B**, *performed by Dr. B. Bilican***)**. Furthermore, even though there was some clonal variation between M337V-1 and M337V-2, there was not a detectable significant difference on average in the expression levels of MNs specific transcripts such as *HB9* and *ChAT* **(Fig. 15 C-D**, *performed by Dr. B. Bilican***)**.

Having established that TDP-43 expression does not significantly vary between M337V and Control MNs, we next analysed the biochemical profile of this protein in differentiated cultures. Immunoblot analysis on samples extracted from $ChAT^+$ MN cultures revealed that M337V iPSC derived cultures appear to present an accumulation of TDP-43 full length in both the soluble **(Fig. 15 E**, *performed by Dr. B. Bilican***)** and detergent resistant **(Fig. 15 F**, *performed by Dr. B. Bilican***)** fractions. We then quantified the difference between the two clones of the mutant line and Control-1 by the Semi-quantitative densitometric analysis on the immunoblots bands, revealing a three to four-fold increase in soluble TDP-43 and a 1.5 fold increase in detergent-resistant TDP-43 **(Fig. 15 G-H**, *performed by Dr. B. Bilican***)**.

Figure 15: Expression and Biochemistry of TDP-43 in iPSC-derived Motor Neurones. (A-D) qRT-PCR analysis of TARDBP, histone deacetylase 6 (HDAC6), HB9, and ChAT expression in MN-containing neuronal cultures (n = 3). (E-F) Western blot analysis of soluble (E) and detergent resistant (F) TDP-43 in M337V-1, M337V-2, and Cont-2 MN-containing cultures. Three independent extractions are shown for each cell line. β3-Tubulin was the loading control for soluble fractions (E), and Ponceau S reversible membrane staining was the loading control for detergent-resistant fractions (F). (G) Semi-quantitative analyses of band signal intensity for soluble TDP-43 Immunoblot analysis. Levels of soluble TDP-43 normalized to β3-tubulin, Cont-2 set to 1: M337V-1 = 3.67 ± 0.58; M337V-2 = 4.54 ± 0.01; Cont-2 = 1.0 ± 0.24. M337V-1 vs. M337V-2, n.s.; M337V-1 vs. Cont-2, $P = 0.013$; M337V-2 vs. Cont-2, $P < 0.001$, n = 3 in- dependent extractions. (H) Semi-quantitative analyses of band signal intensity for detergent resistant TDP-43 immunoblot analysis. Levels of detergent-resistant TDP-43 normalized to Ponceau S, Cont-2 set to 1: M337V-1 = 1.52 ± 0.08; M337V-2= 1.67 ± 0.10; Cont-2 = 1.0 ± 0.16. M337V-1 vs. M337V-2, not significant; M337V-1 vs. Cont- 2, $P = 0.04$; M337V-2 vs. Cont-2, $P < 0.03$, n = 3 independent extractions

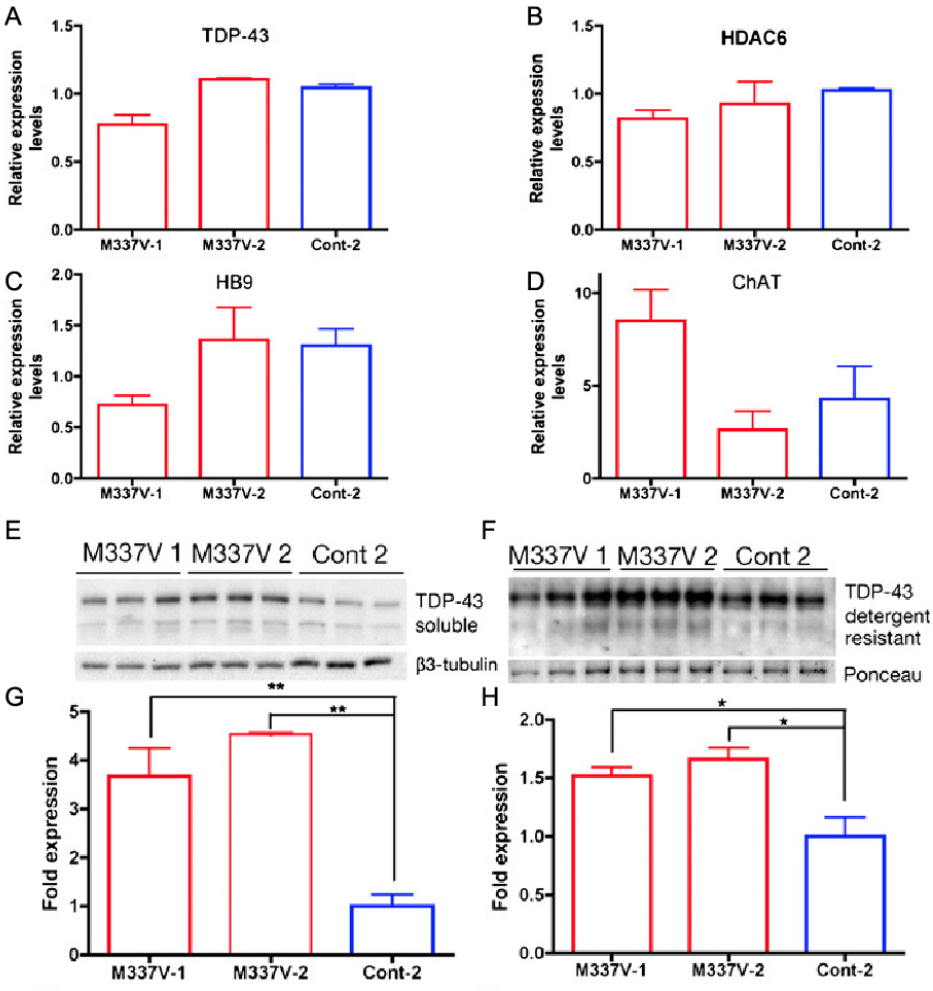
A
TDP-43
Relative expression levels
1.5
1.0
0.5
0.0
M337V-1
M337V-2
Cont-2
B
HDAC6
Relative expression levels
C
HB9
2.0
D
ChAT
10
5
E
M337V 1 M337V 2 Cont 2
TDP-43 soluble
β3-tubulin
F
M337V 1 M337V 2 Cont 2
TDP-43 detergent resistant
Ponceau
G
Fold expression
**
H
Fold expression
*

4.2) Localisation of TDP-43 in iPSC-derived Motor Neurones

In order to analyse the behaviour and localisation of TDP-43 in differentiated iPSC-derived MNs several different commercially available antibodies directed against different epitopes of TDP-43 were screened. As described before, the normal TDP-43 localisation in neurons is predominantly nuclear, with some discrete small foci of accumulation in the cytoplasm and -especially- in neurites, in response to neuronal activity[40]. A panel of 4 antibodies with different specificity for different forms of TDP-43 (nominally the full length 43 kDa form, the 25 and 35 kDa degradation cleavage products) was optimised, based on commercially available antibodies used in previous publications. The immunostainings were performed on fixed MN cultures at the end of their maturation phase, after the expression of SMI-32 and Chat. All antibodies tested were able to detect TDP-43 in fixed cultures, although with deferent degree of signal strength and specificity **(Fig. 16 A-D)**. After these batch testing phase, a Rabbit polyclonal antibody raised against the full-length protein was selected, due to its intense signal in the immunofluorescence set up used, specificity of the recognition to the antigen and practicality of use in double immunostaining set ups with the antibodies tested during the optimization of the protocols. Using this antibody we did not observe any abnormality in the localisation of TDP-43 in MNs generated from the M337V iPSC line **(Fig. 16E)** at the end of the maturation protocol compared with Control iPSC-derived MNs.

Interestingly, we observed that strongly SMI-32 positive cells in the MN culture seemed to have an increased amount of nuclear TDP-43 compared to SMI-32 negative neurons **(Fig. 16F).** Densitometric quantification of TDP-43 immunostaining revealed that SMI-32^{+} presents an average 20% increase in the amount of nuclear TDP-43 (SMI-32^{+} 1.236 ± 0.07, SMI-32^{-} 1.032 ± 0.05, $p<0,05$) **(Fig. 16G)**. Despite this difference, we were unable to detect any increase in the nuclear TDP-43 densitometry comparing M337V and Control SMI-32^{+} cells **(Fig. 16H)**.

Figure 16: Localisation of TDP-43 in iPSC-derived Motor Neurones. (A-D) Optimisation of four different TDP-43 antibodies in mature Control iPSC-derived MNs (identified by Chat and SMI32 co-positivity): A' and B') two polyclonal antibodies target to the n-terminal portion of the protein; C') a polyclonal antibody targeted to the c-terminal portion of the protein; D') a monoclonal antibody generated by immunization against the full length recombinant TDP-43. All antibodies show a predominantly nuclear localization in neurons, with absence of discrete aggregates of large size. (E) TDP-43 staining on M37V iPSC-derived MNs does not reveal substantial mislocalisation or aggregation (F) Immunofluorescence analysis of nuclear TDP-43 in SMI-32+ and SM-I32− cells. (G) Densitometric quantification of nuclear TDP-43 in SMI-32+ and SMI-32- neurons [$p<0,001$ n=30 cells per group over 3 independent fields]. (H) Densitometric analysis of nuclear TDP-43 in SMI-32+ and SMI-32− cells. No significant difference between M337V and control groups ($n > 20$ cells)

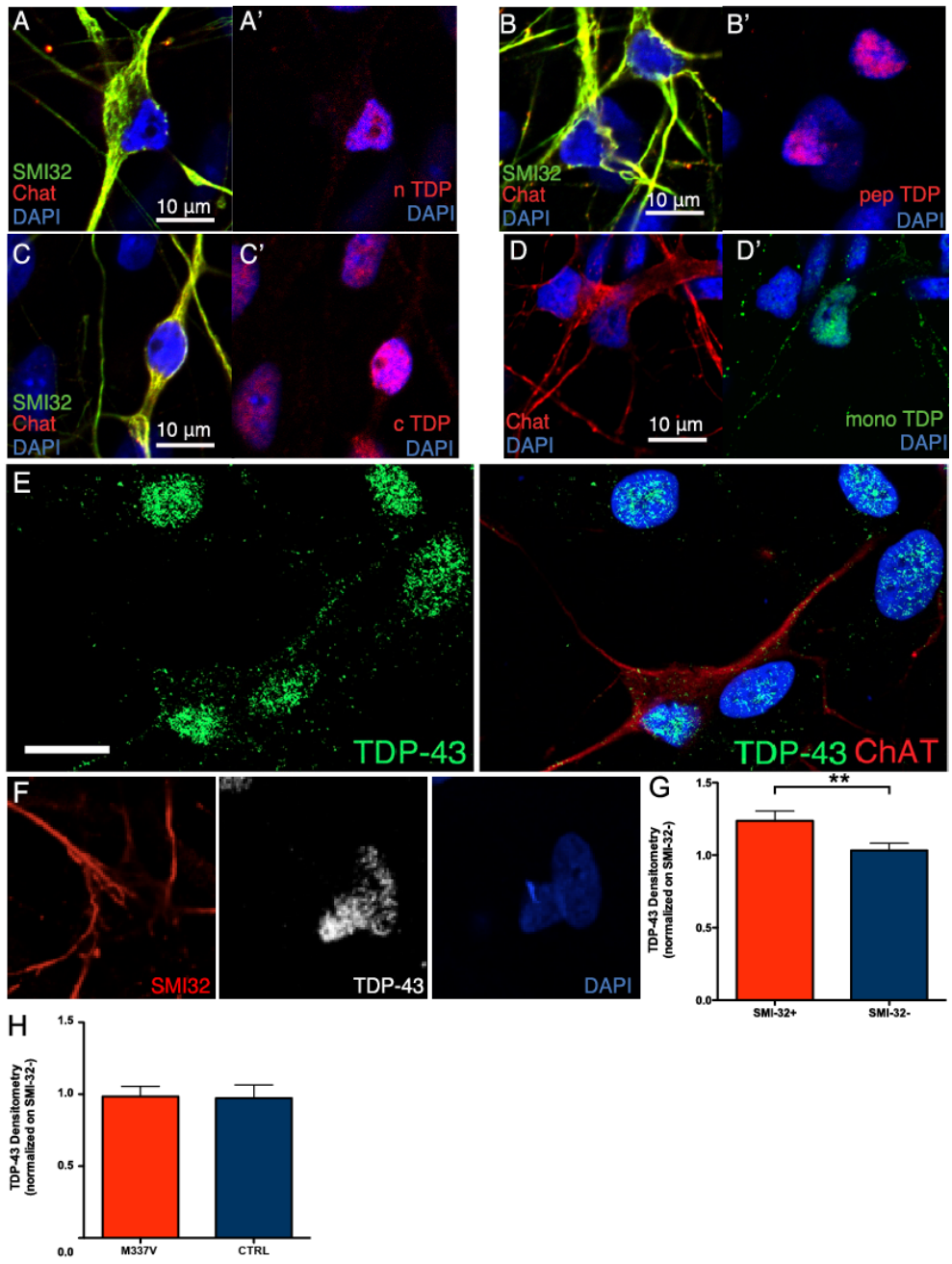
A
SMI32
Chat
DAPI
10 µm
A'
n TDP
DAPI
B
SMI32
Chat
DAPI
10 µm
B'
pep TDP
DAPI
C
SMI32
Chat
DAPI
10 µm
C'
c TDP
DAPI
D
Chat
DAPI
10 µm
D'
mono TDP
DAPI
E
TDP-43
TDP-43 ChAT
F
SMI32
TDP-43
DAPI
G
**
TDP-43 Densitometry
(normalized on SMI-32-)
1.5
1.0
0.5
0.0
SMI-32+
SMI-32-
H
TDP-43 Densitometry
(normalized on SMI-32-)
1.5
1.0
0.5
0.0
M337V
CTRL

4.3) Expression and Biochemistry of TDP-43 in iPSC-Astrocytes

As the M337V iPSC-derived MNs demonstrated a tendency to accumulate TDP-43 in both soluble and detergent resistant fractions without a corresponding increase in *TARDBP* mRNA expression, it was of particular interest to clarify whether the astrocytes displayed the same biochemical phenotype.

Using quantitative RT-PCR analysis we determined that mutation-carrying astrocytes do not present an increased expression of TARDBP mRNA, nor they display any significant difference in the expression of TDP-43 downstream target HDAC6 **(Fig. 17A, top panels** *performed by Dr. B. Bilican***)**. Moreover, as for the MNs expression analysis we also wanted to check that generally the expression profile was not altered by the M337V mutation. For this reason we performed quantitative RT-PCR analysis on two astrocyte specific transcripts, S100β and GFAP, but we could not detect any difference in their expression levels comparing M337V and Control iPSC-derived astrocytes **(Fig. 17A, bottom panels** *performed by Dr. B. Bilican***)**.

We then proceeded to analyse the TDP-43 protein levels in iPSC-derived astrocytes; immunoblot analysis revealed that mutation carrying astroglial cultures present a increase in soluble TDP-43 levels, without the corresponding increase in detergent resistant levels observed in the MNs **(Fig. 17B** *performed by Dr. B. Bilican***)**. This increase in soluble TDP-43 was quantified to be 2-fold compared to control astrocytes, with semi-quantitative densitometric analysis of three independent protein extractions **(Fig. 17C** *performed by Dr. B. Bilican***)**.

Figure 17: Expression and Biochemistry of TDP-43 in iPSC-Astrocytes. (A) qRT-PCR expression analysis of iPSC-derived astrocytes shows no significant difference [$p>0.05$ for all pairs, unpaired t-test] in mRNA levels of TARDBP, HDAC6, S100β or GFAP; results are presented as expression fold increase normalized to M337V-1. (B) Representative western blot from soluble and detergent resistant TDP-43 analysis of M337V-1, M337V-2, and CTRL-1 astrocytes. (C) Semiquantitative analyses of soluble TDP-43 band signal intensity was accomplished using ImageJ on three independent extractions [M337V-1 1.993 ±0.38 SEM, M337V-2 1.917± 0.37 SEM, CTRL-1 1.107 ±0.26 SEM, $p=0.003$, repeated measures ANOVA).

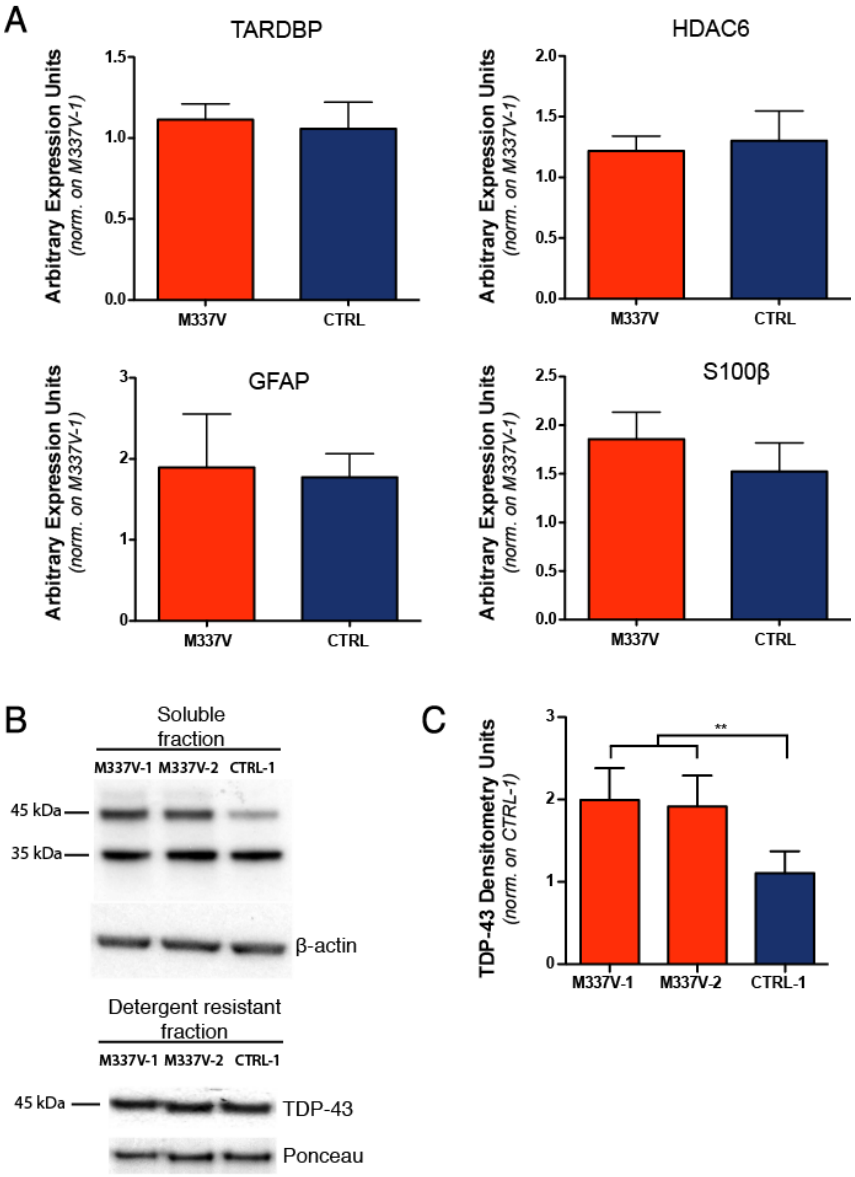
A
TARDBP
HDAC6
GFAP
S100β
Arbitrary Expression Units
(norm. on M337V-1)
M337V
CTRL
B
Soluble fraction
M337V-1 M337V-2 CTRL-1
45 kDa
35 kDa
β-actin
Detergent resistant fraction
M337V-1 M337V-2 CTRL-1
45 kDa
TDP-43
Ponceau
C
TDP-43 Densitometry Units
(norm. on CTRL-1)
**
M337V-1
M337V-2
CTRL-1

4.4) Localisation of TDP-43 in iPSC-Astrocytes

The next step in the project was to study the localisation of TDP-43 in iPSC-derived astrocytes. For this purpose, sub-confluent astrocytes monolayer cultures differentiated from APCs in CNTF for 14 days were immuno-labelled with antibodies against GFAP and TDP-43 and then imaged with a confocal microscope. High-resolution images were then used to perform densitometric analysis with ImageJ. In order to be able to determine any changes in TDP-43 localisation, single astrocytes within the fields of view were manually analysed by first determining and delimitating the nuclear and cytoplasmic regions of each cell using DAPI and FAP respectively, and then measuring the density of TDP-43 fluorescent signal from these regions **(Fig. 18A)**. The densitometric analysis was performed on 25 astrocytes per field, using a total of 12 different fields for every iPSC lines, over four different biological replicates. This quantification revealed that astrocytes derived from the mutant iPSC line present a 2-fold increase in the amount of cytoplasmic TDP-43 compared to control astrocytes **(Fig. 18 B-D)**. Interestingly nuclear TDP-43 levels appear to remain unchanged between M337V control iPSC-derived astrocytes.

Figure 18: Localisation of TDP-43 in iPSC-Astrocytes. (A) Example of region-based densitometric TDP-43 analysis in astrocytes. Nuclear region was manually drawn based on DAPI, cytoplasmic region was manually drawn based on GFAP. (B-C) Representative confocal images of TDP-43/GFAP immunolabelling used for densitometric analysis. (D) Densitometric quantification of TDP-43 localization by confocal microscopy showing a significant increase of cytoplasmic TDP-43 in M337V astrocytes. [M337V nuclear 1.088 ± 0.091 SEM, cytoplasmic 1.806 ± 0.127 SEM; CTRL nuclear 1.006 ± 0.049 SEM, cytoplasmic 1.009 ± 0.050 SEM. Results are presented as densitometric signal fold increase normalized to the control, n=4 independent experiments. *** for $p<0.001$].

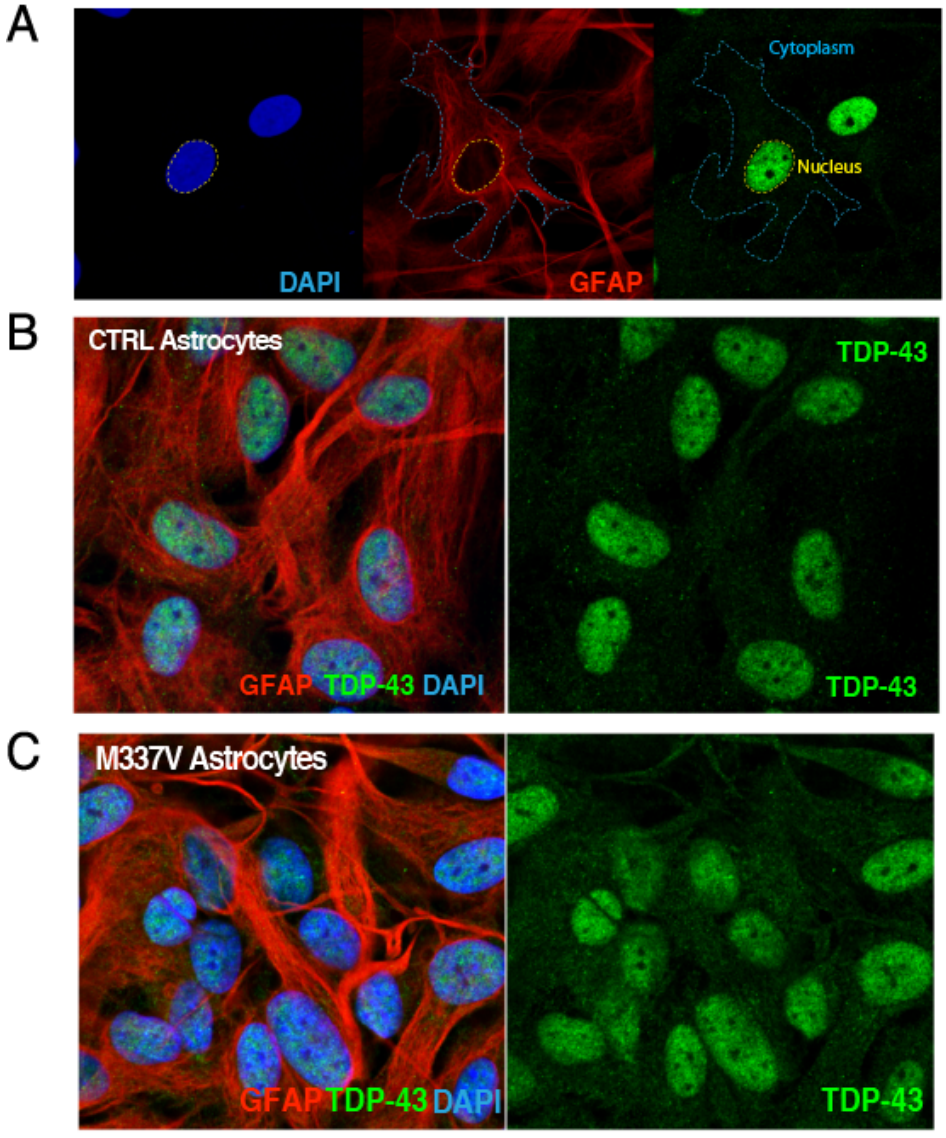
A
DAPI
GFAP
Cytoplasm
Nucleus
B
CTRL Astrocytes
GFAP TDP-43 DAPI
TDP-43
TDP-43
C
M337V Astrocytes
GFAP TDP-43 DAPI
TDP-43
D
TDP-43 Densitometry Units
(norm. on CTRL-1)
M337V
CTRL
***
2.5
2.0
1.5
1.0
0.5
0.0
Nuclear
Cytoplasmic

4.5) Ectopic TDP-43 expression in iPSC-Astrocytes

The results presented in the previous sections of this chapter indicate that the M337V TDP-43 mutation in astrocytes determines increased levels of soluble full length TDP-43, and that this accumulation of protein is mainly localised in the cytoplasm. These findings represent a strong indication of a TDP-43 phenotype in our vitro system, in particular it must be highlighted that this is the first comprehensive in vitro fALS study to look at TDP-43 in isolated patient-derived astrocytes. For this reason it is of the utmost importance to determine that the cytoplasmic accumulation of TDP-43 is really due to the presence of the M337V mutation, rather than ascribable to an *in vitro* artefact. Also, the experiments presented so far do clearly demonstrate that the accumulation observed is a direct effect of the presence of the mutation on TDP-43, or part of a secondary mechanism due to differences in the genetic background.

To clarify this point we choose to analyse exogenous TDP-43 expressed in Control-iPSC derived astrocytes, in order to eliminate any differences due to the genetic background of the iPSC lines and focus on the effect of the M337V mutation on TDP-43 localisation.

Control iPSC-derived astrocytes were first co-transfected with a plasmid encoding either WT or M337V TDP-43 fused to mApple, under the control of a constitutive promoter, and a plasmid constitutively expressing eGFP **(Fig. 19A)**. Transient transfection leads to different expression levels within the population, and in the case of TDP-43 exogenous expression this is accompanied by a diverse range of localisation within the same transfected populations. In particular, some astrocytes would present a mostly nuclear localisation of the ectopic TDP-43 **(Fig. 19A, top panel)**, while other equally fluorescent cells would display high levels of cytoplasmic ectopic TDP-43 **(Fig. 19A, bottom panel)**. The transfected populations were then analysed to determine the relative expression levels of exogenous TDP-43, in order to subdivide the population in groups. The intensity of the constitutively expressed eGFP was used as a normaliser of the densitometric measurement on the exogenous TDP-43 signal. The normalised exogenous

TDP-43 signal quantification was then used to arbitrarily divide the transfected population into 5 different expression groups (A to F) from low to high relative expression of exogenous TDP-43 **(Fig. 19B)**.

Within the different expression groups, the localization of exogenous TDP-43 was then analysed. Astrocytes with prominent nuclear localization of transfected WT or M337V TDP43-mApple were grouped and compared to astrocytes with nuclear-and-cytoplasmic or exclusively cytoplasmic fluorescence. Interestingly, these results showed a strong influence of expression levels on TDP-43 localization. Elevated expression levels were directly related to cytoplasmic mislocalisation of TDP-43 **(Fig 19C)**, as it has been previously reported[70]. However, while WT TDP-43 displayed a dynamic range of localization correlating with expression levels, M337V TDP-43 showed an inherent bias towards cytoplasmic localization **(Fig 19D)**. Notably, this effect was particularly evident when the low expression levels groups from the WT and M337Vtransfected population were compared directly **(Fig. 19E).**

These results confirm that the observed changes in localization of TDP-43 in iPSC-derived astrocytes are in fact due to the presence of the M337V mutation on TARDBP, which causes localisation bias towards the cytoplasm leading to an accumulation of the protein.

Figure 19: Ectopic TDP-43 expression in iPSC-Astrocytes. (A) Representative images of cytoplasmic and nuclear-only TDP43:mApple-transfected astrocytes showing the criteria for inclusion of astrocytes in either cytoplasmic [top panels] or nuclear [bottom panels]. (B) Stratification of TDP-43:mApple-expressing astrocytes into six groups based on their relative expression levels; groups A–F contain astrocytes with progressively increasing exogenous TDP-43 expression levels. (C) Analysis of exogenous WT TDP-43 localization on stratified relative expression groups. The localization of WT TDP-43 was significantly related to relative expression levels (Nuclear vs Cytoplasmic TDP-43: A=n.s., B=n.s., C=n.s., D=$p<0.05$, E=$p<0.01$, F=$p<0.001$). Data pooled from three independent experiments (D) Analysis of exogenous M337 TDP-43 localization on stratified relative expression groups. M337V TDP-43 remained localized mainly to the cytoplasm regardless of expression level (nuclear vs cytoplasmic TDP-43: A–F=$p<0.001$). Data pooled from three independent experiments. (E) Comparison of ectopic TDP-43 localization in astrocytes from the lowest relative expression level groups [group A in panels d and e]. At low expression levels 73.6%± 3.31 of astrocytes from the TDP43M337V:mApple group present mainly or exclusively cytoplasmic localization of the protein, compared to 44.51%%± 1.64 in the TDP43WT:mApple (*=$p<0.05$; **=$p<0.01$, 1-way ANOVA).

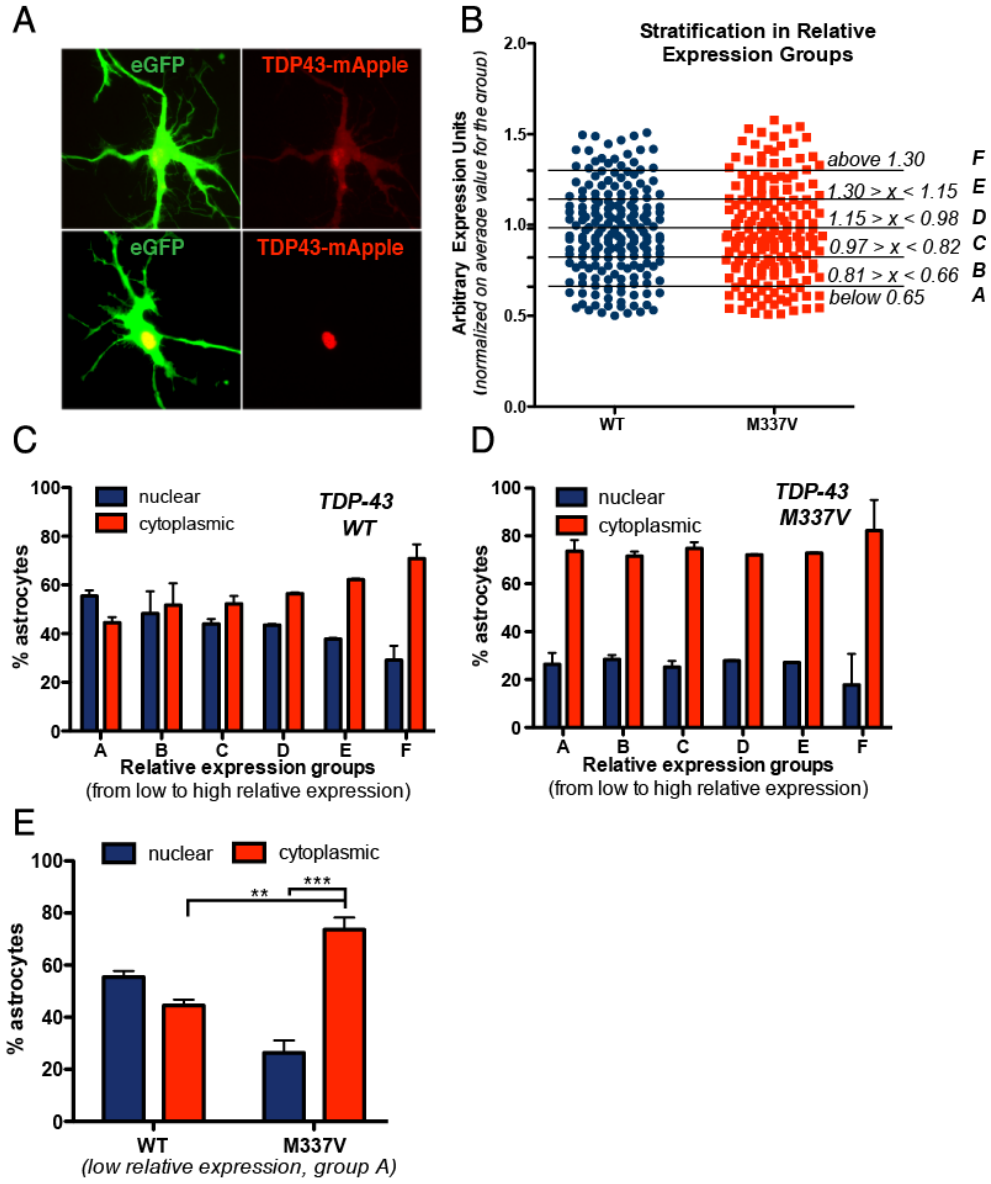
A
eGFP
TDP43-mApple
eGFP
TDP43-mApple
B
Stratification in Relative Expression Groups
Arbitrary Expression Units
(normalized on average value for the group)
2.0
1.5
1.0
0.5
0.0
above 1.30 F
1.30 > x < 1.15 E
1.15 > x < 0.98 D
0.97 > x < 0.82 C
0.81 > x < 0.66 B
below 0.65 A
WT
M337V
C
nuclear
cytoplasmic
TDP-43 WT
% astrocytes
100
80
60
40
20
0
A B C D E F
Relative expression groups
(from low to high relative expression)
D
nuclear
cytoplasmic
TDP-43 M337V
% astrocytes
100
80
60
40
20
0
A B C D E F
Relative expression groups
(from low to high relative expression)
E
nuclear
cytoplasmic
**
***
% astrocytes
100
80
60
40
20
0
WT
M337V
(low relative expression, group A)

4.6) Conclusions

TDP-43 profiling in iPSC-derived differentiated cells revealed that this platform reproduces key feature of the pathological signature described of TDP proteinopathies. In particular we were able to detect accumulation of both soluble and detergent resistant TDP-43 in mature MNs-containing cultures, despite the expression levels of *TARDBP* appear to be unchanged in the M337V iPSC-derived cultures compared to controls. Interestingly, also in astrocytes TDP-43 protein levels were increased in the mutation carrying cultures without any significant changes to the mRNA expression levels. These results suggest that the differences in protein levels observed in both neurons and glia arise from a post-translational mechanism, rather than increased abundance of the transcript. Moreover, the mutant protein does not seem to interfere with the auto-regulatory feedback mechanism proposed for TDP-43 control of mRNA levels [29,42]. Of relevance is that possible to detect a difference in the way MNs and astrocytes process the mutant protein: while in MN cultures both soluble and detergent resistant are significantly increased, in astrocytes the detergent resistant levels are unchanged. This could underline a fundamental difference in the way these cell types manage the accumulation of M337V TDP-43.

In terms of TDP-43 localisation, although biochemically M337V MN cultures present a significant difference compared to controls, we did not observed overt mislocalisation of the protein in iPSC-derived MNs. This could be due to the age of the MN cultures, as most of the evidences for accumulation and aggregation come from post-mortem sample analysis.

Interestingly however, it was possible to determine with the experiments reported in this section, that the M337V mutation causes cytoplasmic accumulation of the protein in astrocytes. Moreover, this cytoplasmic accumulation is a direct consequence of a localisation bias caused by the mutation, as the exogenous TDP-43 experiments on control astrocytes demonstrated.

Chapter 5: Survival Analysis in isolated cultures

5.1) Introduction to in vitro Survival Analysis in iPSC-derived cultures

As discussed in the previous chapters, part of the phenotype described for TDP proteinopathies, and ALS in particular, is the mislocalisation and aggregation of TDP-43 in the cytoplasm of MNs and glial cells.

Although the exact molecular mechanism responsible for this pathology is still not clear, what causes the disease's symptoms is ultimately the specific death of MNs. Also, it has been shown in several in vitro and in vivo systems that expression of mutant TDP-43 is in itself toxic to neurons[67,70,207].

For this reason, one of the most important aspects to verify in establishing a patient iPSC-derived model for ALS is whether there is a survival difference between mutation carrying and control cells.

However, in trying to determine a survival difference between iPSC-derived cultures one encounters several specific problems, mainly related to the intrinsic heterogeneity of the culture itself. In particular, one of the major problems is that the efficiency of differentiation into the particular cell type of interest (in this case MNs) is generally less than 100% (*see Results Chapter 1*), determining that the cultures analysed are always a mixture of the cell type of interests with other neuronal, glial or other unrelated cell types. For this reason, it is generally more difficult to rely on unbiased population based assays (like general LHD-release based population assays), and one need to specifically identify the cell type of interest, for example by staining several replicates for MN-specific protein HB9 and determining the exact percentage of MNs in the culture over time.

This methodology however can present an additional challenge, determined by the fact that stem cells and progenitor differentiation in vitro is not perfectly synchronized, especially when considering relatively short periods of time (i.e. weeks)[208]. In the specific example of staining several replicates of MN cultures at time 0 and two weeks later to determine $HB9^{+}$ cells

survival over time, in an unsynchronized culture MN-progenitors would be differentiating at different speed, determining "newly-born" HB9+ cells in between the beginning of the experiment and the final time-point. Therefore part of (if not all) the percentage of MNs lost to problems in cell survival during the experiment would be masked by the generation of new neurons from the asynchronous progenitors. This in turns means that only a relatively large toxic effect can be observed with such experiments. To perform survival analysis in our iPSC-derived cultures we collaborated with the Finkbeiner lab, at the Gladstone Institute in San Francisco: between 2005 and 2009 they established a technique to perform high-content screening based on a automated microscope system[209,210]. This technique was initially optimized on primary neuronal cultures and successfully used to create in vitro models of protein toxicity and aggregation for ALS and Huntington's Disease[70,211,212].

This methodology is based on transfecting the population of interest with a cellular fluorescent reporter, identifying the positive cells after transfection and then following them over time using an automated microscope **(Fig. 20A)**. Using this method it is possible to follow the survival of the single cells within the population rather than the population as a whole, using the same survival analysis equations used in drug screenings[213,214] and register also very small effects on survival and relative risk of cell death. To perform this particular survival analysis on our iPSC-derived cultures it was necessary to first optimise a protocol to insert fluorescent reporters in the iPSC-derived cultures. For the MN survival analysis we used a HB9-eGFP reporter originally generated in the Goldman lab[175]. An electroporation based transfection was optimised in order to introduce the reporter into maturing iPSC-derived MNs and then confirmed the identity of the eGFP positive cells with immunostaining for MN-specific markers **(Fig. 20B)**.

While the MNs cultures are heterogeneous (*see Results Chapter 2.1.2*) the differentiated astrocytes cultures derived from iPSC lines with the protocol described above (*see Results Chapter 2.1.3*) are highly enriched in $GFAP^{+}/S100\beta^{+}$ cells (>90%). Therefore it was possible to perform the

experiment by using a plasmid encoding for a fluorescent protein driven by a constitutive promoter **(Fig. 20C)**; as an additional control for the astrocyte survival analysis cultures were analysed by immunostaining at the end of the experiment to confirm that the majority of cells expressed the astrocyte marker GFAP **(Fig. 20C)**.

Figure 20: Survival Analysis on iPSC-derived cultures using automated longitudinal microscopy. (A) Schematic representation of in vitro High Content Screening experiment using automated longitudinal microscopy. (B) Representative images of co-immunolabelling of HB9-eGFP^{+} transfected cells and motor neuronal markers, to confirm the identity of the transfected cells. (C) Representative images of pGW1-mApple transfected astrocytes cultures (on the right) at the beginning of a survival experiment, and a immunostaining for GFAP taken at the end of a survival experiment (on the left).

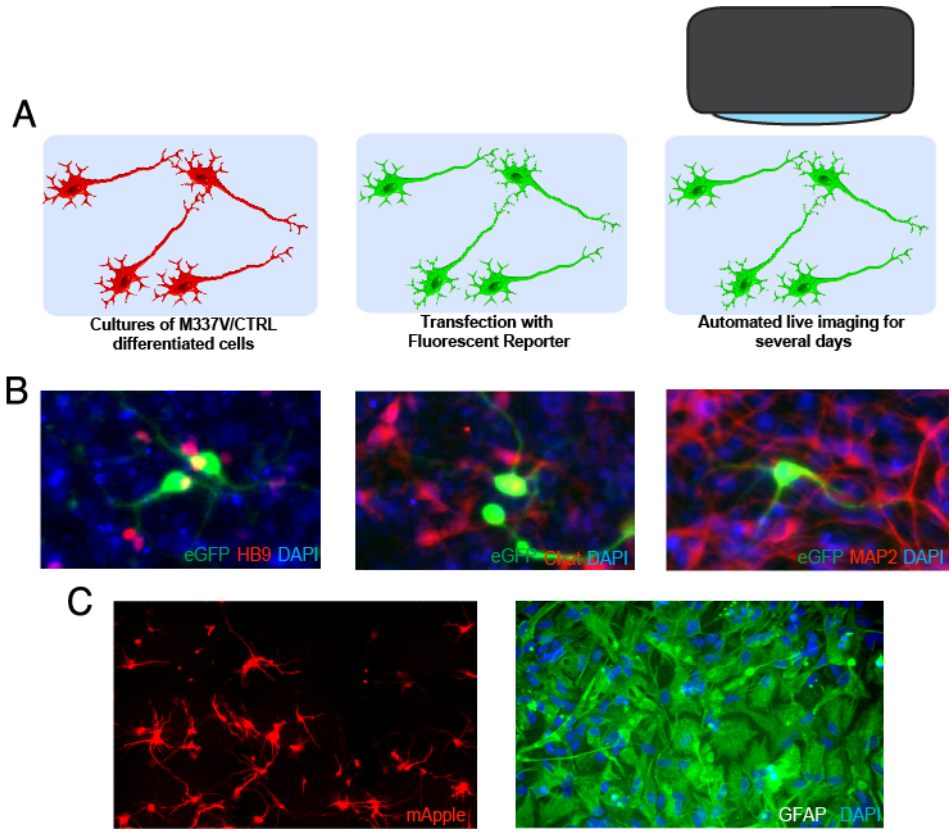
A
Cultures of M337V/CTRL differentiated cells
Transfection with Fluorescent Reporter
Automated live imaging for several days
B
eGFP HB9 DAPI
eGFP ChaT DAPI
eGFP MAP2 DAPI
C
mApple
GFAP DAPI

5.2) Survival Analysis in iPSC-derived MNs

To study the survival analysis in M337V iPSC-derived MNs neurospheres based cultures (*see Results Chapter 1.2.3)* four weeks into their maturation phase where dissociated to single cells suspension and then transfected with the HB9-eGFP reporter plasmid using a NEON electroporation system, and then plated on a 96-well plate. The automated imaging started 24 hours after transfection and proceeded for 10 days at regular daily intervals. Images were then assembled into time-lapses and analysed to determine survival for every transfected neuron. In particular, the time of cell death for all transfected cells within the fields of analysis was determined applying the criteria previously described by Arrasate and colleagues[209] **(Fig. 21A),** and the data was then used to determine the risk of death for the MNs populations derived from the different iPSC lines and plot cumulative risk curves **(Fig. 21B)**. Interestingly, results showed that under basal conditions, the cumulative risk curves for the two clones of the M337V line were clustering together at significantly higher cumulative risk levels compared to both control iPSC lines. Moreover, MNs derived from both clones of the mutant iPSC lines presented over two fold-increase in cumulative Hazard Ratio (cHR) compared to MNs derived from CTRL-1 iPSC line **(Fig. 21C)**. Given that the two lines for each genotype were presenting very similar behaviour in this highly sensitive analysis of cumulative risk of death and cHR, it was possible to cluster the different genotype together, averaging the contribution to survival of the different iPSC lines **(Fig. 21D)**. The analysis of cHR by genotype revealed that the presence of the M337V mutation in mature MNs confer a 2.65 fold increase in the relative risk of death (cHR M337V 2.6516, cHR CTRL 1; $p=2x10^{-16}$) compared to Control MNs under basal conditions.

Figure 21: Survival Analysis of iPSC-derived MNs. (A) Representative images from a typical survival analysis of HB9:EGFP-expressing MNs; cell fate was followed over 10 days, and cell death was determined by loss of fluorescence or dissolution of the cell itself (note as one of the astrocytes [red arrow] survives for the whole experiment, while in the same field, another cell [blue arrow] displays morphologic changes and disappears). (B) Real-time survival analysis of M337V-1, M337V-2, CTRL-1 and CTRL-2 iPSC-derived MNs under basal conditions. (C) Comparison between cumulative Hazard ratios between M337V-1, M337V-2 and CTRL-2 iPSC-derived MNs compared to CTRL-1 derived MNs. [CTRL-1 as HR=1; CTRL-2 HR=0,7262; M337V-1 HR=2,1942; M337V-2 HR=2,3231, for M337V-1 and M337V-2 vs. CTRL-1 $p<0,001$]. (D) Real-time survival analysis of MN cultures clustered by genotype, $p<0.001$.

All experiments represent averaging of 3 independent replicates

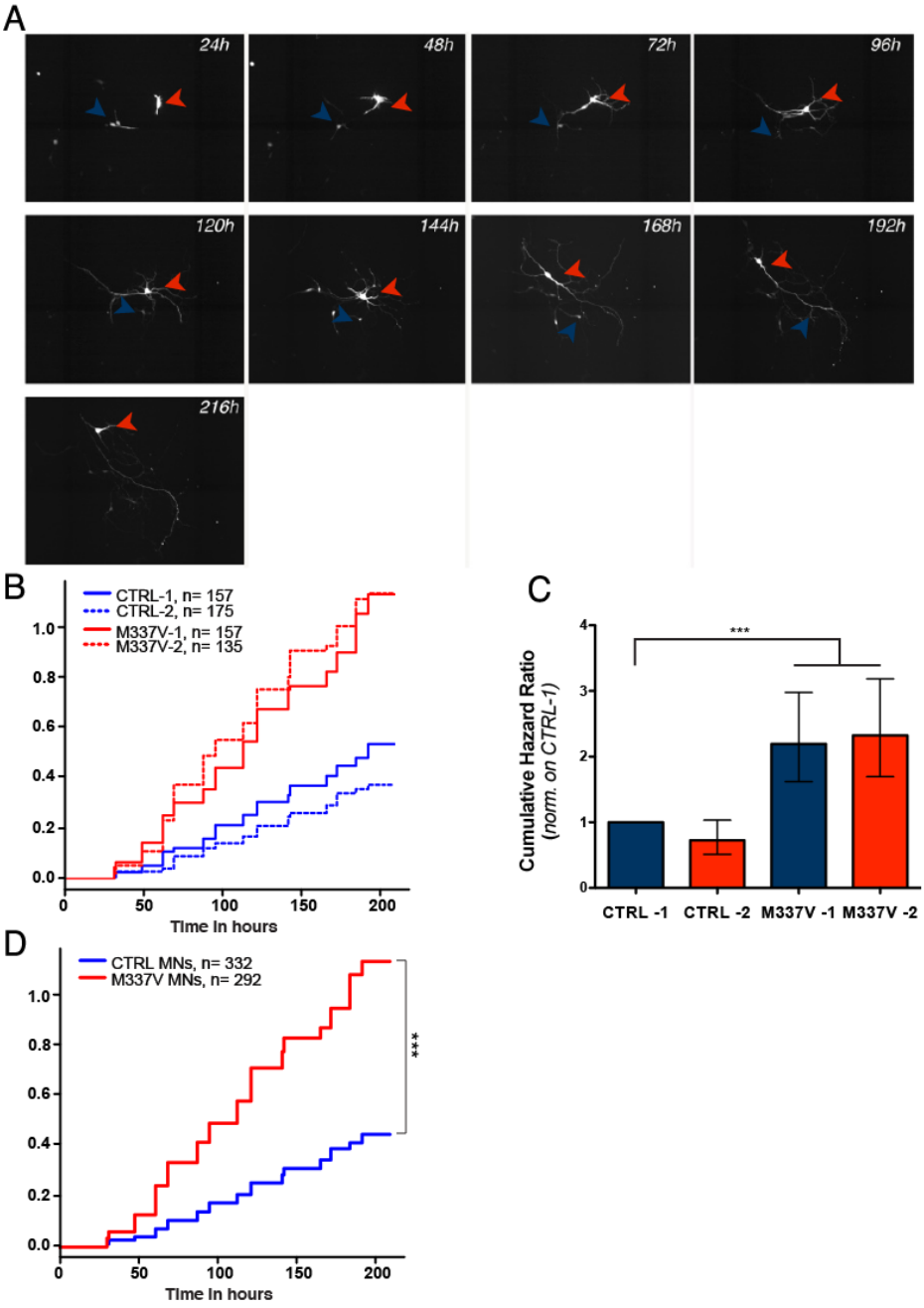
A
24h
48h
72h
96h
120h
144h
168h
192h
216h
B
CTRL-1, n= 157
CTRL-2, n= 175
M337V-1, n= 157
M337V-2, n= 135
Time in hours
C
Cumulative Hazard Ratio
(norm. on CTRL-1)
***
CTRL -1
CTRL -2
M337V -1
M337V -2
D
CTRL MNs, n= 332
M337V MNs, n= 292
***
Time in hours

5.3) Survival Analysis in iPSC-derived Astrocytes

After having established that the M337V mutation confers an intrinsic increased risk of death to MNs, we wanted to verify whether the same toxic effect could be found in astrocytes carrying the mutation. For this purpose differentiated iPSC-derived astroglial cultures were transfected using a plasmid expressing the fluorescent protein mApple under the control of a constitutive viral promoter (CMV); these cultures were then imaged every 24 hours for 10 days with automated longitudinal microscopy. As for the MN survival analysis the time of cell death was determined for all transfected cells within the fields of analysis **(Fig. 22A)** and then used to plot cumulative risk curves for astrocytes derived from the different iPSC lines **(Fig. 22B)**. Similarly to what observed for the survival analysis in MN cultures, the cumulative risk of astrocytes derived from the two clones of the M337V line clustered together at significantly higher cumulative risk levels compared to both control iPSC lines. Cumulative Hazard Ratio (cHR) analysis between astrocytes derived from the different iPSC lines revealed that both M337V iPSC clones present over two fold-increased risk of death compared with astrocytes derived from CTRL-1 iPSCs **(Fig. 21C)**. Finally, the analysis of cumulative hazard in astrocytes cultures clustered by genotype revealed a 2.5-fold greater risk of death associated with the TDP-43 M337V mutation in comparison with controls under basal conditions (cHR M337V 2.6516, cHR CTRL 1; $p=2x10^{-16}$) **(Fig. 21D)**, similarly to what observed in MNs cultures.

Figure 22: Survival Analysis of iPSC-derived Astrocytes. (A) Representative images from a typical survival analysis of EGFP-expressing astrocytes; cell fate was followed over 10 days, and cell death was determined by loss of fluorescence or dissolution of the cell itself (note as one of the astrocytes [red arrow] survives for the whole experiment, while in the same field, another cell [blue arrow] displays morphologic changes at 97 h and disappears by 140 h). (B) Real-time survival analysis of M337V-1, M337V-2, CTRL-1 and CTRL-2 iPSC-derived astrocytes cultures under basal conditions. (C) Comparison between cumulative Hazard ratios between M337V-1, M337V-2 and CTRL-2 iPSC-derived Astrocytes compared to CTRL-1 derived MNs. [CTRL-1 as HR=1; CTRL-2 HR=0,8503; M337V-1 HR=2,0733; M337V-2 HR=2,3796, for M337V-1 and M337V-2 vs. CTRL-1 $p<0,001$]. (D) Real-time survival analysis of MN cultures clustered by genotype, $p<0.001$.
All experiments represent averaging of 3 independent replicates

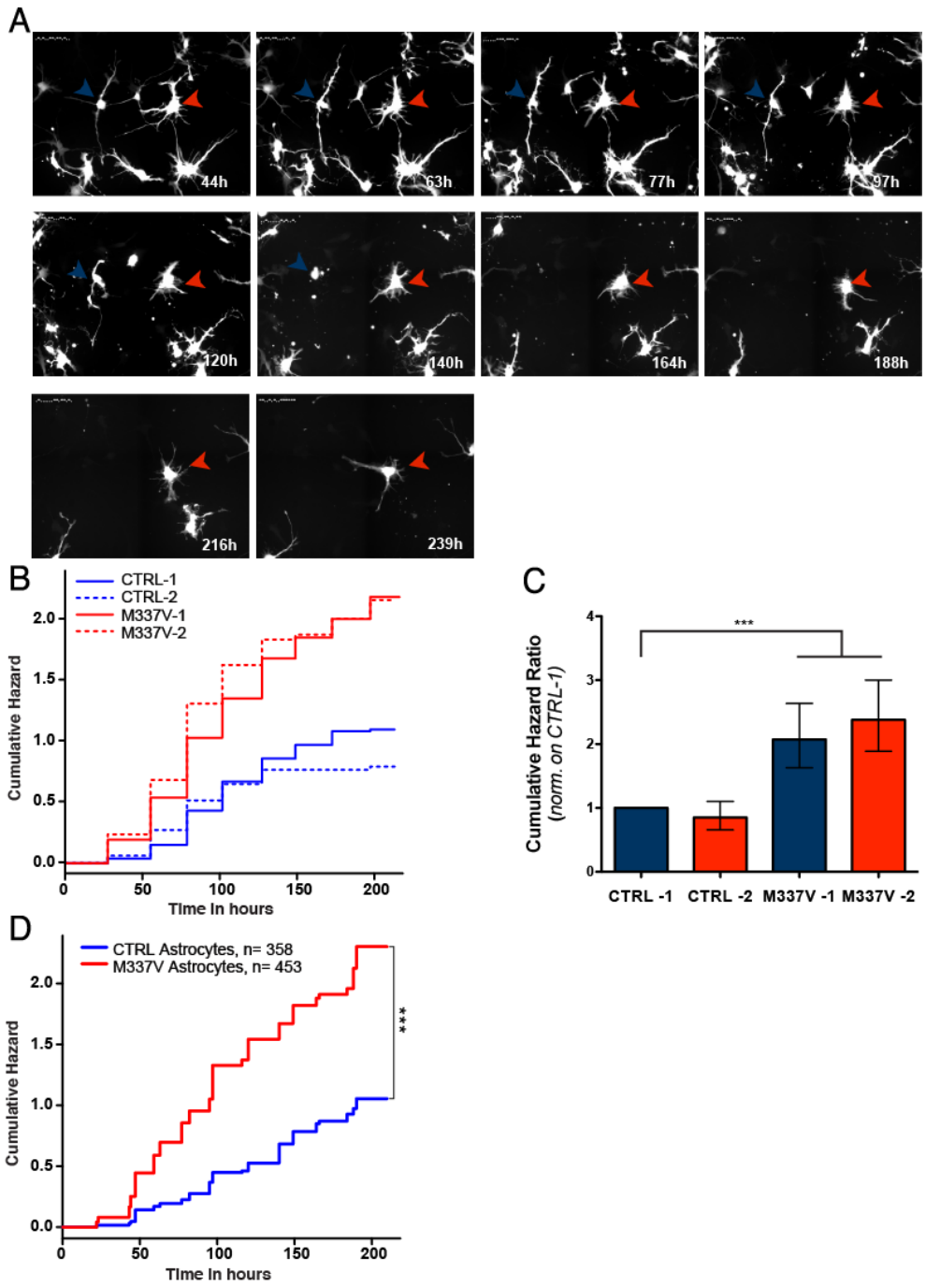
A
44h
63h
77h
97h
120h
140h
164h
188h
216h
239h
B
CTRL-1
CTRL-2
M337V-1
M337V-2
Cumulative Hazard
Time in hours
C
Cumulative Hazard Ratio
(norm. on CTRL-1)
***
CTRL -1
CTRL -2
M337V -1
M337V -2
D
CTRL Astrocytes, n= 358
M337V Astrocytes, n= 453
Cumulative Hazard
Time in hours
***

5.4) Dissection of M337V toxicity mechanism by drug screening

Having established that the presence of the M337V mutation confers an intrinsic toxicity under basal conditions in both MNs and astrocytes demonstrates that the iPSC-based platform to model fALS does not only recapitulate the molecular phenotypes (as accumulation of TDP-43 and cytoplasmic mislocalisation) as demonstrated in Chapter 2, but it also present a measurable survival difference between mutant carrying and control cells. This is a particularly interesting aspect of the in vitro phenotype because having a measurable difference in survival allows in principle to use the automated microscopy set up to test potentially modifying disease compounds. This approach can therefore be used both as a proof of principle for drug testing strategies but also to try to dissect the toxicity mechanism by using already established compounds that affects specific cellular pathways. In particular we used specific compounds to elucidate whether the toxicity observed in M337V carrying cells could be recued (and if so to what degree) by acting specifically on caspase-mediated apoptosis and autophagy.

5.4.1) Apoptosis and M337V Toxicity

To determine if the observed cell death is due to increased apoptosis, we evaluated the effect of an already established pan-caspase inhibitor, QVD-oph[215], on the risk of death of M337V astrocytes, as measured by automated longitudinal microscopy. Treatment with the pan-caspase inhibitor successfully decreased the overall cumulative hazard of both M337V and control astroglial cultures **(Fig. 23A)**. In particular, QVD-treated control astrocytes showed a cHR of 0.33 ($p = 5.07 \times 10\text{-}11$, log-rank test) compared to the vehicle-treated group. On the M337V background, QVD-treatment similarly produced a significantly decrease in cHR, which passed from 2.66 in the vehicle-treated group ($p = 8.13*10\text{-}12$, log-rank test, compared with vehicle-treated CTRL astrocytes) to 0.72 in the QVD-treated group ($p = 0.0145$, log-rank test, compared with vehicle-treated CTRL astrocytes.

Therefore the presence of a non-reversible caspase inhibitor decreased the risk of death over threefold in both genotypes. However, when the M337V and WT QVD-treated groups were compared directly, the M337V astrocytes still displayed a significantly greater hazard ratio than WT astrocytes (2.19, p = 2.32 x 10-7, log-rank test)**(Fig. 23B)**. The comparison of hazard ratios between M337V and control astrocytes with QVD or vehicle-only treatment revealed that caspase inhibition did decrease the overall toxicity observed in astrocytes cultures but in fact failed to significantly lower the observed mutant TDP43-specific toxicity **(Fig. 23C)**.

Figure 23: Caspase-independent toxicity of M337V TDP-43 in Astrocytes. (A) Real-time survival analysis of M337V and control iPSC-derived astrocytes in the presence of 10 μM QVD-oph. The inhibition of caspase activation reduces the risk of death in M337V and control astrocytes (with CTRL+vehicle as a reference, HR for M337V+vehicle 2.61, $p=8.13x10^{-12}$; HR for M337V+QVD 0.72, p=0.0145; HR for CTRL+QVD 0.33, p=5.07x10-11). (B) Direct comparison of QVD-treated M337V and Control iPSC-derived astrocytes (C) Comparison between cumulative hazard ratio of M337V astrocytes in QVD-treated and vehicle–treated groups. [Vehicle treated M337V vs CTRL astrocytes cHR=2.60; QVD-treated M337V vs. CTRL astrocytes cHR=2.20. The error bars represent 95% confidence intervals].

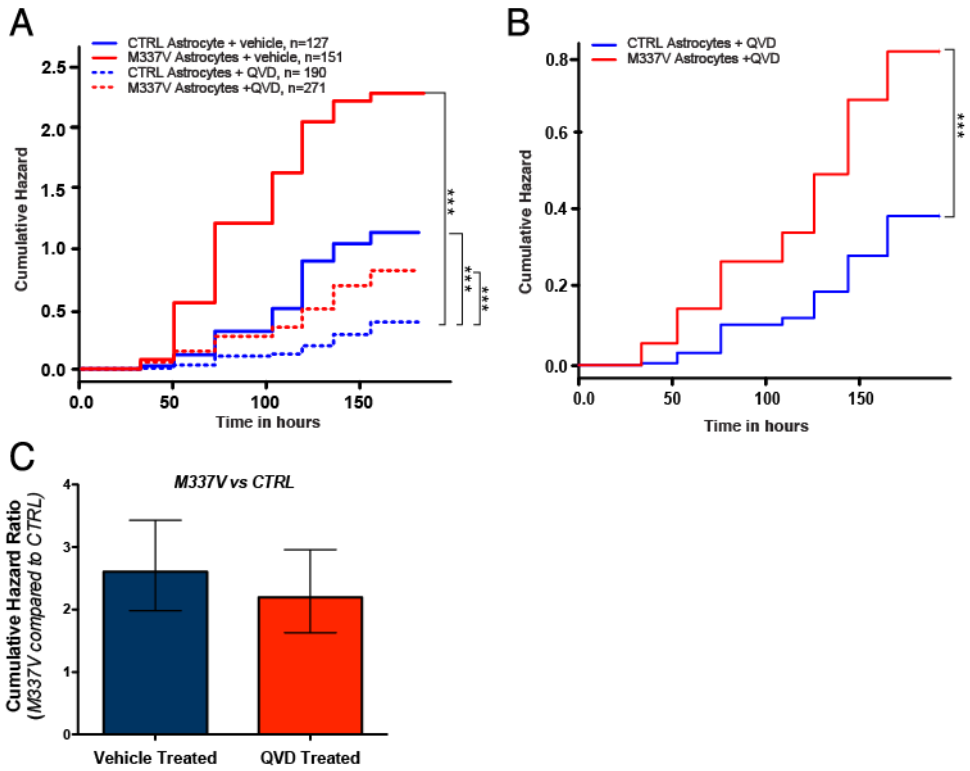
A
CTRL Astrocyte + vehicle, n=127
M337V Astrocytes + vehicle, n=151
CTRL Astrocytes + QVD, n= 190
M337V Astrocytes +QVD, n=271
Cumulative Hazard
Time in hours
***
***
***
B
CTRL Astrocytes + QVD
M337V Astrocytes +QVD
Cumulative Hazard
Time in hours
***
C
M337V vs CTRL
Cumulative Hazard Ratio
(M337V compared to CTRL)
Vehicle Treated
QVD Treated

5.4.2) Autophagy and M337V Toxicity

Autophagy is one of the major cellular recycling pathways. Used to remove long-lived proteins, aggregates and organelles, it involves sequestration of material inside double-membrane vesicles called autophagosomes, which fuse to lysosomes in order to degrade vesicle contents [216]. Autophagic recycling has been recently shown to be very important for neuronal survival, as mice deficient in autophagy spontaneously develop neurodegeneration with age[217]. Deficient autophagic clearance might be one of the causes of accumulation of misfolded proteins that potentially leads to neurodegenerative proteinopathies[218]. More importantly, it has been shown that autophagy plays a role in TDP-43 accumulation and toxicity [219] and more recently autophagy inducers have been shown to ameliorate the phenotype of a TDP-43 proteinopathy model [220].

Tsvetkov and colleagues from Steve Finkbeiner group, have characterised the function of a library of FDA-approved compound based on their affinity with a known Akt inhibitor, 10-[4-(N-diethylamino)butyl]-2-chlorophenoxazine (10-NCP) [221]. In particular they demonstrated that the use of these compounds can significantly decrease the cumulative risk of death measured by automated longitudinal microscopy in an in vitro primary model of Huntington's disease.

Thanks to an on-going collaboration, it was possible to test the effect of some of these compounds on the M337V TDP-43 toxicity observed in both MNs and astrocytes. In particular, three compounds were selected: 10-NCP, together with two already characterised compounds from this library, already in use as neuropsychiatric drugs, Fluphenazine (FPZ), and Methyl-Trimeprazine (MTM) **(Fig. 24A)**.

Treatment of M337V-derived MN cultures with these three compound revealed that while 10-NCP and MTM failed to significantly decrease the cumulative risk of death compared to control MNs, in contrast FPZ had a significant effect and partially recued the toxicity observed **(Fig. 24B)**. Interestingly, when this approach was performed on Control iPSC-derived MNs both FDA-approved drugs demonstrated the ability to increase the

cumulative risk of death, as a side effect. In particular, while 10-NCP did not seems to have a significant effect on the control MNs, MTM increased their cHR to 1.49 (p=0.005) and FPZ had a particularly marked toxic effect, rising the cHR to 1.76 (p=0.0002)**(Fig. 24C)**.

The effect of these three compounds on TDP-43 toxicity was then tested in iPSC-derived astrocytes cultures. Interestingly, all compounds seemed to have a more powerful effect and homogeneous behaviour in astrocytes, compared to what observed in MNs. In fact, all three compounds were able to positively affect the TDP-43 toxicity observed in M337V iPSC-derived astrocytes (M337V vehicle cHR as baseline; M337V FPZ cHR=0.66, p=0.0013; M337V 10-NCP cHR=0.61, p=0.0006; M337V MTM cHR=0.61, p=0.00025) **(Fig. 24D)**, while they did not have any negative effect on the cumulative risk of death observed in control astrocytes populations (CTRL vehicle cHR as baseline; CTRL FPZ cHR=1.18, p=0.22; CTRL 10-NCP cHR=1.12, p=0.48; CTRL MTM cHR=1.06, p=0.67) **(Fig. 24E)**.

The data obtained from the autophagy inducers was then analysed by combining effect of the three treatments and factoring the different genotypes, in both MNs and astrocytes. In general, Autophagy inducers were not able to rescue the toxicity observed in mutation carrying cells, reducing the cHR registered for M337V MNs and collapsing the cumulative risk curve to the baseline. They did however have a negative effect on the overall survival of the control MNs cultures **(Fig. 24F)**. On the contrary, in astrocytes the autophagy inducers were able to significantly reduce the cumulative risk in the mutation carrying cells without having an overall negative effect on the control iPSC-derived astrocytes **(Fig. 24G)**. The rescue of autophagy inducers was however incomplete even in astrocytes, as the cHR of the M337V-treated group was reduced compared to the M337V vehicle treated group, but still significantly higher than the vehicle treated Control astrocytes (M337V vehicle cHR=2.53, $p=2.55x10^{-11}$; M337V ATPhGYi cHR=1.56, p=0.000313; CTRL vehicle as 1).

Figure 24: M337V toxicity is partially rescued by Autophagy inducers compounds. (A) Formula structures of the three autophagy inducers used in these experiments. (B) Real-time survival analysis of M337V iPSC-derived MN in the presence of autophagy inducers. (with vehicle as a reference, FPZ cHR=0.79, p=0.028; MTM cHR=0.96, p=0.691; 10-NCP cHR=0.86, p=0.17). (C) Real-time survival analysis of CTRL iPSC-derived MN in the presence of autophagy inducers. (with vehicle as a reference, FPZ cHR=1.76, p=0.0001; MTM cHR=1.49, p=0.0056; 10-NCP cHR=1.28, p=0.108). (D) Real-time survival analysis of M337V iPSC-derived Astrocytes in the presence of autophagy inducers. (with vehicle as a reference, FPZ cHR=0.66, p=0.0013; MTM cHR=0.61, p=0.0003; 10-NCP cHR=0.61, p=0.0006). (E) Real-time survival analysis of CTRL iPSC-derived Astrocytes in the presence of autophagy inducers. (with vehicle as a reference, FPZ cHR=1.18, p=0.218; MTM cHR=1.06, p=0.673; 10-NCP cHR=1.26, p=0.474). (F) Analysis of cumulative plots combining the effect of autophagy inducers (ATPhGYi) on the different genotypes of MNs (with CTRL-vehicle as a reference, M337V vehicle cHR=2.01, $p=1.08x10^{-16}$; CTRL ATPhGYi cHR=1.50, p=0.00146; M337V ATPhGYi cHR=1.74, $p=1.09x10^{-05}$). (G) Analysis of cumulative plots combining the effect of autophagy inducers (ATPhGYi) on the different genotypes of MNs (with CTRL-vehicle as a reference, M337V vehicle cHR=2.53, $p=2.55x10^{-11}$; CTRL ATPhGYi cHR=1.13, p=0.307; M337V ATPhGYi cHR=1.56, p=0.000313).

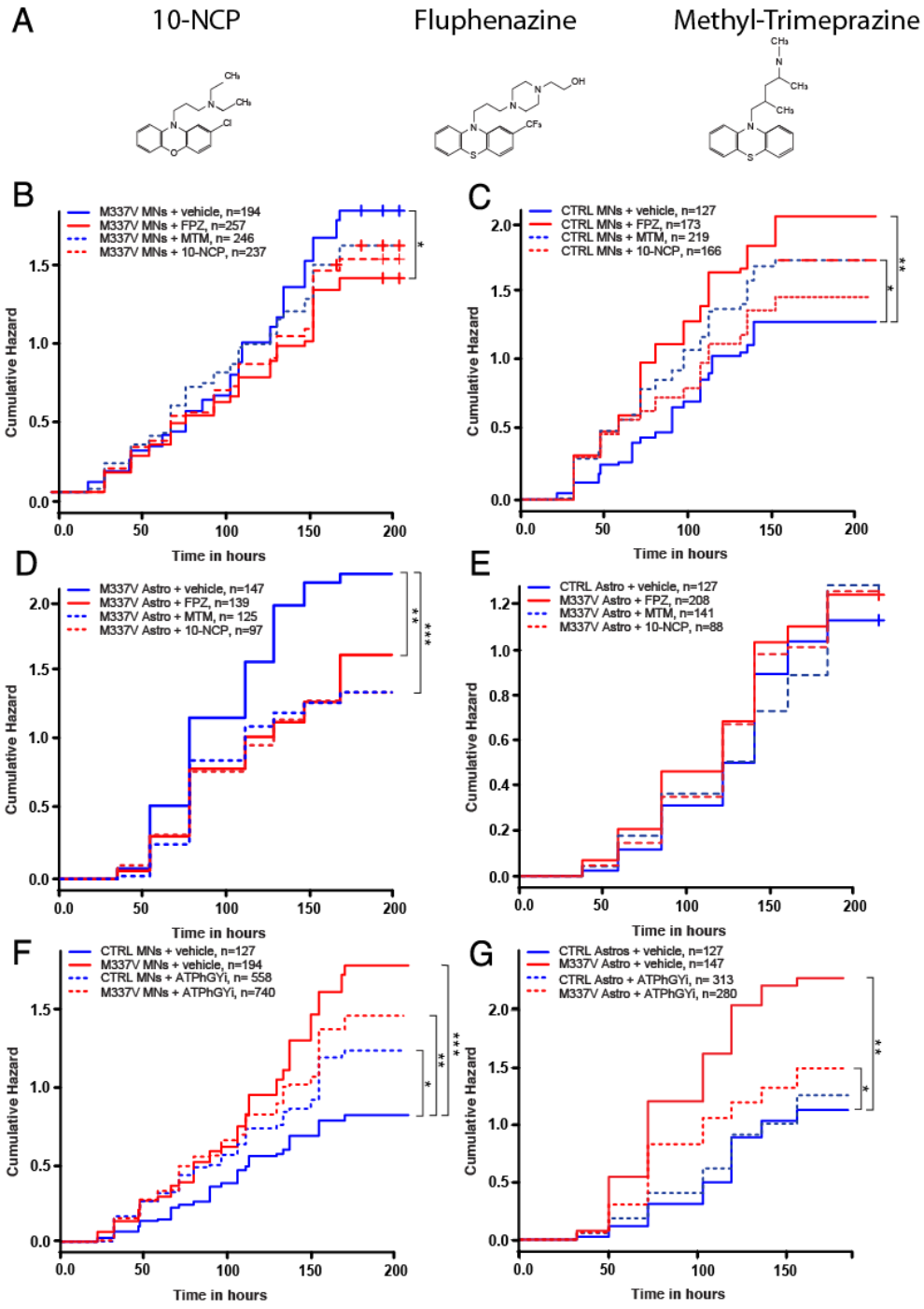
A
10-NCP
Fluphenazine
Methyl-Trimeprazine
B
M337V MNs + vehicle, n=194
M337V MNs + FPZ, n=257
M337V MNs + MTM, n= 246
M337V MNs + 10-NCP, n=237
C
CTRL MNs + vehicle, n=127
CTRL MNs + FPZ, n=173
CTRL MNs + MTM, n= 219
CTRL MNs + 10-NCP, n=166
D
M337V Astro + vehicle, n=147
M337V Astro + FPZ, n=139
M337V Astro + MTM, n= 125
M337V Astro + 10-NCP, n=97
E
CTRL Astro + vehicle, n=127
M337V Astro + FPZ, n=208
M337V Astro + MTM, n=141
M337V Astro + 10-NCP, n=88
F
CTRL MNs + vehicle, n=127
M337V MNs + vehicle, n=194
CTRL MNs + ATPhGYi, n= 558
M337V MNs + ATPhGYi, n=740
G
CTRL Astros + vehicle, n=127
M337V Astro + vehicle, n=147
CTRL Astro + ATPhGYi, n= 313
M337V Astro + ATPhGYi, n=280
Cumulative Hazard
Time in hours

5.5) Conclusions

The experiments presented in this chapter show that in the iPSC-based model established for this project it is possible to detect a survival difference between in both MNs and astrocytes, when comparing M337V and control genotypes under basal conditions.

In ALS, the most relevant pathological phenomenon is arguably the loss of MNs that determines the symptoms in the first place. For this reason the ability to reproduce this selective vulnerability in vitro is of great importance, not only because it allows to study the mechanism of such toxicity but it also offers a clinically relevant measurable outcome for disease modifying compound screening.

Interestingly, a similar toxicity under basal conditions was observed also in highly enriched astrocytes cultures. Although several in vitro models have shown that mutant TDP-43 can be toxic in several different systems (from immortalized cell lines to primary cultures), this study demonstrates for the first time that TDP-43 can exert a direct toxicity in astrocytes. These findings represent the first report of cell-autonomous astrocyte toxicity in a mutant iPSC line and would be compatible with the idea that, at least initially or in part, reactive astrogliosis observed in ALS might not be simply a response to neuronal injury but a consequence of direct mutation-mediated astrocyte toxicity.

One of the key aims of establishing a reliable in vitro model for ALS is the elucidation of the pathways involved in the specific loss of cells observed in the patients, and ultimately the possibility to test different therapeutic strategies directly on patient derived material.

In this context, we were able to prove that the difference in survival between mutant and control astrocytes was not abolished by QVD-treatment, which suggests that the M337V TDP-43 toxicity in astrocytes can be attributed largely to caspase-independent mechanisms.

Moreover, treatment with autophagy inducers was partially able to ameliorate the survival of both M337V MNs and astrocytes, despite these drugs showed the tendency to increase the cumulative risk of death in

control MNs. This is potentially an important results, because together with recently published work on a TDP-43 animal model[220], highlights the potential role of autophagy in ALS pathogenesis, and with it the possibility to act on this pathway to improve survival of mutation carrying cells.

Chapter 6: Survival Analysis in isolated cultures

Mutations on SOD1 were the first genetic causes of ALS to be discovered, therefore most research efforts in the last years have been focused on mtSOD1-fALS models. However, thanks to recent discovery of other genetic variants linked to fALS (such as TDP-43, FUS, C9ORF17) [5,15,22] we have now a better understanding of contribution of other genes in this disease. Of particular importance was the discovery that nearly all cases of ALS (as well ad half of the total number of cases for FTLD) present a pathological signature compatible with a TDP proteinopathy[222]. The only notable exceptions to this observation are those fALS cases determined by mutations on SOD1 which count for a minority all fALS cases. This suggest that the most influential model for ALS research in the last 25 years might not be the one from which we can draw conclusions applicable to the majority of cases.

For these reasons it is of crucial importance to understand whether the same characteristics of SOD1 ALS pathology apply to TDP-43 proteinopathies.

One finding of particular relevance that the field gained from the study of SOD1 fALS models is that this form of the disease can be regarded partially as a non-cell autonomous neurodegenerative disorder (NCA-ND).

In fact, both in vitro and in vivo models convincingly demonstrated that astrocytes carrying SOD1 mutations mediate, at least in part, disease progression in SOD1 fALS[147,150-152]. Understanding whether the TDP-43 mutation carrying astrocytes have a comparable neurotoxic effect is thus of great interest.

Results presented in previous chapters showed that the M337V mutation impairs survival in isolated cultured under basal conditions (*see Chapter 3*) and increase TDP-43 levels. The same analytic approach was then used to examine the survival and morphology of MNs cocultured with either M337V or control astrocytes.

6.1) Analysis of TDP-43 in MN-Astrocytes cocultures

To study the effect of mutation carrying astrocytes on TDP-43 levels a physical coculture system was established starting from the differentiated iPSC cultures optimized so far. Astrocytes monolayers for the cocultures were prepared by differentiating APCs cultures for 14 days in the presence of CNTF (as described in Chapter 1.X) and then plated on a matrigel coated microscopy grade culture-chamber slide, to favour the long-term attachment of the astrocytes without compromising the imaging quality. Astrocyte cultures were maintained on the chamber slide for a period of three days before plating the neurons.

Motor neurons for the cocultures were generated from both genotypes of iPSC lines as described in the previous chapters from neurospheres. After two weeks in their maturation phase, patterned neurospheres were dissociated to single cells using papain and then plated on top of either M337V or Control iPSC-derived astrocyte culture previously prepared. The cocultures were maintained for a period of three weeks and then fixed for analysis.

Immuno-staining for both MN and astrocytes markers was performed (SMI-32 and GFAP) to confer the identity of the cells to be analysed, in addition to TDP-43 staining to compare the protein levels between different cultures **(Fig. 25A)**. The immune-labelled cultures were imaged with a confocal microscope in order to be able to focus the analysis on the MN TDP-43 (on top), restricting the influence of the astrocyte TDP-43 signal (coming from the monolayer at the interface with the culture slide). Moreover, the MNs to be analysed were selected based on the possibility to single out their signal from the underneath astrocytes: in particular the criterium was a minimal presence of GFAP signal within the space occupied by the analysed MNs, within a imaging section of 1 A.U. {calculated on the TDP-43 staining, since the fluorochrome used has the longest wave-length compared to the others}. Selected MNs were manually analysed by drawing regions of interests based on SMI-32 staining. The TDP-43 signal from within the

region of interest was then measured. Quantification of the densitometric analysis revealed that TDP-43 levels fluctuate between the different genotypes and cocultures conditions, but no significant difference was registered **(Fig. 25 B)**.

Figure 25: TDP-43 analysis in MNs-Astrocytes coculture. (A) Representative immunostaining image for 3-week old MN-Astrocytes cocultures, labelled with antibodies against SMI-32, GFAP and TDP43. (B) Densitometric quantification of TDP-43 signal by confocal microscopy comparing MNs from both Control and M337V iPSC lines plated on either genotype of astrocytes for 5 weeks. [M337V MNs on M337V Astro 1.166 ± 1.2 SEM, M337V MNs on CTRL Astro 1.000 ± 0.07 SEM; CTRL MNs on M337V Astro 0.951 ± 0.07 SEM, CTRL MNs on CTRL Astro 1.00 ± 0.2 SEM. Results are presented as densitometric signal fold increase normalized to the same genotype of MNs plated on CTRL astrocytes, n=3 independent experiments.].

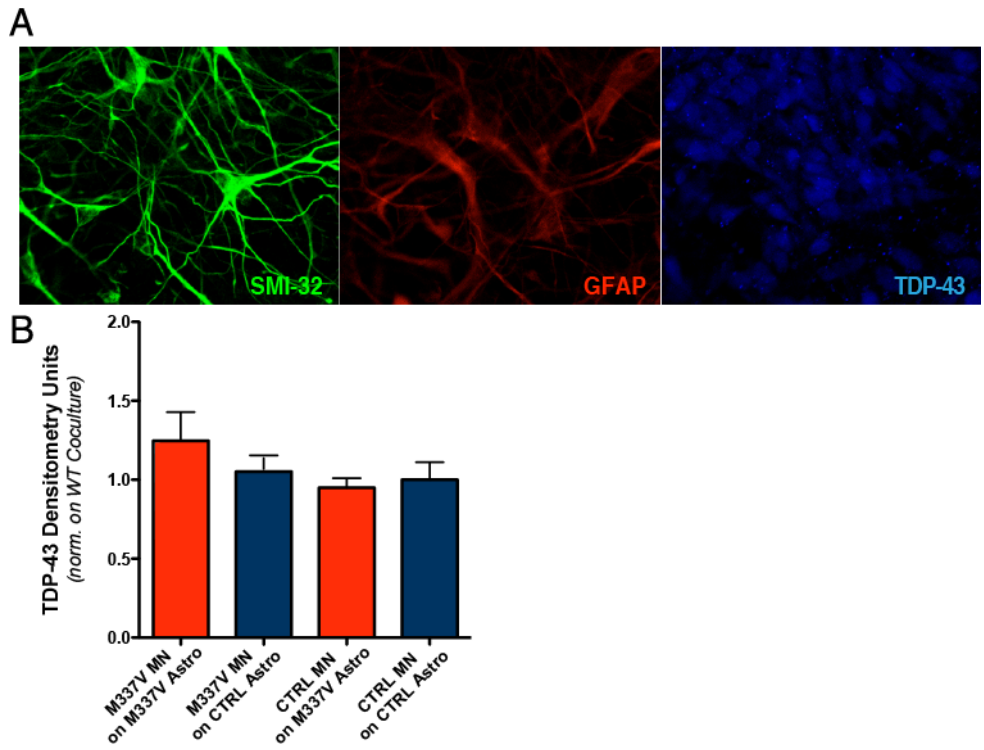
A
SMI-32
GFAP
TDP-43
B
TDP-43 Densitometry Units
(norm. on WT Coculture)
2.0
1.5
1.0
0.5
0.0
M337V MN on M337V Astro
M337V MN on CTRL Astro
CTRL MN on M337V Astro
CTRL MN on CTRL Astro

6.2) Morphological Analysis in MN-Astrocytes cocultures

Astrocytes-neuronal interactions are fundamental to many different key processes in neuronal development and maturation. Among others, one of the key roles played by astrocytes is the regulation of neurite growth. Astrocytes are able to promote neurite growth by providing various diffusible and non-diffusible cues [223,224]. In contrast, reactive astrocytes around sites of neurodegeneration or injuries generally produce growth-inhibitory extracellular matrix (ECM) proteins suppressing the extension of regenerating axons [225]. In the context of NCA-ND, and ALS in particular, the measurement of neurites length has been used as a parameter of neural health and development, when cocultured with mutation carrying astrocytes, (e.g. mutant SOD1 fALS primary astrocytes) [226].

One practical obstacle to a reliable measurement of neurite outgrowth in complex cultures such as iPSC-derived MNs is the difficulty in distinguishing reliably the different cell's neurites with immunostaining (for reference see Fig. 25 A, panel SMI-32). To overcome this obstacle it is possible to use fluorescent reporters instead of immunolabelling to identify the cells to analyse. The non-complete efficiency of the transfection process insures that virtually all neurons expressing the fluorescent reporter will not be overlapping, or in the immediate vicinity of another transfected cell, allowing to reliably assign each neurite to the correct neurons and to measure their length.

To asses whether iPSC-derived mutation carrying astrocytes present an impaired capability to promote neurite outgrowth, Control and M337V iPSC-derived MNs (derived as described in Chapter 1) were transfected with the pHB9:eGFP fluorescent reporter (as described in Chapter 3) and then plated on astrocytes monolayer derived from either genotypes iPSC lines. The cocultures were maintained for a period of three weeks post plating and then imaged with automated live microscopy **(Fig. 26 A)**. Images of HB9:eGFP^{+} cells were then analysed using the NeuronJ software package [227,228] by tracing the length of the visible neurites. The

quantification of the average neurite length was then compared for the different coculture conditions. Results from this experiment revealed that M337V astrocytes do not seem to present an impairment in their ability to promote neurites outgrowth, independently from the genotype of the cocultured MNs **(Fig. 26 B)**.

Figure 26: TDP-43 analysis in MNs-Astrocytes coculture. (A) Representative immunostaining image for 3-week old MN-Astrocytes cocultures, expressing the MN specific reporter HB9::eGFP. (B) Quantification of average neurite length comparing MNs from both Control and M337V iPSC lines plated on either genotype of astrocytes for 3 weeks. Measure are presented in n. of pixels [M337V MNs on M337V Astro 242.9 ± 13.75 SEM, M337V MNs on CTRL Astro 231.4 ± 12.7 SEM; CTRL MNs on M337V Astro 238.1 ± 25.03 SEM, CTRL MNs on CTRL Astro 254.5 ± 33.88 SEM].

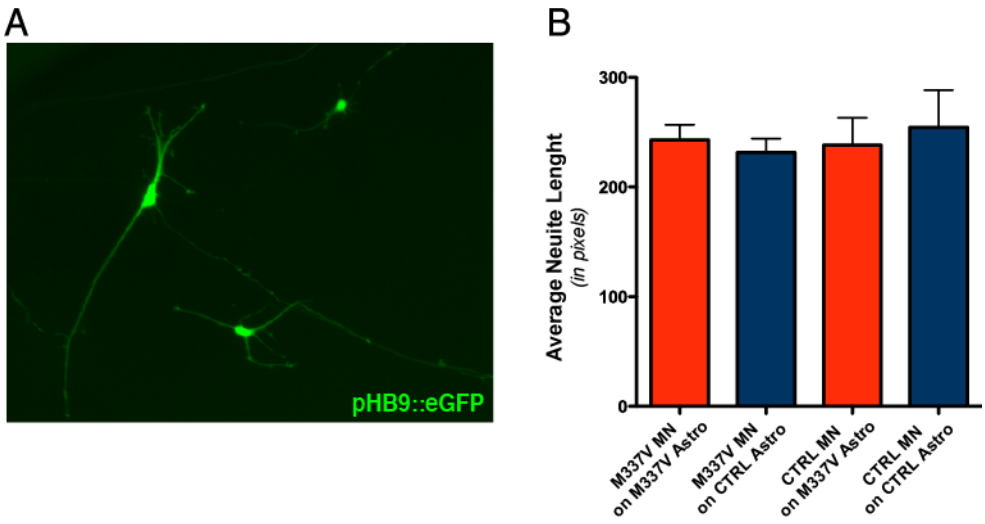
A
pHB9::eGFP
B
Average Neuite Lenght
(in pixels)
300
200
100
0
M337V MN
on M337V Astro
M337V MN
on CTRL Astro
CTRL MN
on M337V Astro
CTRL MN
on CTRL Astro

6.3) Survival Analysis in MN-Astrocytes cocultures

To determine whether, as demonstrated *in vitro* and *in vivo* for SOD1 fALS, TDP-43 mutation carrying astrocytes are negatively affecting the survival of MNs, survival analysis of astrocytes-MNs coculture was undertaken using the longitudinal microscopy approach adopted for the analysis of isolated cultures. Control and mutant iPSC-derived neurospheres were dissociated and transfected with the HB9::eGFP reporter at the end of the MN induction protocol, after two weeks of culture in their maturation phase (as described in Chapter 3). Transfected MNs were then plated on a monolayer of differentiated astrocytes derived from either the mutant or control iPSC line. The coculture was imaged with automated longitudinal microscopy every 24 hours for 10 days to perform survival analysis.

The effect of control and mutant astrocyte background on the survival of Control MN cultures was tested first. Results of this comparison revealed that cumulative risk of death of wild-type MNs cultured on mutant astrocytes was not significantly different from that of WT MNs cultured on WT astrocytes, suggesting that mutant astrocytes do exert a significant toxic effect to wild-type MNs **(Fig. 27 A)**.

Subsequently, the survival of mutant M337V MNs in coculture with astrocytes was determined. Similarly to what observed for Control iPSC-derived MNs, mutation-carrying astrocytes did not exert non-cell-autonomous toxic effects MNs carrying the M337V TDP-43 mutation **(Fig. 27 B).**

As an internal control for these experiments the MNs populations from wither genotype were also plated in isolation and analysed in parallel. This experiment confirmed that the M337V MNs used in the coculture experiments presented greater cell-autonomous vulnerability than healthy or control MNs as shown before (*see Chapter 3.2*) **(Fig. 27 C)**.

Interestingly, when cocultured with astrocytes of either genotype, the cell-autonomous vulnerability previously observed in isolated mutant MNs was no longer evident **(Fig. 27 D)**. These results suggest that, independently from the genetic background of the astrocytes, coculture conditions rescue

the survival difference associated with the TDP-43 M337V mutation in motor neuronal cultures and –importantly- that TDP-43 mutant astrocytes do not exert an in vitro toxic effect on neurons.

The lack of a significant non-cell autonomous toxic effect was also reproduced when the same experiments were repeated using a pan neuronal MAP2::mApple reporter instead of the MN specific HB9::eGFP. In particular, as shown for the MNs, both wild-type and M337V MAP2 positive neurons did show decreased viability when cocultured with TDP-43 mutation carrying astrocytes **(Fig. 28 A-B)**, nor they presented any difference in viability when compared directly **(Fig. 28 C)**.

The results obtained from these coculture survival experiments suggests that –contrary to what observed for SOD1 astrocytes- TDP-43 mutation carrying astroglia are not toxic to MNs. Given the important implications of these observation, it was of utmost importance to be able to confirm that the absence of significant non-cell autonomous effects did not represent merely a false negative result, originated by the inadequacy of the detection system used.

To answer this particular concern, the same longitudinal microscopy approach was used to determine the survival of iPSC-derived MNs cocultured with primary murine astrocytes overexpressing the G93A mutant human SOD1. A number of *in vitro* experiments have convincingly demonstrated that mutant SOD1 astrocytes are toxic to cocultured MNs [147,151,152], and for this reason this particular experiment represent a ideal "positive control" to determine the reliability of the previous observations.

Indeed the results showed clearly that –as previously reported- MNs plated on mutant SOD1 overexpressing astrocytes present a significantly increased risk of death compared to MNs cocultured with wild-type SOD1 astrocytes **(Fig 28 D)**. This result confirms that the longitudinal live microscopy based survival analysis adopted for the coculture experiments is capable of detecting non-cell autonomous effects determined by astrocytes on MNs, supporting the idea that the absence of a increased toxicity in MNs cultured

with M337V iPSC-derived astrocytes is due to a difference in pathogenic mechanism between SOD1 fALS and TDP-43 fALS.

Figure 27: TDP-43 analysis in MNs-Astrocytes coculture I. (A) Real-time survival analysis of Control iPSC-derived MNs plated on either M337V or control iPSC-derived astrocytes. Mutant astrocytes are not toxic to cocultured WT MNs (with WT MNs on WT astrocytes as a reference, HR for WT MNs on M337V astrocytes 0.98, p=0.68). (B Real-time survival analysis of M337V iPSC-derived MNs plated on either M337V or control iPSC-derived astrocytes. Mutant astrocytes are not toxic to cocultured WT MNs (with WT MNs on WT astrocytes as a reference, HR for WT MNs on M337V astrocytes 0.83, p=0.2). (C) Real-time survival analysis of MNs cultured in isolation (n=3), demonstrating cell-autonomous toxicity of mutant TDP43 (with WT as a reference, HR for M337V 2.02, p 8.91x10-7) (D) Longitudinal analysis of both genotypes of MNs plated on either Control or M337V astrocytes. Both Control and M337V astrocytes improved the survival of Control MNs. M337 astrocytes had no detectable toxicity to cocultured MNs. All graph represent pooled data from three independent experiments.

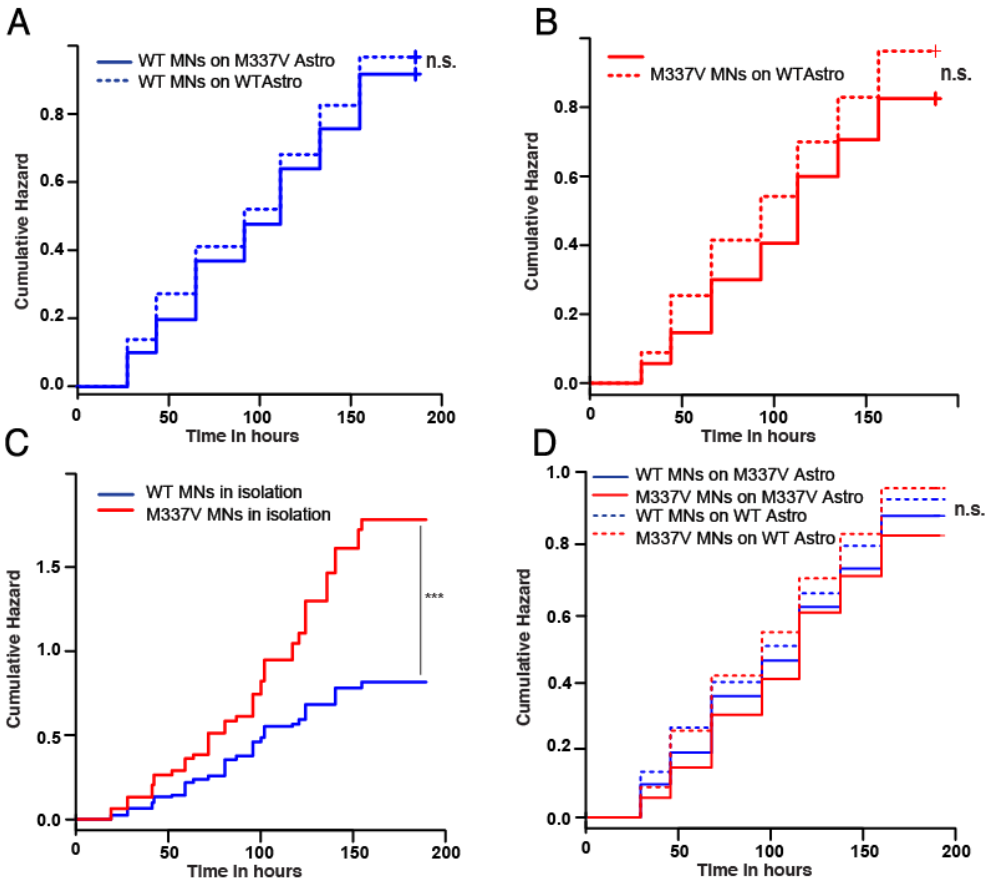
A
WT MNs on M337V Astro
WT MNs on WTAstro
n.s.
Cumulative Hazard
Time in hours
B
M337V MNs on WTAstro
n.s.
Cumulative Hazard
Time in hours
C
WT MNs in isolation
M337V MNs in isolation
***
Cumulative Hazard
Time in hours
D
WT MNs on M337V Astro
M337V MNs on M337V Astro
WT MNs on WT Astro
M337V MNs on WT Astro
n.s.
Cumulative Hazard
Time in hours

Figure 28: TDP-43 analysis in MNs-Astrocytes coculture II. (A) Real-time survival analysis of Control iPSC-derived MAP2+ cells plated on either M337V or control iPSC-derived astrocytes. Mutant astrocytes are not toxic to cocultured neurons (with Control Neurons on WT astrocytes as a reference, HR for WT Neurons on M337V astrocytes 1.08, p=0.58). (B Real-time survival analysis of M337V iPSC-derived MAP2+ cells plated on either M337V or control iPSC-derived astrocytes. Mutant astrocytes are not toxic to cocultured M337V Neurons (with M337V Neurons on WT astrocytes as a reference, HR for M337V Neurons on M337V astrocytes 1.079 , p=0.57). (C) Longitudinal analysis of both genotypes of MAP2+ neurons plated on either WT or M337V astrocytes. (D) Real-time survival analysis of WT MNs cultured on a layer of murine primary astrocytes overexpressing either WT human SOD1 or mutant human SOD1 (n=3), demonstrating non-cell autonomous toxicity of mutant SOD1 astrocytes (with WT SOD1 Astrocytes coculture as a reference, HR for MUT SOD1 coculture 2.46, p 5.05x10-10).

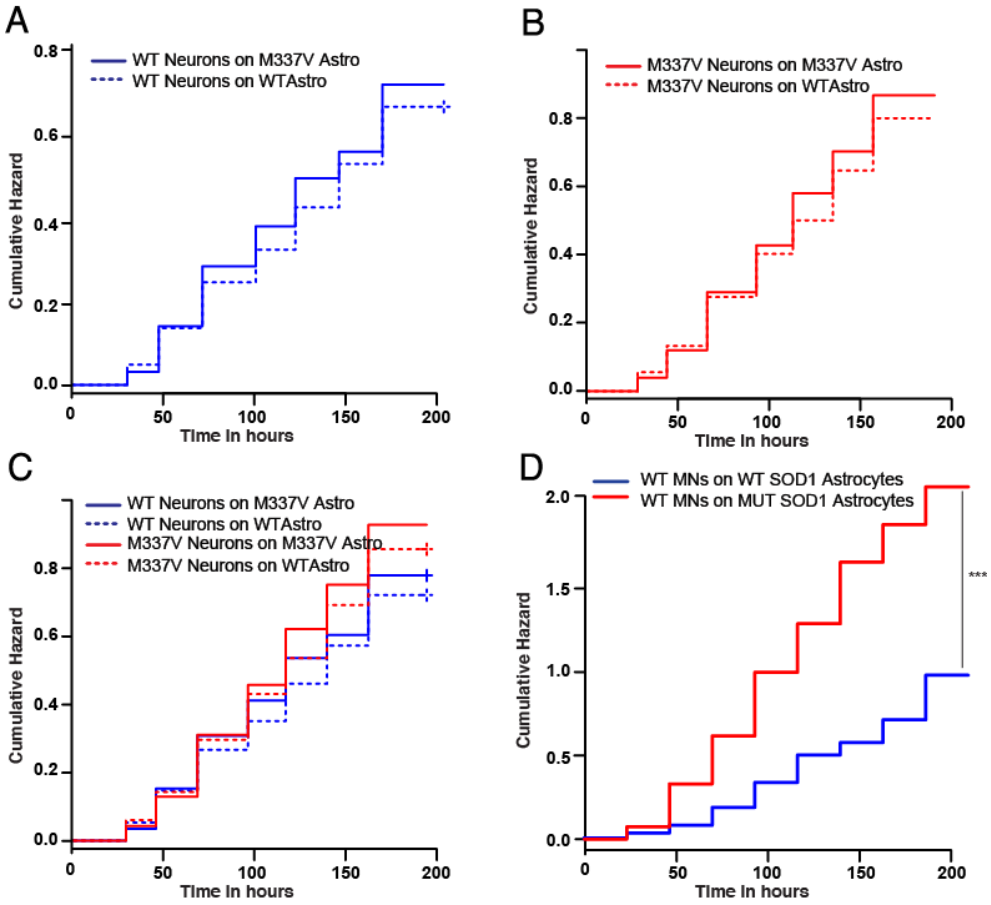
A
WT Neurons on M337V Astro
WT Neurons on WTAstro
Cumulative Hazard
Time in hours
B
M337V Neurons on M337V Astro
M337V Neurons on WTAstro
Cumulative Hazard
Time in hours
C
WT Neurons on M337V Astro
WT Neurons on WTAstro
M337V Neurons on M337V Astro
M337V Neurons on WTAstro
Cumulative Hazard
Time in hours
D
WT MNs on WT SOD1 Astrocytes
WT MNs on MUT SOD1 Astrocytes
***
Cumulative Hazard
Time in hours

6.4) Conclusions

Recent *in vitro* and *in vivo* experiments convincingly demonstrated that in SOD1 fALS models astrocytes mediate, at least in part, disease progression [147,150-152]. However, observations from SOD1 models might not be directly applicable to all ALS cases. In fact, the most common pathological features amongst ALS cases is TDP-43 pathology, which is notably absent from SOD1 fALS cases [5]. Understanding whether the TDP-43 mutation carrying astrocytes can determine a non-cell autonomous neurotoxic effect is thus of great interest.

The results presented in this chapter address the question of non-cell autonomy in the iPSC based platform, using both molecular techniques and longitudinal analysis.

In particular, no difference was detected by immune-labelling densitometric analysis in the TDP-43 levels between MNs of either genotypes plated on the M337V astrocytes compared equivalent cocultures with the control astrocytes. This method of analysis gives a reliable comparison between the different groups, but it is not as powerful as the biochemical analysis by immunoblotting used to determine the levels of TDP-43 in isolated cultures. It has not been possible to undertake immunoblotting analysis in the cocultures due to the lack of an optimized protocol to separate the MN component from the astrocytes monolayer at the time of sample harvesting. This could be solve in future studies by optimizing a fluorescent cells sorting protocol coupled with HB9::eGFP reporter transfection.

Astrocytes derived from the mutant iPSC line did not also show any significant differences in their ability to promote axonal outgrowth in MNs, when compared to wild-type astrocytes.

Interestingly the survival of control MNs plated on mutant astrocytes and equivalent MNs cocultured with control astrocytes did not show any significant decreases in viability, suggesting that mutant astrocytes might not be contributing to the pathogenesis in the same way SOD1 mutant astrocyte do. Importantly, by using the same longitudinal microscopic based

methodology on a already established non-cell autonomous toxicity model (coculture with G93A SOD1 overexpressing astrocytes), it was possible to confirm the ability of this experimental system to address cellular autonomy in iPSC based cellular models as has previously been shown in xeno-cultures.

Together these findings suggest that the absence of non-cell autonomous astrocyte mediated toxicity under basal conditions of mutant TDP-43 reflects underlying differences in pathogenic mechanism and warrant further studies using the platform described in this thesis to study sporadic and other familial ALS iPSC lines.

Chapter 7: Discussion and Future Work

This study describes the establishment of a patient iPSC-based platform to model ALS *in vitro*. In particular, the final aim was to use the established system to address question of cell-autonomy and astrocyte-neuronal interactions in the context of TDP-43 fALS and TDP proteinopathies in general. To accomplish this goal, it was initially necessary to obtain suitable population of both motor neurones and astrocytes from the TDP-43 mutation carrying iPSC lines and controls.

7.1) Generation of Motor Neurones and Astrocytes from iPSC lines

The protocol used to generate reliably population of MNs from the iPSC lines was optimised to mimic closely the different phases that *in vivo* specify the MN identity.

The first step in CNS development during embryonic development is the generation of the neural tube, which entails the specification of the neuroepithelial identity from the previously pluripotent cells. This step was reproduced in vitro by applying the dual SMAD inhibition system[184], which takes advantage of a small molecule inhibitors to selectively block the Activin/TGF-β (SB431542) and dorsomorphine, an analogue of BMP4 inhibitor Noggin, to reproduce in the cultured pluripotent colonies the same neural specification effect that specifies the neuroepithelium *in vivo*.

After the neural tube formation the regional identities are determined along the rostro-caudal axis first and then along the dorso-ventral axis. This dual stage patterning was reproduced *in vitro* by first treating the neural progenitors with retinoic acid to obtain a homogeneously caudalised population, and then exposing them an analogue of sonic hedgehog (SHH) to shift their expression profile towards a ventral identity. Importantly, *in vivo* as well as in the cultures, the generation of regionally specified progenitors able to give rise to specific neuronal populations is a process that takes places over a relatively long period of time. For this reason, separating the MN generation protocol into different phases offers an

additional practical advantage, besides mimicking closely the embryonic development: because every phase is separate, it has been possible to optimise every step separately to obtain a maximised efficiency (ex. maximum percentage of Nestin/Sox1 positive cells at the end of the neuralisation phase, maximised percentage of HoxB4 positive caudalised progenitors after retinoic acid treatment, etc.).

The same strategy to mimic the *in* vivo neural development was adopted in the development of a protocol to generate astroglial cells from the iPSC lines. As seen in the Introduction, gliogenesis is a highly regulated process that occurs at a specific time during development; the astrocytes generation protocol was modelled to incorporate the same signalling that regulates the generation of astrocytes in the developing embryo.

Moreover, as for the MN protocol, the generation of astrocytes was divided into two separate phases, to optimise separately the induction of astrocyte progenitors and the differentiation and maturation of these progenitors into functional astroglial.

In the first phase of the protocol, pro-gliogenic signalling was used to generate enriched and scalable astroglial progenitors starting from patterned neural precursors (directly from the final phase of the MN protocol). As previously demonstrated with several *in vivo* and *in vitro* experiments, the prolonged propagation of neural precursors in the presence of LIF and EGF but without FGF2 promotes glial commitment and expansion, resulting in efficient astrocyte progenitor cells (APC) fate specification [108,110,113,229]. Optimisation of the mechanical chopping, culturing technique and the transition between neurospheres to monolayer cultures, allowed to obtain highly enriched APC cultures, featuring ≃ 80% cells co-positive for Vimentin and NFIA. The separation of this protocol into generation of APCs and differentiation of the progenitors into functional astrocytes offers practical advantages, as the APCs monolayer cultures can be propagated in the presence of FGF2 and EGF, allowing to significantly reduce the amount of starting material necessary for an experiment, but they can also be cryopreserved, allowing to perform experiments with the same batches of

cells over long periods of times. From the enriched APC cultures it was then possible to obtain high purity (>90%) populations of differentiated astrocytes, co-positive for GFAP and S100β.

The protocol here described represent a considerable advancement compared to the already published methodologies to obtain astroglial from pluripotent cells, in particular in terms of time needed to complete the protocol.

In particular, it has been reported by Krencik and co-workers that neural progenitors cultured in suspension in EGF and FGF2 for prolonged period of times (3-9 months) will progressively lose their neurogenic potential, while increasing their ability to generate functional astroglia [124], in a fashion similar to what happens in the nervous system during development, and leading to a highly enriched GFAP+/S100B+ population by day 180 in culture. The EGF-LIF conversion based protocol here described allows to obtain similarly enriched population of APCs starting from MN-generating neurospheres with a much shorter period of time needed for efficient glial specification of the culture (6 weeks to obtain APCs and 2 weeks to differentiate them into astrocytes). However, to properly compare the two protocols it needs to be noted that they present several differences: firstly, the methodology described by Krencik and colleagues has a shorter patterning phase compared to the MN-specific patterning protocol used here; secondly, in this study the APC-enrichment is started at a stage when the neurospheres have already undergone growth factors withdrawal, to generate MN cultures, which in turn can further help the process of astroglial fate specification [230].

For the purposes of this study it was crucial to ensure that the astrocyte populations generated for the coculture studies were coming from a population of iPSC-derived neurospheres in which the TDP-43 M337V toxicity and miss-localization was already established and confirmed. The addition of pro-gliogenic signalling in culture –together with the propagation of the neurospheres- allowed a reduction in the time needed to

obtain an efficient switch between neuronal and astroglial differentiation potential in MN-patterned progenitors.

Other published protocols obtain a high astrocytes yield from cultured neural progenitors, but in most cases they either make use of serum containing media[192] or they present a high percentage of cells in culture that still express neuronal markers[193].

Conversely, the protocol optimized in this study allows to obtain highly enriched astrocytes population in a chemically defined environments, while at the same time minimizing the amount of neuronal cells present in the cultures.

7.2) Functional Characterisation of iPSC-derived differentiated cultures

Having a population of cells that reproduces *in* vitro the expression profile of a determined population *in vivo* is obviously the starting point for any disease modelling study. In the case of this study, specific marker combinations were used to identify the desired cell types as they arise in the culture: for MNs the markers used are HB9, SMI-32 and ChAT; for astrocytes the combination of GFAP and S100B indicate the desired astrocyte lineage. However, it is also obvious that the mere expression of proteins found in the desired cells –taken alone- does not constitute a solid base to validate hypothesis and test potential treatments. The neurons and astrocytes generated *in vitro* need to resemble their *in vivo* counterparts beyond the expression profile, and present comparable functional properties. To test the validity of the protocols optimised for this study, a battery of functional test for both iPSC-derived MNs and astrocytes was devised.

MNs Functional Characterisation

As a first functional assay for the MNs, electrophysiological characterisation was performed on 10-weeks old cultures. Whole-cell patch clamp recordings showed repetitive firing of action potentials, and spontaneous excitatory post-synaptic currents. Moreover, this characterisation revealed that at this stage MNs present functional NMDA,

AMPA and $GABA_A$ receptors. Taken together these results indicate that the maturation protocol allows the MNs to reach a developmental stage advanced enough to exhibit the basic neuronal functional properties, and to be considered electrophysiologically active.

To further test their functionality, the iPSC-derived MNs were cocultured with differentiated murine myofibers, derived from C2C12 cells.

The NMJ formation assay revealed that the iPSC-derived MNs have the potential of inducing the clustering of nicotinic receptors when making contact with a fused myofibers. This particular experiment represent the current standard for the field [191,194] but it present some limitations: particularly, because of the absence of a defined tri-dimensional environment the structure formed by he's- or iPSC-derived MNs and differentiated C2C12 is very different from the NMJ described *in vivo* [231], and so far no long term study on these "putative" NMJ *in vitro* exists. Moreover, further issues might be raised by the difference of species between the MNs and the C2C12.

However, the conclusion that can safely be drawn from such functional characterisation –limited as they are- is that at the end of the maturation protocol optimised, when cultured with an established model of myofibers *in vitro*, the iPSC-derived MNs have the potential of initiate the clustering of receptors on the muscle cells, which in itself represent the first step of the NMJ formation. More studies concerning the functional properties of these *in vitro* putative NMJs are necessary to fully elucidate the functional potential of iPSC-derived MNs.

Overall, considered the results of these functional assays, it is possible to consider the iPSC-derived MNs used in these study as a suitable population to use in further mechanistic studies.

Also, interestingly, in the functional studies undertaken, it was not possible to observe any difference in the behaviour of the TDP-43 mutation carrying MNs compared to the controls. These would suggest that the M337V mutation per se does not impair either the development of MNs or their maturation, nor it prevents them to acquire an electrophysiologically active

profile. It needs to be observed, however, that in most animal models degeneration and NMJ defects reported at early stages [232]: these effects of the mutations might not be observed in this *in vitro* system due to the limitations of the NMJ formation assays, or to the limited time that the myofibers and MNs are actually kept in coculture.

Astrocytes Functional Characterisation

One of the aims of this project was to determine whether astrocytes carrying the M337V TDP-43 mutations are toxic to MNs similarly to what observed for SOD1 astrocytes. To evaluate the potential toxic effect it is necessary to account for gain of toxic effects as well as loss of support functions.

For this reason it is extremely important that the astrocytes used in the study present a functional profile very close to what observed for astroglial *in vivo*. Moreover, a thorough functional characterisation is also necessary to prove that the novel protocol optimised in this study is effectively generating *bona fide* astroglial cells.

The functional characterisation of the astrocytes used in this study was focused on determining their ability to uptake glutamate, promote synaptogenesis, and propagate intercellular calcium waves (ICW).

The results of the glutamate uptakes assay revealed that the astrocytes generated with the EGF-LIF enrichment protocol are capable of clearing excesses of L-glutamate from the media in a time dependent fashion. Importantly, this uptake was abolished by both absence of sodium and application of a specific metabotropic amino acid transporter inhibitor (PDC), which indicates the uptake observed is dependent on the activity of EAAT1. Interestingly, the presence of the M337V mutation did not impair the glutamate clearance ability in the astrocytes cultures, having both mutant and control astrocytes performing similarly in terms of both rate of clearance and total amount of cleared glutamate. This is a particularly relevant point, as the impairment of glutamate clearance and consequent excitotoxicity are thought to play a key role in MN toxicity observe in models of SOD1 fALS. In particular, it has been previously shown that

MNs are particularly sensitive to excitotoxicity [233,234], and there are some evidences of increased plasmatic levels of glutamate and decreased expression of glutamate transporters in patient samples[235].

This particular experiment however, presents an intrinsic limitation due to the *in vitro* culture conditions: in the CNS most of the glutamate is cleared from the synaptic clefts by the activity of EAAT2, another astrocytes specific metabotropic transporter. In fact, it is mostly EAAT2 that is found down regulated in SOD1 fALS models and patient samples [236]. However, while EAAT1 is expressed in astrocytes upon maturation, the expression of EAAT2 is regulated by neuronal activity, neuronal networks maturation and other soluble factors [237]. It is therefore expressed at low levels in isolated astrocytes cultures, particularly in pure astrocytes populations differentiated *in vitro*. The results presented in this study indicate that M337V TDP-43 does not impair the glutamate uptake mediated mostly by EAAT1, however future experiments will need to address the effect of this mutation on EAAT2 dependent glutamate uptake, by coculturing the developing astrocyte with neurons from an early stage or by inducing an higher expression of EAAT2 by other means (for example, the application of Ceftriaxone[238]).

Besides the maintenance of the neuronal environment, another important function of astrocytes is to promote synapse formation and maintenance (*see* Introduction). The second functional assay performed on the iPSC-derived astrocytes addressed their ability of promoting the formation of mature synapses in cocultured neurons. The results of these tests revealed that the iPSC-derived astrocytes are able to increase the number of mature synapses formed by the cocultured neurons, compared with isolated neuronal cultures, but they also revealed that the presence of the M337V mutation did not impair this synaptogenesis ability. In fact both genotypes of astrocytes performed equally in terms of number of mature synaptic vesicles observed in the cocultured neurons.

The IPSC-derived astrocytes were also able to generate and propagate ICW in response to soluble cues and mechanical stimuli. In the present study the

presence of ICWs was determined by a stimulation paradigm and following live imaging. Future studies will need to compare the speed of propagation and the number of cells involved in these calcium waves, and possibly compare directly the ICW generated by iPSC-derived astrocytes with those from primary astrocytes, in order to better characterise this particularly important feature of astroglial cells and its development *in vitro*.

Taken together, the presence of ICW in *in vitro* generated astrocytes indicates, their ability to promote synaptogenesis and the glutamate uptake capacity demonstrate that the protocol optimised for this study not only produces GFAP and S100B positive cells that look like astrocytes, but *in vitro* functional astrocytes that can be effectively used to study and model the involvement of astroglial cells in disease pathogenesis and progression.

7.3) Phenotypical characterisation of the iPSC-based TDP-43 model

One of the most important aspects to consider in the establishment of a TDP-43 *in vitro* model is whether it recapitulates the aspects of the TDP-43 pathology described in the disease. To investigate whether the iPSC-platform recapitulates TDP-43 pathology, after the directed differentiation protocols for both MNs and astrocytes were optimised and validated, a battery of molecular and survival assays was undertaken.

Modelling the MN Component of ALS with iPSC

As seen in the Introduction chapters, TDP-43 proteinopathies and ALS in particular are characterised primarily by accumulation and mislocalisation of this protein, coupled with the specific loss of neurons (MNs in the case of ALS) that ultimately causes the symptoms.

Interestingly, in this study MNs generated from patient-derived iPSC line carrying a pathogenic TDP-43 mutation recapitulate key aspects of TDP-43 proteinopathies in vitro, including cell-autonomous neuronal degeneration and the accumulation of insoluble TDP-43.

The fist molecular characterisation was focused on TDP-43 biochemistry; mutation-carrying MNs presented significantly higher levels of soluble and

detergent-resistant TDP-43. This result is particularly interesting considering that TDP-43 is intrinsically prone to aggregation, and it has been shown that ALS-linked mutations increase its toxicity and tendency to aggregate[239] [67]. Previously, increased stability of mutant TDP-43 proteins had been reported only in isogenic transformed cell lines [240].

Interestingly, although M337V MNs had increased TDP-43 levels compared to control neurons, they expressed equivalent levels of TARDBP mRNA.

This would suggest that differences in TDP-43 protein levels result from a post-translational mechanism rather than from transcriptional differences.

Moreover, the mutant TDP-43 in iPSC-derived MNs do not appear to interfere with the proposed autoregulatory feedback mechanism proposed for the control of TDP-43 mRNA levels[29,42]. One of the possibilities to explain this differences is that missense mutations in the C-terminal domain of the protein might inhibit the turnover of mutant TDP-43 or alternatively negatively effect protein quality control pathways.

These biochemical studies are important as they recapitulate one of the key feature of the pathology, but they also present a limitation due to the starting cellular material. In fact, the samples used represent a mixed cultures containing up to 50% HB9 positive cells, mixed with other spinal cord patterned neuronal cell types as well as a small percentage of progenitors and glial cells. Further studies will need to confirm the biochemistry experiments performed on the mixed MN cultures, by using a purified population of spinal cord MNs.

Besides the biochemical signature, one of the other important molecular features of TDP-43 proteinopathies is the mislocalisation of this protein from the nucleus to the cytoplasm. Despite the higher biochemically levels of TDP-43 observed in M337V neurons detected, it was not possible to detect a significant mislocalisation of TDP-43 immunostaining densitometric analysis. However, this analysis revealed that SMI-32+ neurons had higher levels of nuclear TDP-43 *in vitro*, indicating the possibility that TDP-43 protein levels can differ between neuronal subtypes.

Both M337V and Control iPSC-derived MNs presented a punctate TDP-43 pattern compatible with the involvement of TDP-43 in nucleocytoplasmic shuttling of RNA, the association of TDP-43 with RNA granules in somatodendrites, and the presence of TDP-43 in the microsome fraction of brainstem samples, suggesting active transport of TDP-43 along the axons [241 40,242].

Ubiquitinated TDP-43 aggregates were not observed in the iPSC-derived MNs, despite being one of the most striking features of reported from the post-mortem samples. This could indicate, together with the absence of nuclear TDP-43 clearance, that these phenomena represent a later stage of the pathology, while the *in vitro* iPSC-derived MNs are representative of a much earlier time-point on the pathogenesis timeline.

The presence of elevated TDP-43 protein levels in mutation carrying MNs is important evidence that the iPSC-based platform can be used as a model for this class of diseases. However, it is also equally important that the *in vitro* system recapitulates the event that is the direct cause of the disease in the patients, namely the loss of MNs.

Several cellular and transgenic models of TDP-43 expression established that elevated levels of wild-type and mutant TDP-43 can be highly toxic [243,244]. Moreover, it has been shown that the levels of cytoplasmic, rather than nuclear, TDP-43 correlate with cellular toxicity [70].

Importantly, this study has shown that the presence of the M337V TDP-43 mutation significantly increased the risk of death of iPSC-derived MNs under basal conditions, as measured by longitudinal fluorescence live microscopy of MNs, suggesting an inherent cell-autonomous toxicity of the mutation in MNs.

In summary, these findings show that patient-derived TDP-43 M337V neurons recapitulate key biochemical aspects of TDP-43 proteinopathies and provide evidence that the M337V mutation in TDP-43 is toxic to iPSC-derived MNs.

Shortly after these results on the MN component of the iPSC-based platform were published[245], another research group reported a study on iPSC-derived MNs generated from TDP-43 fALS patients[246]. Importantly, the results presented by Egawa and colleagues confirm most of the finding of the present study, particularly the fact that the mutation per se does not impair MN specification or differentiation, the presence of TDP-43 punctate cytoplasmic staining and the elevated protein levels found in both the soluble and insoluble fraction. There are however some differences in the results that are worth noticing. In particular, the Japanese study reported increased levels of *Tardbp* mRNA levels in the mutation carrying cells, and they also do not report a survival difference between M337V and Control MNs.

The difference in the results regarding the TDP-43 expression levels between this study and the results published by Egawa and colleagues can be attributed to several different causes. First, for the present study one patient line carrying the M337V mutation was used, while the Japanese study uses three different lines carrying respectively a Q343R, a M337V and a G298S mutations. Egawa and co-workers report that the clones of the M337V line they analysed presented *Tardbp* mRNA equivalent to control MNs, while all other lines presented increased levels: future studies will need to address the levels of TDP-43 expression increasing the numbers of patients recruited for the iPSC generation, and the number of clones used for each line. Another difference between the two studies is the cellular samples used: while in this project a mixed MN-containing of spinal cord patterned cultures were used to determine the mRNA levels, in the study presented by Egawa *et al.* the MNs were purified with Fluorescence Activated Cell Sorting (FACS) and a HB9 fluorescent reporter.

Egawa and co-workers also do not report an intrinsic toxicity in MNs as a consequence of the M337V mutation, while in this study we demonstrated that the cumulative risk of death in MNs significantly increases when the mutation is present. One probable explanation for this discrepancy is again to be found in the different set-ups used for the survival experiment. Egawa

and colleagues used a fluorescent based system (IN Cell Analyser 2000, from GE Healthcare) for the survival analysis, counting the number of HB9 positive cells in the culture at different time-points: interestingly they observe a decreased in percentage of survival after 4 days, that is then absent from the later time points[246]. In the live imaging system used for the present study every MN is followed individually which allows a more precise estimation of the risk of death, compared with counting the total number of HB9::GFP positive cells at every time point. These differences in the techniques used for these experiments, together with the variation in the number of lines used can explain the differences in the reported results.

Modelling the Astroglial Component of ALS with iPSC

Having established that the iPSC-based platform can recapitulate key aspects of ALS pathology –at least for what concerns the MN component-, the same molecular phenotyping techniques were applied to population od M337V iPSC-derived astrocytes, to investigate TDP-43 localisation, accumulation and effects on survival in astrocytes.

As shown for the MN populations, M337V expressing astrocytes displayed elevated levels of soluble TDP-43 protein, without presenting an associated increase in *Tardbp* mRNA.

These results, together with the data from the MNs, further support the idea that the M337V mutation affects TDP-43 protein levels via a post-translational mechanism.

It is also of interest that in astrocytes as in MNs, TDP-43 does not seem to negatively auto-regulate its own mRNA, as reported in established stable lines [240].

Conversely to what observed in the MN cultures derived from the same iPSC lines, mutant astrocytes do not show increased levels of detergent-resistant TDP-43 levels together with the accumulation of the protein in the soluble fraction. The reasons for this difference in the behaviour of the mutant protein are unclear, but it would indicate a different cell-specific processing mechanism of protein accumulation.

Along with accumulation of soluble TDP-43, mutant astrocytes also displayed inherent mislocalisation of TDP-43 to the cytoplasm. Interestingly, the increased cytoplasmic TDP-43 levels were not accompanied by a corresponding depletion of nuclear TDP-43 levels, further supporting the idea that the additional TDP-43 is due to increased stability and/or slower clearance.

It is interesting to notice that the loss of TDP-43 nuclear localization has been linked to neuronal degeneration in TDP-43 proteinopathies in animal models and cellular systems (*see Introduction*).

Although cytoplasmic TDP-43 levels were increased, in the mutant astrocytes it was not possible to detect any TDP-43 aggregates, as described in some post-mortem patient samples (Glial Cytoplasmic Inclusion, GCI [247])

As discussed for the MN data, the absence of TDP-43 inclusions and nuclear clearance in astrocytes further support the idea that these events occur at later stage in the pathology, in which case iPSC-platform would be more suitable to model the earlier stages of the disease development, offering an invaluable window on the pathogenic mechanisms of TDP proteinopathies.

Survival analysis of M337V iPSC-derived astrocytes revealed that the presence of the mutation confers a significantly greater risk of death, when compared to Control iPSC-derived astrocytes under basal conditions. The increase in cumulative risk determined by the M337V mutation registered in astrocytes was of similar magnitude to that observed for MNs (HR for M337V Astrocytes is 2.5 compared to controls, while HR for M337V MNs is 2.65 compared to controls).

This results represents the first report of cell-autonomous astrocyte toxicity in a mutant iPSC line, and they are consistent with the idea that, at least initially or in part, reactive astrogliosis observed in ALS might not be simply a secondary response to neuronal injury but a consequence of direct mutation-mediated astrocyte toxicity.

Taken together, these results show that mutation-carrying astrocytes present both a mislocalisation of TDP-43 and a cell-autonomous survival deficit analogous to what observed in MNs, but the results do not indicate whether these two events are linked by causality or if they both are a by-product of another pathological mechanism. Because it was possible to detect both the mislocalisation and the decreased survival in astrocytes, they offer the possibility to elucidate the link between these two phenomena.

Barmada and colleagues showed using ectopic TDP-43 expression in primary rodent neuronal cultures that the localisation and expression levels of the protein are the parameters that mostly influence ectopic-TDP-43 toxicity.

Interestingly, the ectopic M337V and WT TDP-43 expression studies on isogenic control astrocytes reported here (*see Results Chapter 2.5*), demonstrate that the M337V mutation confers an inherent bias towards cytoplasmic localization. In turn, the observation that cytoplasmic localization is associated with an increased risk of death offers an interesting correlation between the increased cytoplasmic TDP-43 of iPSC-derived astrocytes and their lower survival, compared to controls. These findings would support the idea that, as observed in primary neurons, the mutation influences TDP-43 localisation, and in turn this causes the observed toxicity. Importantly, these experiments involved isogenic human astrocytes, so the differences in mislocalisation and toxicity can be attributed specifically to the presence of a disease-associated mutation in TDP-43, and not to potential influences of differences in genetic background. Future studies will be necessary to elucidate the mechanism involved in the change of TDP-43 localisation caused by the mutation. As TDP-43 shuttles between the nucleus and cytoplasm regularly, one of the possible explanation would be that the mutation influences the protein ability to interact with the nuclear import mechanism, an hypothesis suggested by Nishimura and colleagues: their results show that the deletion of the nuclear localisation signal in TDP-43 causes accumulation of the

protein in the cytoplasm, and recapitulate to some extent other features of the pathology[65].

7.4) Drug Studies as a proof of principle

The availability of a human iPSCs based model for TDP-43 proteinopathies that present a measurable phenotype, offers the opportunity to test battery of compounds directly on patient cells and measure their ability to modify the observed phenotype. This particular approach can be used to test potential disease-modifying drugs, but at the same time it offers the opportunity to gain insights on the molecular mechanisms behind the observed phenotype.

In this study we identified a cell autonomous toxicity determined by the presence of the M337V mutation on both MNs and astrocytes. Importantly, the use of survival analysis by longitudinal microscopy allowed to have a precise measurement of the cellular toxicity, through the study of cumulative hazard ratios between the different groups. The same approach was adopted to establish two proof of principles drug studies, that both provided insights on the disease mechanism and indicated some possible therapeutic strategies.

Apoptosis Involvement in M337V Toxicity

The first proof-of-principle drug test performed addressed the question of caspases activation in the TDP-43 toxicity observed in astrocytes.

The treatment of both mutant and control astrocytes with the pan-caspase inhibitor QVD resulted in a three- to fourfold improvement in cell survival on both genetic backgrounds, indicating that in the in vitro system, part of the cell death observed is due to apoptosis by caspases activation. It is interesting to notice that not only the mutant astrocytes but also the control populations presented a significant decrease in the basal levels of cell death registered, indicating that a degree of basal cell death is a feature of the *in vitro* system.

However, when the QVD-treated groups were compared directly, the M337V astrocytes still had a significantly increased risk of death compared to control astrocytes, as measured by Cox proportional hazards analysis. This result suggests that the difference in survival between M337V and control astrocytes can be largely attributed to caspase-independent mechanisms. Indirect support for this caspase-independent mechanism of toxicity in astrocytes is based on the absence of TDP-43 aggregates or significant increase of TDP-43 cleavage products in mutant astrocytes, both of which are associated with caspase activity[248,249].

Autophagy Involvement in M337V Toxicity

The second proof-of-principle drug studies on the iPSC platform was performed in collaboration with Steven Finkbeiner's lab, at the Gladstone Institute (San Francisco, CA), and was focused on testing the effect of a autophagy inducers compounds on the measured TDP-43 toxicity in both MNs and astrocytes.

Autophagy has been indicated as an important pathway involved in TDP-43 clearance and neurodegeneration in several studies[219,250,251]

In particular, Wang and co-workers showed that rapamycin protects against TDP43-mediated neurodegeneration in transgenic mice expressing mutant (A315T) TDP43, confirming a beneficial effect for autophagic upregulation in an animal model of FTD. However, the potential of autophagy as a disease modifying pathway to be manipulated in therapeutic strategies has not be clearly proven, as conflicting evidences have been published. In particular, besides the work present by Wang *et al.*, one other study has suggested that upregulation is beneficial in an animal model of ALS [252], while others have shown that autophagy can enhance neurodegeneration and muscle atrophy [253,254].

The compounds tested in the present study (10-NCP, MTM, and FPZ) have been shown to determine a robust enhancement in autophagic flux even at low concentration. All three compounds have also being shown to significantly enhance the clearance of TDP-43 in primary neurons and

prevented cytoplasmic mislocalisation of TDP-43 (*data not shown, Barmada et al. 2013 unpublished)*.

In the iPSC-platform, treatment with autophagy inducers partially rescued the survival deficit of both M337V MNs and astrocytes, despite showing some tendency to increase the cumulative risk of death in control MNs.

In particular, FPZ proved to be affective in decreasing the cumulative risk of death associated with the M337V mutation in MNs, but it also presented a side toxic effect on the control populations. In astrocytes, the induction of autophagy proved to be able to largely rescue the survival deficit in mutation carrying cells, without drastically increasing the risk of death in control population.

Overall, these results indicate that there could be a beneficial effect in inducing autophagy in TDP43-proteinopathies, and indicate autophagic inducers could be a valid therapeutic option for ALS and other TDP-43 proteinopathies. Clearly, this proof-of-principles study was conducted on a limited number of lines, all coming from the same TDP-43 fALS patient. The inducers will need to be tested a greater number of patient lines, and in particular the repertoire of iPSC will need to include several sporadic patient derived lines, to be able to evaluate the usefulness of this therapeutic approach on the vast majority of ALS cases.

However, besides these limitations, there remains a critical need for effective treatments for ALS and TDP-43 proteinopathies in general. It needs to be considered that the clinical effectiveness of ALS therapies derived from animal models is undermined by several factors: inadequate pre-clinical testing, imprecise model systems, species specific differences or a combination of all the above contributes often to a high rate of failure [255,256]. Thus, more faithful model systems are required: iPSC–based systems and drug screening can potentially bridge the gap between animal models and the clinical application of novel therapies, provided that they accurately recapitulate the relevant mechanisms of disease.

7.5) Cocultures and Non-cell autonomy

Recently, several in vitro and in vivo models have convincingly demonstrated that astrocytes are, at least in part, responsible for disease progression in SOD1 fALS [147,150-152]. However, since SOD1 fALS cases - unlike the great majority of sporadic and familial ALS cases- do not present the features of TDP-43 proteinopathies [5], understanding whether the TDP-43 mutation carrying astrocytes have a similar non-cell autonomous neurotoxic effect is of great importance. Interestingly, this study has not only shown for the first time that the M337V mutation causes cell-autonomous toxicity in MNs, but it also highlighted a previously unrecognised TDP-43 pathology in the mutation carrying astrocytes, indicating that the astroglial activation in fALS might have a more prominent role other than just a secondary response to neuronal death. On this background, the same longitudinal microscopy based survival analysis approach was applied to MN-astrocytes cocultures, to elucidate whether the astrocytes TDP pathology can indeed cause further MN death.

Importantly, no significant difference was detected in the survival of control MNs plated on mutant astrocytes and equivalent MNs cocultured with control astrocytes, which would suggests the absence of a marked non-cell autonomous toxic effect.

To exclude that this particular result was a false negative due to lack of sensitivity rather than an indication of a radical difference between SOD1 and TDP-43 fALS, the same technical set up was tested using control iPSC-derived MN cocultures on primary mouse astrocytes over-expressing either human wild-type SOD1 or G93A SOD1. These primary astrocytes cultures derived from transgenic mice have previously been used to determine that mutant SOD1 confers to astroglial cells the ability to initiate and accelerate the progression of neuronal toxicity[147]. Results of this experiments confirmed the ability of this experimental system to address cellular autonomy in iPSC based models as has previously been shown in xeno-cultures, confirming in turn that the results obtained from the cocultures with M337V astrocytes do not represent a false negative. It has been shown

in SOD1 fALS rodent model that mutation-carrying astrocytes are responsible for the progression but not the onset of the symptoms. Therefore, one of the potential hypothesis proposed to explain the absence of a non-cell autonomous effects in the iPSC-based model is that as the effect exerted on control MNs might be too small to be detected, and that the M337V astrocytes would negatively influence the survival of mutation carrying MNs.

However, when the experiment was performed with M337V MNs, the results indicated that M337V astrocytes not only did not decrease the survival of mutant neurons, coculture with either genotype of neurons actually rescued the survival deficit observed in isolated M337V MN cultures. As a control for this experiments the same MN populations used for the cocultures where also plated in isolation, where the M337V TDP-43 specific cell autonomous toxicity was replicated. Although this results seems at first counterintuitive, considered that previously in this study a cell-autonomous TDP toxicity was discovered in the astrocytes, it needs to be considered that the presence of the M337V mutation did not impair any of the astrocytes functionalities measured. In this context, one of the possible explanations for rescued toxicity in coculture conditions is that a population of functional astrocytes (even if carrying a potentially toxic mutation) will generally increase the health of a neuronal culture, by regulating the extracellular environment, providing neurotrophins and mechanical support. In this scenario, one of the possible limitations of this survival analysis is the actual length of the analysis itself. It is possible that besides the initial increase in general health, over long periods of time (longer than the 248 hours used here) the mutation carrying astrocytes will be less efficient in maintaining MN survival, or they might provide a relatively small toxic insult that is not detectable over short periods of time but accumulates observed the curse of several weeks or months.

It need to be observed however, that in the other coculture experiments performed (characterisation of synapses and synaptogenesis ability, morphological analysis in MN-astrocytes cocultures) it was not possible to

detect any difference in the performance of M337V astrocytes over controls, even if the coculture was protracted for 3 weeks.

To solve this issues future survival analysis in cocultures will need to be optimised to be able to prologue the analysis over the course of several weeks. Also, to convincingly address this issue, future studies will focus on the transplantation of iPSC-derived astrocytes *in vivo*, using fALS rodent models.

Notwithstanding the necessity of further validation this results in other patient derived iPSC-lines and animal models, they suggest a potential radical difference in the consequence of astroglial-neuronal interaction, at least when modelled under basal conditions in vitro, between SOD1 and TDP-43 fALS.

Interestingly, it has been recently shown that astrocytes derived from post-mortem sporadic ALS and SOD1 fALS patient material have a non-cell-autonomous toxic effect on mouse ES–derived MNs, indicating that the concept of astrocyte-mediated toxicity could be extended to sporadic motor neuron disease [226]. Again, this further support the need to expand the experiments presented here to include more independently derive iPSC-lines representative of both fALS and sporadic cases.

However, it need to be considered also that reactive astrogliosis is defined by a number of phenotypic changes in astrocytes [257] and the extent of mechanistic overlap between the SOD1 fALS and sALS astroglia mediated motor neuron toxicity have not been addressed, and remains to be independently confirmed.

It is also important to note that at present no group reported non-cell autonomous toxicity of SOD1 fALS or sporadic ALS iPSC-derived astrocytes. One potential explanation is that generating astrocytes *in vitro* from iPSCs in the absence of degenerating neurons does recapitulate the entirety of the pathogenic mechanisms, due to the lack of some of the as yet uncharacterized, mutation-specific or more general reactive properties of *in vivo* astroglia.

Nevertheless, the platform described here is ideal to study both the reactive properties of in vitro generated astrocytes and the potential differences between astrocytes generated from sporadic and other fALS iPSC lines.

7.6) Conclusion and Ongoing Work

Although this study was limited to a single patient line with sub-clones and controls, it demonstrate the utility of patient-specific iPSC lines in modelling the molecular pathogenesis of adult neurodegenerative and their potential as a platform to test novel therapeutic approaches.

The iPSC-based platform established can be further expanded and improved by including more fALS and sporadic patient-derive lines, but its usefulness can also be increased by performing more detailed molecular some of which are currently ongoing.

In particular, a collaboration is currently ongoing with Tom Maniatis lab at Columbia University (NY), to study the consequences of M337V TDP-43 mutation on the expression profile and splicing of both MN and astrocytes, by using total mRNA deep sequencing techniques (RNA-seq [258]).

It is also important to consider that the iPSC-based platform does not present a stand-alone modelling technique, and to exploit its full potential needs to be paired with *in vivo* analysis. To this end, the establishment of a protocol to transplant the iPSC-derived astrocytes rodent animal models is currently ongoing. The focus of this particular experiment will be to determine whether the mutation carrying astrocytes can affect long-term neuronal survival in a wild-type animal and in a TDP-43 fALS rodent model.

The drug-screening capacity of the platform, couple with the longitudinal imaging set-up will be also further expanded, including different classes of compound to test therapeutic approaches and probe the molecular mechanisms of TDP toxicity. The study with the autophagy inducers in

collaboration with Steven Finkbeiner's lab is currently on-going and its results will be published shortly.

In conclusion, this study established a novel platform to address the biological consequence of somatic mutations on human iPSC–derived MNs and astroglia but also to dissect the contribution of glial-neuronal cross-talk in neurodegenerative processes. The application of the platform to study the non-cell-autonomous component of TDP-43 proteinopathies, and the description of a previously unrecognized cell autonomous TDP-43 toxic effect on astrocytes further highlight the potential of using patient-derived iPSCs to gain a deeper understanding of the molecular pathogenesis of neurodegenerative disorders.

REFERENCES

1. Boillee, S. *et al.* Onset and progression in inherited ALS determined by motor neurons and microglia. *Science* **312**, 1389–1392 (2006).
2. Lobsiger, C. S. & Cleveland, D. W. Glial cells as intrinsic components of non-cell-autonomous neurodegenerative disease. *Nat Neurosci* **10**, 1355–1360 (2007).
3. Shaw, C. E. Capturing VCP: another molecular piece in the ALS jigsaw puzzle. *Neuron* **68**, 812–814 (2010).
4. Sinaki, M. & Mulder, D. W. Amyotrophic lateral sclerosis: relationship between serum creatine kinase level and patient survival. *Arch Phys Med Rehabil* **67**, 169–171 (1986).
5. Lagier-Tourenne, C. & Cleveland, D. W. Rethinking ALS: the FUS about TDP-43. *Cell* **136**, 1001–1004 (2009).
6. Leigh, P. N. & Swash, M. Cytoskeletal pathology in motor neuron diseases. *Adv Neurol* **56**, 115–124 (1991).
7. Leigh, P. N. *et al.* Ubiquitin-immunoreactive intraneuronal inclusions in amyotrophic lateral sclerosis. Morphology, distribution, and specificity. *Brain* **114 (Pt 2)**, 775–788 (1991).
8. Delisle, M. B. & Carpenter, S. Neurofibrillary axonal swellings and amyotrophic lateral sclerosis. *J Neurol Sci* **63**, 241–250 (1984).
9. Bruijn, L. I., Miller, T. M. & Cleveland, D. W. Unraveling the mechanisms involved in motor neuron degeneration in ALS. *Annu Rev Neurosci* **27**, 723–749 (2004).
10. Forman, M. S., Trojanowski, J. Q. & Lee, V. M.-Y. TDP-43: a novel neurodegenerative proteinopathy. *Curr Opin Neurobiol* **17**, 548–555 (2007).
11. Song, J. H., Huang, C. S., Nagata, K., Yeh, J. Z. & Narahashi, T. Differential action of riluzole on tetrodotoxin-sensitive and tetrodotoxin-resistant sodium channels. *J. Pharmacol. Exp. Ther.* **282**, 707–714 (1997).
12. Orrell, R. W. Motor neuron disease: systematic reviews of treatment for ALS and SMA. *Br Med Bull* **93**, 145–159 (2010).
13. Rosen, D. R. Mutations in Cu/Zn superoxide dismutase gene are associated with familial amyotrophic lateral sclerosis. *Nature* **364**, 362 (1993).
14. Rosen, D. R. *et al.* A frequent ala 4 to val superoxide dismutase-1 mutation is associated with a rapidly progressive familial amyotrophic lateral sclerosis. *Hum Mol Genet* **3**, 981–987 (1994).
15. Sreedharan, J. *et al.* TDP-43 mutations in familial and sporadic amyotrophic lateral sclerosis. *Science* **319**, 1668–1672 (2008).
16. Van Deerlin, V. M. *et al.* TARDBP mutations in amyotrophic lateral sclerosis with TDP-43 neuropathology: a genetic and histopathological analysis. *Lancet Neurol* **7**, 409–416 (2008).
17. Gitcho, M. A. *et al.* TDP-43 A315T mutation in familial motor neuron disease. *Ann Neurol* **63**, 535–538 (2008).

18. Daoud, H. *et al.* Contribution of TARDBP mutations to sporadic amyotrophic lateral sclerosis. *J. Med. Genet.* **46**, 112–114 (2009).
19. Corrado, L. *et al.* High frequency of TARDBP gene mutations in Italian patients with amyotrophic lateral sclerosis. *Hum. Mutat.* **30**, 688–694 (2009).
20. Kwiatkowski, T. J. *et al.* Mutations in the FUS/TLS gene on chromosome 16 cause familial amyotrophic lateral sclerosis. *Science* **323**, 1205–1208 (2009).
21. Vance, C. *et al.* Mutations in FUS, an RNA processing protein, cause familial amyotrophic lateral sclerosis type 6. *Science* **323**, 1208–1211 (2009).
22. Renton, A. E. *et al.* A Hexanucleotide Repeat Expansion in C9ORF72 Is the Cause of Chromosome 9p21-Linked ALS-FTD. *Neuron* **72**, 257–268 (2011).
23. Dejesus-Hernandez, M. *et al.* Expanded GGGGCC Hexanucleotide Repeat in Noncoding Region of C9ORF72 Causes Chromosome 9p-Linked FTD and ALS. *Neuron* **72**, 245–256 (2011).
24. Morris, H. R., Waite, A. J., Williams, N. M., Neal, J. W. & Blake, D. J. Recent advances in the genetics of the ALS-FTLD complex. *Curr Neurol Neurosci Rep* **12**, 243–250 (2012).
25. Ou, S. H., Wu, F., Harrich, D., García-Martínez, L. F. & Gaynor, R. B. Cloning and characterization of a novel cellular protein, TDP-43, that binds to human immunodeficiency virus type 1 TAR DNA sequence motifs. *J Virol* **69**, 3584–3596 (1995).
26. Ayala, Y. M. *et al.* Human, Drosophila, and C.elegans TDP43: nucleic acid binding properties and splicing regulatory function. *J Mol Biol* **348**, 575–588 (2005).
27. Sephton, C. F. *et al.* TDP-43 is a developmentally-regulated protein essential for early embryonic development. *J Biol Chem* (2009).doi:10.1074/jbc.M109.061846
28. Buratti, E. & Baralle, F. E. Multiple roles of TDP-43 in gene expression, splicing regulation, and human disease. *Front Biosci* **13**, 867–878 (2008).
29. Polymenidou, M. *et al.* Long pre-mRNA depletion and RNA missplicing contribute to neuronal vulnerability from loss of TDP-43. *Nat Neurosci* **14**, 459–468 (2011).
30. Sephton, C. F. *et al.* Identification of neuronal RNA targets of TDP-43-containing ribonucleoprotein complexes. *Journal of Biological Chemistry* **286**, 1204–1215 (2011).
31. Buratti, E. *et al.* Nuclear factor TDP-43 and SR proteins promote in vitro and in vivo CFTR exon 9 skipping. *EMBO J* **20**, 1774–1784 (2001).
32. Buratti, E. & Baralle, F. E. Characterization and functional implications of the RNA binding properties of nuclear factor TDP-43, a novel splicing regulator of CFTR exon 9. *J Biol Chem* **276**, 36337–36343 (2001).
33. Bose, J. K., Wang, I.-F., Hung, L., Tarn, W.-Y. & Shen, C.-K. J. TDP-43 overexpression enhances exon 7 inclusion during the

survival of motor neuron pre-mRNA splicing. *J Biol Chem* **283**, 28852–28859 (2008).
34. Xu, Y.-F. *et al.* Wild-type human TDP-43 expression causes TDP-43 phosphorylation, mitochondrial aggregation, motor deficits, and early mortality in transgenic mice. *Journal of Neuroscience* **30**, 10851–10859 (2010).
35. Kim, S. H., Shanware, N., Bowler, M. J. & Tibbetts, R. S. ALS-associated proteins TDP-43 and FUS/TLS function in a common biochemical complex to coregulate HDAC6 mRNA. *J Biol Chem* (2010).doi:10.1074/jbc.M110.154831
36. Lee, J.-Y., Nagano, Y., Taylor, J. P., Lim, K. L. & Yao, T.-P. Disease-causing mutations in parkin impair mitochondrial ubiquitination, aggregation, and HDAC6-dependent mitophagy. *J Cell Biol* **189**, 671–679 (2010).
37. Chiang, P.-M. *et al.* Deletion of TDP-43 down-regulates Tbc1d1, a gene linked to obesity, and alters body fat metabolism. *Proc Natl Acad Sci USA* (2010).doi:10.1073/pnas.1002176107
38. Tollervey, J. R. *et al.* Characterizing the RNA targets and position-dependent splicing regulation by TDP-43. *Nat Neurosci* **14**, 452–458 (2011).
39. Wu, L.-S. *et al.* TDP-43, a neuro-pathosignature factor, is essential for early mouse embryogenesis. *Genesis* **48**, 56–62 (2010).
40. Wang, I.-F., Wu, L.-S., Chang, H.-Y. & Shen, C.-K. J. TDP-43, the signature protein of FTLD-U, is a neuronal activity-responsive factor. *J Neurochem* **105**, 797–806 (2008).
41. Cohen, T. J., Lee, V. M.-Y. & Trojanowski, J. Q. TDP-43 functions and pathogenic mechanisms implicated in TDP-43 proteinopathies. *Trends Mol Med* (2011).doi:10.1016/j.molmed.2011.06.004
42. Ayala, Y. M. *et al.* TDP-43 regulates its mRNA levels through a negative feedback loop. *EMBO J* **30**, 277–288 (2011).
43. Igaz, L. M. *et al.* Dysregulation of the ALS-associated gene TDP-43 leads to neuronal death and degeneration in mice. *J Clin Invest* **121**, 726–738 (2011).
44. Winton, M. J. *et al.* Disturbance of nuclear and cytoplasmic TAR DNA-binding protein (TDP-43) induces disease-like redistribution, sequestration, and aggregate formation. *J Biol Chem* **283**, 13302–13309 (2008).
45. Caragounis, A. *et al.* Zinc induces depletion and aggregation of endogenous TDP-43. *Free Radic Biol Med* **48**, 1152–1161 (2010).
46. Colombrita, C. *et al.* TDP-43 is recruited to stress granules in conditions of oxidative insult. *J Neurochem* **111**, 1051–1061 (2009).
47. McDonald, K. K. *et al.* TAR DNA-Binding Protein 43 (TDP-43) Regulates Stress Granule Dynamics via Differential Regulation of G3BP and TIA-1. *Hum Mol Genet* (2011).doi:10.1093/hmg/ddr021
48. Dewey, C. M. *et al.* TDP-43 is directed to stress granules by sorbitol, a novel physiological osmotic and oxidative stressor. *Mol Cell Biol* **31**, 1098–1108 (2011).
49. Anderson, P. & Kedersha, N. Stress granules: the Tao of RNA

triage. *Trends Biochem Sci* **33**, 141–150 (2008).
50. Anderson, P. & Kedersha, N. RNA granules: post-transcriptional and epigenetic modulators of gene expression. *Nat Rev Mol Cell Biol* **10**, 430–436 (2009).
51. Liu-Yesucevitz, L. *et al.* Tar DNA binding protein-43 (TDP-43) associates with stress granules: analysis of cultured cells and pathological brain tissue. *PLoS ONE* **5**, e13250 (2010).
52. Neary, D. *et al.* Frontotemporal lobar degeneration: a consensus on clinical diagnostic criteria. in *Neurology* **51**, 1546–1554 (1998).
53. McKhann, G. M. *et al.* Clinical and pathological diagnosis of frontotemporal dementia: report of the Work Group on Frontotemporal Dementia and Pick's Disease. *Arch. Neurol.* **58**, 1803–1809 (2001).
54. Mackenzie, I. R., Rademakers, R. & Neumann, M. TDP-43 and FUS in amyotrophic lateral sclerosis and frontotemporal dementia. *Lancet Neurol* **9**, 995–1007 (2010).
55. Liscic, R. M., Grinberg, L. T., Zidar, J., Gitcho, M. A. & Cairns, N. J. ALS and FTLD: two faces of TDP-43 proteinopathy. *Eur. J. Neurol.* **15**, 772–780 (2008).
56. Lomen-Hoerth, C., Anderson, T. & Miller, B. The overlap of amyotrophic lateral sclerosis and frontotemporal dementia. *Neurology* **59**, 1077–1079 (2002).
57. Mackenzie, I. R. A. & Feldman, H. H. Ubiquitin immunohistochemistry suggests classic motor neuron disease, motor neuron disease with dementia, and frontotemporal dementia of the motor neuron disease type represent a clinicopathologic spectrum. *J Neuropathol Exp Neurol* **64**, 730–739 (2005).
58. Caselli, R. J. *et al.* Rapidly progressive aphasic dementia and motor neuron disease. *Ann Neurol* **33**, 200–207 (1993).
59. Tsuchiya, K. *et al.* Rapidly progressive aphasia and motor neuron disease: a clinical, radiological, and pathological study of an autopsy case with circumscribed lobar atrophy. *Acta Neuropathol* **99**, 81–87 (2000).
60. Tsuchiya, K. *et al.* Atypical amyotrophic lateral sclerosis with dementia mimicking frontal Pick's disease: a report of an autopsy case with a clinical course of 15 years. *Acta Neuropathol* **101**, 625–630 (2001).
61. Neumann, M. *et al.* Ubiquitinated TDP-43 in Frontotemporal Lobar Degeneration and Amyotrophic Lateral Sclerosis. *Science* **314**, 130–133 (2006).
62. Arai, T. *et al.* TDP-43 is a component of ubiquitin-positive tau-negative inclusions in frontotemporal lobar degeneration and amyotrophic lateral sclerosis. *Biochem Biophys Res Commun* **351**, 602–611 (2006).
63. Mackenzie, I. R. A. *et al.* Nomenclature and nosology for neuropathologic subtypes of frontotemporal lobar degeneration: an update. *Acta Neuropathol* **119**, 1–4 (2010).
64. Mackenzie, I. R. A. *et al.* Pathological TDP-43 distinguishes

sporadic amyotrophic lateral sclerosis from amyotrophic lateral sclerosis with SOD1 mutations. *Ann Neurol* **61**, 427–434 (2007).
65. Nishimura, A. L. *et al.* Nuclear import impairment causes cytoplasmic trans-activation response DNA-binding protein accumulation and is associated with frontotemporal lobar degeneration. *Brain* **133**, 1763–1771 (2010).
66. Igaz, L. M. *et al.* Expression of TDP-43 C-terminal Fragments in Vitro Recapitulates Pathological Features of TDP-43 Proteinopathies. *J Biol Chem* **284**, 8516–8524 (2009).
67. Johnson, B. S. *et al.* TDP-43 is intrinsically aggregation-prone, and amyotrophic lateral sclerosis-linked mutations accelerate aggregation and increase toxicity. *J Biol Chem* **284**, 20329–20339 (2009).
68. Iguchi, Y. *et al.* TDP-43 depletion induces neuronal cell damage through dysregulation of Rho family GTPases. *J Biol Chem* **284**, 22059–22066 (2009).
69. Cohen, T. J., Hwang, A. W., Unger, T., Trojanowski, J. Q. & Lee, V. M.-Y. Redox signalling directly regulates TDP-43 via cysteine oxidation and disulphide cross-linking. *EMBO J* **31**, 1241–1252 (2011).
70. Barmada, S. J. *et al.* Cytoplasmic mislocalization of TDP-43 is toxic to neurons and enhanced by a mutation associated with familial amyotrophic lateral sclerosis. *Journal of Neuroscience* **30**, 639–649 (2010).
71. Kraemer, B. C. *et al.* Loss of murine TDP-43 disrupts motor function and plays an essential role in embryogenesis. *Acta Neuropathol* **119**, 409–419 (2010).
72. Wu, L.-S., Cheng, W.-C. & Shen, C.-K. J. Targeted depletion of TDP-43 expression in the spinal cord motor neurons leads to the development of amyotrophic lateral sclerosis-like phenotypes in mice. *Journal of Biological Chemistry* **287**, 27335–27344 (2012).
73. Wegorzewska, I., Bell, S., Cairns, N. J., Miller, T. M. & Baloh, R. H. TDP-43 mutant transgenic mice develop features of ALS and frontotemporal lobar degeneration. *Proc Natl Acad Sci USA* **106**, 18809–18814 (2009).
74. Zhou, H. *et al.* Transgenic Rat Model of Neurodegeneration Caused by Mutation in the TDP Gene. *PLoS Genet* **6**, e1000887 (2010).
75. Tian, T. *et al.* TDP-43 potentiates alpha-synuclein toxicity to dopaminergic neurons in transgenic mice. *Int. J. Biol. Sci.* **7**, 234–243 (2011).
76. Shan, X., Chiang, P.-M., Price, D. L. & Wong, P. C. Altered distributions of Gemini of coiled bodies and mitochondria in motor neurons of TDP-43 transgenic mice. *Proc Natl Acad Sci USA* **107**, 16325–16330 (2010).
77. Wils, H. *et al.* TDP-43 transgenic mice develop spastic paralysis and neuronal inclusions characteristic of ALS and frontotemporal lobar degeneration. *Proc Natl Acad Sci USA* **107**, 3858–3863 (2010).

78. Tsai, K.-J. *et al.* Elevated expression of TDP-43 in the forebrain of mice is sufficient to cause neurological and pathological phenotypes mimicking FTLD-U. *J Exp Med* **207**, 1661–1673 (2010).
79. Stallings, N. R., Puttaparthi, K., Luther, C. M., Burns, D. K. & Elliott, J. L. Progressive motor weakness in transgenic mice expressing human TDP-43. *Neurobiol Dis* **40**, 404–414 (2010).
80. Zhou, H. *et al.* Transgenic Rat Model of Neurodegeneration Caused by Mutation in the TDP Gene. *PLoS Genet* **6**, e1000887 (2010).
81. Armakola, M., Hart, M. P. & Gitler, A. D. TDP-43 toxicity in yeast. *Methods* **53**, 238–245 (2011).
82. Giordana, M. T. *et al.* TDP-43 redistribution is an early event in sporadic amyotrophic lateral sclerosis. *Brain Pathol.* **20**, 351–360 (2010).
83. Romano, M., Feiguin, F. & Buratti, E. Drosophila Answers to TDP-43 Proteinopathies. *J Amino Acids* **2012**, 356081 (2012).
84. Voigt, A. *et al.* TDP-43-mediated neuron loss in vivo requires RNA-binding activity. *PLoS ONE* **5**, e12247 (2010).
85. Fiesel, F. C. *et al.* Knockdown of transactive response DNA-binding protein (TDP-43) downregulates histone deacetylase 6. *EMBO J* **29**, 209–221 (2010).
86. Godena, V. K. *et al.* TDP-43 regulates Drosophila neuromuscular junctions growth by modulating Futsch/MAP1B levels and synaptic microtubules organization. *PLoS ONE* **6**, e17808 (2011).
87. Li, Y. *et al.* A Drosophila model for TDP-43 proteinopathy. *Proc Natl Acad Sci USA* **107**, 3169–3174 (2010).
88. Lin, M.-J., Cheng, C.-W. & Shen, C.-K. J. Neuronal function and dysfunction of Drosophila dTDP. *PLoS ONE* **6**, e20371 (2011).
89. Kabashi, E. *et al.* Gain and loss of function of ALS-related mutations of TARDBP (TDP-43) cause motor deficits in vivo. *Hum Mol Genet* **19**, 671–683 (2010).
90. Vaccaro, A. *et al.* Methylene blue protects against TDP-43 and FUS neuronal toxicity in C. elegans and D. rerio. *PLoS ONE* **7**, e42117 (2012).
91. Uchida, A. *et al.* Non-human primate model of amyotrophic lateral sclerosis with cytoplasmic mislocalization of TDP-43. *Brain* **135**, 833–846 (2012).
92. Gendron, T. F., Josephs, K. A. & Petrucelli, L. Review: transactive response DNA-binding protein 43 (TDP-43): mechanisms of neurodegeneration. *Neuropathol Appl Neurobiol* **36**, 97–112 (2010).
93. Feiguin, F. *et al.* Depletion of TDP-43 affects Drosophila motoneurons terminal synapsis and locomotive behavior. *FEBS Lett* **583**, 1586–1592 (2009).
94. Lu, Y., Ferris, J. & Gao, F.-B. Frontotemporal dementia and amyotrophic lateral sclerosis-associated disease protein TDP-43 promotes dendritic branching. *Mol Brain* **2**, 30 (2009).
95. Sofroniew, M. V. & Vinters, H. V. Astrocytes: biology and pathology. *Acta Neuropathol* **119**, 7–35 (2010).
96. Markiewicz, I. & Lukomska, B. The role of astrocytes in the

physiology and pathology of the central nervous system. *Acta Neurobiol Exp (Wars)* **66**, 343–358 (2006).
97. Gage, F. H. Mammalian neural stem cells. *Science* **287**, 1433–1438 (2000).
98. Qian, X. *et al.* Timing of CNS cell generation: a programmed sequence of neuron and glial cell production from isolated murine cortical stem cells. *Neuron* **28**, 69–80 (2000).
99. Sun, Y. *et al.* Neurogenin promotes neurogenesis and inhibits glial differentiation by independent mechanisms. *Cell* **104**, 365–376 (2001).
100. Namihira, M., Kohyama, J., Abematsu, M. & Nakashima, K. Epigenetic mechanisms regulating fate specification of neural stem cells. *Philos. Trans. R. Soc. Lond., B, Biol. Sci.* **363**, 2099–2109 (2008).
101. Hsieh, J. & Gage, F. H. Epigenetic control of neural stem cell fate. *Curr. Opin. Genet. Dev.* **14**, 461–469 (2004).
102. Takizawa, T. *et al.* DNA methylation is a critical cell-intrinsic determinant of astrocyte differentiation in the fetal brain. *Developmental Cell* **1**, 749–758 (2001).
103. Bonni, A. *et al.* Regulation of gliogenesis in the central nervous system by the JAK-STAT signaling pathway. *Science* **278**, 477–483 (1997).
104. Rajan, P. & McKay, R. D. Multiple routes to astrocytic differentiation in the CNS. *J Neurosci* **18**, 3620–3629 (1998).
105. Bugga, L., Gadient, R. A., Kwan, K., Stewart, C. L. & Patterson, P. H. Analysis of neuronal and glial phenotypes in brains of mice deficient in leukemia inhibitory factor. *J Neurobiol* **36**, 509–524 (1998).
106. Koblar, S. A. *et al.* Neural precursor differentiation into astrocytes requires signaling through the leukemia inhibitory factor receptor. *Proc Natl Acad Sci USA* **95**, 3178–3181 (1998).
107. Nakashima, K., Yanagisawa, M., Arakawa, H. & Taga, T. Astrocyte differentiation mediated by LIF in cooperation with BMP2. *FEBS Letters* **457**, 43–46 (1999).
108. Viti, J., Feathers, A., Phillips, J. & Lillien, L. Epidermal growth factor receptors control competence to interpret leukemia inhibitory factor as an astrocyte inducer in developing cortex. *Journal of Neuroscience* **23**, 3385–3393 (2003).
109. Mehler, M. F., Mabie, P. C., Zhang, D. & Kessler, J. A. Bone morphogenetic proteins in the nervous system. *Trends Neurosci* **20**, 309–317 (1997).
110. Fukuda, S. *et al.* Potentiation of Astrogliogenesis by STAT3-Mediated Activation of Bone Morphogenetic Protein-Smad Signaling in Neural Stem Cells. *Mol Cell Biol* **27**, 4931–4937 (2007).
111. Mason, I. Initiation to end point: the multiple roles of fibroblast growth factors in neural development. *Nat Rev Neurosci* **8**, 583–596 (2007).

112. Maric, D., Fiorio Pla, A., Chang, Y. H. & Barker, J. L. Self-renewing and differentiating properties of cortical neural stem cells are selectively regulated by basic fibroblast growth factor (FGF) signaling via specific FGF receptors. *Journal of Neuroscience* **27**, 1836–1852 (2007).
113. Tropepe, V. *et al.* Distinct neural stem cells proliferate in response to EGF and FGF in the developing mouse telencephalon. *Dev Biol* **208**, 166–188 (1999).
114. Gritti, A. *et al.* Epidermal and fibroblast growth factors behave as mitogenic regulators for a single multipotent stem cell-like population from the subventricular region of the adult mouse forebrain. *J Neurosci* **19**, 3287–3297 (1999).
115. Martens, D. J., Tropepe, V. & van der Kooy, D. Separate proliferation kinetics of fibroblast growth factor-responsive and epidermal growth factor-responsive neural stem cells within the embryonic forebrain germinal zone. *Journal of Neuroscience* **20**, 1085–1095 (2000).
116. Burrows, R. C., Wancio, D., Levitt, P. & Lillien, L. Response diversity and the timing of progenitor cell maturation are regulated by developmental changes in EGFR expression in the cortex. *Neuron* **19**, 251–267 (1997).
117. Caric, D. *et al.* EGFRs mediate chemotactic migration in the developing telencephalon. *Development* **128**, 4203–4216 (2001).
118. Fan, G. *et al.* DNA methylation controls the timing of astrogliogenesis through regulation of JAK-STAT signaling. *Development* **132**, 3345–3356 (2005).
119. Sanalkumar, R., Vidyanand, S., Lalitha Indulekha, C. & James, J. Neuronal vs. glial fate of embryonic stem cell-derived neural progenitors (ES-NPs) is determined by FGF2/EGF during proliferation. *J Mol Neurosci* **42**, 17–27 (2010).
120. Koch, P., Opitz, T., Steinbeck, J. A., Ladewig, J. & Brüstle, O. A rosette-type, self-renewing human ES cell-derived neural stem cell with potential for in vitro instruction and synaptic integration. *Proc Natl Acad Sci USA* **106**, 3225–3230 (2009).
121. Zhang, S. C., Wernig, M., Duncan, I. D., Brüstle, O. & Thomson, J. A. In vitro differentiation of transplantable neural precursors from human embryonic stem cells. *Nat Biotechnol* **19**, 1129–1133 (2001).
122. Glaser, T., Pollard, S. M., Smith, A. & Brüstle, O. Tripotential differentiation of adherently expandable neural stem (NS) cells. *PLoS ONE* **2**, e298 (2007).
123. Conti, L. *et al.* Niche-independent symmetrical self-renewal of a mammalian tissue stem cell. *PLoS Biol* **3**, e283 (2005).
124. Krencik, R., Weick, J. P., Liu, Y., Zhang, Z.-J. & Zhang, S.-C. Specification of transplantable astroglial subtypes from human pluripotent stem cells. *Nat Biotechnol* (2011).doi:10.1038/nbt.1877
125. Corti, S. *et al.* Embryonic stem cell-derived neural stem cells improve spinal muscular atrophy phenotype in mice. *Brain* **133**, 465–481 (2010).

126. Axell, M. Z., Zlateva, S. & Curtis, M. A method for rapid derivation and propagation of neural progenitors from human embryonic stem cells. *J Neurosci Methods* **184**, 275–284 (2009).
127. Barbeito, L. H. *et al.* A role for astrocytes in motor neuron loss in amyotrophic lateral sclerosis. *Brain Res Brain Res Rev* **47**, 263–274 (2004).
128. Nedergaard, M., Ransom, B. & Goldman, S. A. New roles for astrocytes: redefining the functional architecture of the brain. *Trends Neurosci* **26**, 523–530 (2003).
129. Villegas, S. N., Poletta, F. A. & Carri, N. G. GLIA: A reassessment based on novel data on the developing and mature central nervous system. *Cell Biol Int* **27**, 599–609 (2003).
130. Schmalenbach, C. & Müller, H. W. Astroglia-neuron interactions that promote long-term neuronal survival. *J. Chem. Neuroanat.* **6**, 229–237 (1993).
131. Diniz, L. P. *et al.* Astrocyte-induced synaptogenesis is mediated by transforming growth factor beta signaling through modulation of D-serine levels in cerebral cortex neurons. *Journal of Biological Chemistry* (2012).doi:10.1074/jbc.M112.380824
132. Emirandetti, A., Graciele Zanon, R., Sabha, M. & de Oliveira, A. L. R. Astrocyte reactivity influences the number of presynaptic terminals apposed to spinal motoneurons after axotomy. *Brain Res* **1095**, 35–42 (2006).
133. Ullian, E. M., Harris, B. T., Wu, A., Chan, J. R. & Barres, B. A. Schwann cells and astrocytes induce synapse formation by spinal motor neurons in culture. *Molecular and Cellular Neuroscience* **25**, 241–251 (2004).
134. Ullian, E. M. Control of Synapse Number by Glia. *Science* **291**, 657–661 (2001).
135. Perea, G., Navarrete, M. & Araque, A. Tripartite synapses: astrocytes process and control synaptic information. *Trends Neurosci* **32**, 421–431 (2009).
136. Wolosker, H., Panizzutti, R. & De Miranda, J. Neurobiology through the looking-glass: D-serine as a new glial-derived transmitter. *Neurochem Int* **41**, 327–332 (2002).
137. Bezzi, P. & Volterra, A. A neuron-glia signalling network in the active brain. *Curr Opin Neurobiol* **11**, 387–394 (2001).
138. Rouach, N. *et al.* Gap junctions and connexin expression in the normal and pathological central nervous system. *Biol Cell* **94**, 457–475 (2002).
139. Gordon, G. R. J., Mulligan, S. J. & MacVicar, B. A. Astrocyte control of the cerebrovasculature. *Glia* **55**, 1214–1221 (2007).
140. Ridet, J. L., Malhotra, S. K., Privat, A. & Gage, F. H. Reactive astrocytes: cellular and molecular cues to biological function. *Trends Neurosci* **20**, 570–577 (1997).
141. Liberto, C. M., Albrecht, P. J., Herx, L. M., Yong, V. W. & Levison, S. W. Pro-regenerative properties of cytokine-activated astrocytes. *J Neurochem* **89**, 1092–1100 (2004).

142. Forman, M. S., Trojanowski, J. Q. & Lee, V. M.-Y. Neurodegenerative diseases: a decade of discoveries paves the way for therapeutic breakthroughs. *Nat Med* **10**, 1055–1063 (2004).
143. Yazawa, I. *et al.* Mouse model of multiple system atrophy alpha-synuclein expression in oligodendrocytes causes glial and neuronal degeneration. *Neuron* **45**, 847–859 (2005).
144. Nakayama, K., Suzuki, Y. & Yazawa, I. Binding of neuronal α-synuclein to β-III tubulin and accumulation in a model of multiple system atrophy. *Biochem Biophys Res Commun* **417**, 1170–1175 (2012).
145. Shin, J.-Y. *et al.* Expression of mutant huntingtin in glial cells contributes to neuronal excitotoxicity. *J Cell Biol* **171**, 1001–1012 (2005).
146. Custer, S. K. *et al.* Bergmann glia expression of polyglutamine-expanded ataxin-7 produces neurodegeneration by impairing glutamate transport. *Nat Neurosci* **9**, 1302–1311 (2006).
147. Di Giorgio, F. P., Carrasco, M. A., Siao, M. C., Maniatis, T. & Eggan, K. Non-cell autonomous effect of glia on motor neurons in an embryonic stem cell-based ALS model. *Nat Neurosci* **10**, 608–614 (2007).
148. Nagai, M. *et al.* Astrocytes expressing ALS-linked mutated SOD1 release factors selectively toxic to motor neurons. *Nat Neurosci* **10**, 615–622 (2007).
149. Yamanaka, K. *et al.* Mutant SOD1 in cell types other than motor neurons and oligodendrocytes accelerates onset of disease in ALS mice. *Proc Natl Acad Sci USA* **105**, 7594–7599 (2008).
150. Yamanaka, K. *et al.* Astrocytes as determinants of disease progression in inherited amyotrophic lateral sclerosis. *Nat Neurosci* **11**, 251–253 (2008).
151. Di Giorgio, F. P., Boulting, G. L., Bobrowicz, S. & Eggan, K. C. Human embryonic stem cell-derived motor neurons are sensitive to the toxic effect of glial cells carrying an ALS-causing mutation. *Cell Stem Cell* **3**, 637–648 (2008).
152. Marchetto, M. C. N. *et al.* Non-cell-autonomous effect of human SOD1 G37R astrocytes on motor neurons derived from human embryonic stem cells. *Cell Stem Cell* **3**, 649–657 (2008).
153. Ince, P. G. *et al.* Molecular pathology and genetic advances in amyotrophic lateral sclerosis: an emerging molecular pathway and the significance of glial pathology. *Acta Neuropathol* **122**, 657–671 (2011).
154. Schiffer, D., Cordera, S., Cavalla, P. & Migheli, A. Reactive astrogliosis of the spinal cord in amyotrophic lateral sclerosis. *J Neurol Sci* **139 Suppl**, 27–33 (1996).
155. Vargas, M. R., Pehar, M., Díaz-Amarilla, P. J., Beckman, J. S. & Barbeito, L. Transcriptional profile of primary astrocytes expressing ALS-linked mutant SOD1. *J Neurosci Res* **86**, 3515–3525 (2008).
156. Thomson, J. A. *et al.* Embryonic stem cell lines derived from

human blastocysts. *Science* **282**, 1145–1147 (1998).
157. Hu, B.-Y. & Zhang, S.-C. Directed Differentiation of Neural-stem cells and Subtype-Specific Neurons from hESCs. *Methods Mol Biol* **636**, 123–137 (2010).
158. Li, X.-J. *et al.* Directed differentiation of ventral spinal progenitors and motor neurons from human embryonic stem cells by small molecules. *Stem Cells* **26**, 886–893 (2008).
159. Wada, T. *et al.* Highly efficient differentiation and enrichment of spinal motor neurons derived from human and monkey embryonic stem cells. *PLoS ONE* **4**, e6722 (2009).
160. Lee, H. *et al.* Directed differentiation and transplantation of human embryonic stem cell-derived motoneurons. *Stem Cells* **25**, 1931–1939 (2007).
161. Vajta, G. Somatic cell nuclear transfer in its first and second decades: successes, setbacks, paradoxes and perspectives. *Reprod. Biomed. Online* **15**, 582–590 (2007).
162. Lee, G.-S. *et al.* Improved developmental competence of cloned porcine embryos with different energy supplements and chemical activation. *Mol. Reprod. Dev.* **66**, 17–23 (2003).
163. Takahashi, K. & Yamanaka, S. Induction of pluripotent stem cells from mouse embryonic and adult fibroblast cultures by defined factors. *Cell* **126**, 663–676 (2006).
164. Takahashi, K. *et al.* Induction of Pluripotent Stem Cells from Adult Human Fibroblasts by Defined Factors. *Cell* **131**, 861–872 (2007).
165. Takahashi, K., Okita, K., Nakagawa, M. & Yamanaka, S. Induction of pluripotent stem cells from fibroblast cultures. *Nat Protoc* **2**, 3081–3089 (2007).
166. HD iPSC Consortium Induced pluripotent stem cells from patients with Huntington's disease show CAG-repeat-expansion-associated phenotypes. *Cell Stem Cell* **11**, 264–278 (2012).
167. Lee, G. *et al.* Modelling pathogenesis and treatment of familial dysautonomia using patient-specific iPSCs. *Nature* **461**, 402–406 (2009).
168. Ebert, A. D. *et al.* Induced pluripotent stem cells from a spinal muscular atrophy patient. *Nature* **457**, 277–280 (2009).
169. Soldner, F. *et al.* Generation of isogenic pluripotent stem cells differing exclusively at two early onset Parkinson point mutations. *Cell* **146**, 318–331 (2011).
170. Nguyen, H. N. *et al.* LRRK2 mutant iPSC-derived DA neurons demonstrate increased susceptibility to oxidative stress. *Cell Stem Cell* **8**, 267–280 (2011).
171. Cheung, A. Y. L. *et al.* Isolation of MECP2-null Rett Syndrome patient hiPS cells and isogenic controls through X-chromosome inactivation. *Hum Mol Genet* **20**, 2103–2115 (2011).
172. Park, I.-H. *et al.* Reprogramming of human somatic cells to pluripotency with defined factors. *Nature* **451**, 141–146 (2008).
173. Hajkova, P. *et al.* DNA-methylation analysis by the bisulfite-assisted genomic sequencing method. *Methods Mol Biol* **200**, 143–

154 (2002).
174. Vallier, L., Alexander, M. & Pedersen, R. A. Activin/Nodal and FGF pathways cooperate to maintain pluripotency of human embryonic stem cells. *J Cell Sci* **118**, 4495–4509 (2005).
175. Singh Roy, N. *et al.* Enhancer-specified GFP-based FACS purification of human spinal motor neurons from embryonic stem cells. *Exp Neurol* **196**, 224–234 (2005).
176. Lee, S.-K., Lee, B., Ruiz, E. C. & Pfaff, S. L. Olig2 and Ngn2 function in opposition to modulate gene expression in motor neuron progenitor cells. *Genes Dev* **19**, 282–294 (2005).
177. Arber, S. *et al.* Requirement for the homeobox gene Hb9 in the consolidation of motor neuron identity. *Neuron* **23**, 659–674 (1999).
178. Li, X.-J. *et al.* Specification of motoneurons from human embryonic stem cells. *Nat Biotechnol* **23**, 215–221 (2005).
179. Sasai, Y. *et al.* Xenopus chordin: a novel dorsalizing factor activated by organizer-specific homeobox genes. *Cell* **79**, 779–790 (1994).
180. Hemmati-Brivanlou, A., Kelly, O. G. & Melton, D. A. Follistatin, an antagonist of activin, is expressed in the Spemann organizer and displays direct neuralizing activity. *Cell* **77**, 283–295 (1994).
181. Smith, W. C. & Harland, R. M. Expression cloning of noggin, a new dorsalizing factor localized to the Spemann organizer in Xenopus embryos. *Cell* **70**, 829–840 (1992).
182. Valenzuela, D. M. *et al.* Identification of mammalian noggin and its expression in the adult nervous system. *J Neurosci* **15**, 6077–6084 (1995).
183. Smith, J. R. *et al.* Inhibition of Activin/Nodal signaling promotes specification of human embryonic stem cells into neuroectoderm. *Dev Biol* **313**, 107–117 (2008).
184. Chambers, S. M. *et al.* Highly efficient neural conversion of human ES and iPS cells by dual inhibition of SMAD signaling. *Nat Biotechnol* **27**, 275–280 (2009).
185. Harris, W. A. Specifying motor neurons: up and down and back to front. *Nat Neurosci* **6**, 1247–1249 (2003).
186. Rankin, S. L., Guy, C. S. & Mearow, K. M. Neurite outgrowth is enhanced by laminin-mediated down-regulation of the low affinity neurotrophin receptor, p75NTR. *J Neurochem* **107**, 799–813 (2008).
187. Aglah, C., Gordon, T. & Posse de Chaves, E. I. cAMP promotes neurite outgrowth and extension through protein kinase A but independently of Erk activation in cultured rat motoneurons. *Neuropharmacology* **55**, 8–17 (2008).
188. Welin, D., Novikova, L. N., Wiberg, M., Kellerth, J.-O. & Novikov, L. N. Effects of N-acetyl-cysteine on the survival and regeneration of sural sensory neurons in adult rats. *Brain Res* **1287**, 58–66 (2009).
189. Lee, S. *et al.* A regulatory network to segregate the identity of neuronal subtypes. *Dev Cell* **14**, 877–889 (2008).
190. Carriedo, S. G., Yin, H. Z. & Weiss, J. H. Motor neurons are

selectively vulnerable to AMPA/kainate receptor-mediated injury in vitro. *J Neurosci* **16**, 4069–4079 (1996).
191. Miles, G. B. *et al.* Functional properties of motoneurons derived from mouse embryonic stem cells. *J Neurosci* **24**, 7848–7858 (2004).
192. Juopperi, T. A. *et al.* Astrocytes generated from patient induced pluripotent stem cells recapitulate features of Huntington's disease patient cells. *Mol Brain* **5**, 17 (2012).
193. Emdad, L., D'Souza, S. L., Kothari, H. P., Qadeer, Z. A. & Germano, I. M. Efficient Differentiation of Human Embryonic and Induced Pluripotent Stem Cells into Functional Astrocytes. *Stem Cells Dev* **21**, 404–410 (2012).
194. Hu, B.-Y. *et al.* Neural differentiation of human induced pluripotent stem cells follows developmental principles but with variable potency. *Proc Natl Acad Sci USA* **107**, 4335–4340 (2010).
195. de Vellis, J. & Cole, R. Preparation of mixed glial cultures from postnatal rat brain. *Methods Mol Biol* **814**, 49–59 (2012).
196. Sakai, Y., Rawson, C., Lindburgh, K. & Barnes, D. Serum and trans- forming growth factor p regulate glial fibrillary acidic protein in serum-free-derived mouse embryo cells. *Proc Natl Acad Sci U S A* 1–5 (1990).
197. Johe, K. K., Hazel, T. G., Muller, T., Dugich-Djordjevic, M. M. & McKay, R. D. Single factors direct the differentiation of stem cells from the fetal and adult central nervous system. *Genes Dev* **10**, 3129–3140 (1996).
198. Gross, R. E. *et al.* Bone morphogenetic proteins promote astroglial lineage commitment by mammalian subventricular zone progenitor cells. *Neuron* **17**, 595–606 (1996).
199. Mi, H. & Barres, B. A. Purification and characterization of astrocyte precursor cells in the developing rat optic nerve. *J Neurosci* **19**, 1049–1061 (1999).
200. Deneen, B. *et al.* The transcription factor NFIA controls the onset of gliogenesis in the developing spinal cord. *Neuron* **52**, 953–968 (2006).
201. Andrea Fanelli, F. E. M. R. M. G. S. Temporal and Spatial Analysis of Astrocyte Calcium Waves. 1–4 (2009).
202. Scemes, E. & Giaume, C. Astrocyte calcium waves: what they are and what they do. *Glia* **54**, 716–725 (2006).
203. Grynkiewicz, G., Poenie, M. & Tsien, R. Y. A new generation of Ca2+ indicators with greatly improved fluorescence properties. *J Biol Chem* **260**, 3440–3450 (1985).
204. ATP Released from Astrocytes Mediates Glial Calcium Waves. 1–9 (1998).
205. Abramov, A. Y., Canevari, L. & Duchen, M. R. Changes in intracellular calcium and glutathione in astrocytes as the primary mechanism of amyloid neurotoxicity. *Journal of Neuroscience* **23**, 5088–5095 (2003).
206. Baloh, R. H. TDP-43: The relationship between protein aggregation

and neurodegeneration in ALS and FTLD. *FEBS J* (2011).doi:10.1111/j.1742-4658.2011.08256.x
207. Xu, Y.-F. *et al.* Expression of mutant TDP-43 induces neuronal dysfunction in transgenic mice. *Mol Neurodegener* **6**, 73 (2011).
208. Hong, F. *et al.* Dissecting Early Differentially Expressed Genes in a Mixture of Differentiating Embryonic Stem Cells. *PLoS Comput Biol* **5**, e1000607 (2009).
209. Arrasate, M. & Finkbeiner, S. Automated microscope system for determining factors that predict neuronal fate. *Proc Natl Acad Sci USA* **102**, 3840–3845 (2005).
210. Daub, A., Sharma, P. & Finkbeiner, S. High-content screening of primary neurons: ready for prime time. *Curr Opin Neurobiol* **19**, 537–543 (2009).
211. Dasuri, K. *et al.* Amino acid analog toxicity in primary rat neuronal and astrocyte cultures: Implications for protein misfolding and TDP-43 regulation. *J Neurosci Res* **89**, 1471–1477 (2011).
212. Miller, J. *et al.* Identifying polyglutamine protein species in situ that best predict neurodegeneration. *Nat. Chem. Biol.* **7**, 925–934 (2011).
213. Singh, R. & Mukhopadhyay, K. Survival analysis in clinical trials: Basics and must know areas. *Perspect Clin Res* **2**, 145–148 (2011).
214. Zaman, Q. & Karl, P. Survival analysis in Medical Research. *Interstat* 1–36 (2010).
215. Léveillé, F. *et al.* Suppression of the intrinsic apoptosis pathway by synaptic activity. *Journal of Neuroscience* **30**, 2623–2635 (2010).
216. Rubinsztein, D. C., Gestwicki, J. E., Murphy, L. O. & Klionsky, D. J. Potential therapeutic applications of autophagy. *Nat Rev Drug Discov* **6**, 304–312 (2007).
217. Komatsu, M. *et al.* Loss of autophagy in the central nervous system causes neurodegeneration in mice. *Nature* **441**, 880–884 (2006).
218. Mizushima, N., Levine, B., Cuervo, A. M. & Klionsky, D. J. Autophagy fights disease through cellular self-digestion. *Nature* **451**, 1069–1075 (2008).
219. Caccamo, A. *et al.* Rapamycin rescues TDP-43 mislocalization and the associated low molecular mass neurofilament instability. *J Biol Chem* **284**, 27416–27424 (2009).
220. Wang, I.-F. *et al.* Autophagy activators rescue and alleviate pathogenesis of a mouse model with proteinopathies of the TAR DNA-binding protein 43. *Proc Natl Acad Sci USA* **109**, 15024–15029 (2012).
221. Thimmaiah, K. N. *et al.* Identification of N10-substituted phenoxazines as potent and specific inhibitors of Akt signaling. *J Biol Chem* **280**, 31924–31935 (2005).
222. Kwong, L. K., Neumann, M., Sampathu, D. M., Lee, V. M.-Y. & Trojanowski, J. Q. TDP-43 proteinopathy: the neuropathology underlying major forms of sporadic and familial frontotemporal lobar degeneration and motor neuron disease. *Acta Neuropathol* **114**, 63–70 (2007).
223. Tomaselli, K. J., Neugebauer, K. M., Bixby, J. L., Lilien, J. &

Reichardt, L. F. N-cadherin and integrins: two receptor systems that mediate neuronal process outgrowth on astrocyte surfaces. *Neuron* **1**, 33–43 (1988).
224. Araújo, S. J. & Tear, G. Axon guidance mechanisms and molecules: lessons from invertebrates. *Nat Rev Neurosci* **4**, 910–922 (2003).
225. Silver, J. & Miller, J. H. Regeneration beyond the glial scar. *Nat Rev Neurosci* **5**, 146–156 (2004).
226. Haidet-Phillips, A. M. *et al.* Astrocytes from familial and sporadic ALS patients are toxic to motor neurons. *Nat Biotechnol* (2011).doi:10.1038/nbt.1957
227. E Meijering, M. J. J. C. F. S. P. S. H. H. M. U. Design and Validation of a Tool for Neurite Tracing and Analysis in Fluorescence Microscopy Images. *Cytometry* 1–14 (2004).
228. Popko, J., Fernandes, A., Brites, D. & Lanier, L. M. Automated analysis of NeuronJ tracing data. *Cytometry A* **75**, 371–376 (2009).
229. Rajan, P., Panchision, D. M., Newell, L. F. & McKay, R. D. G. BMPs signal alternately through a SMAD or FRAP-STAT pathway to regulate fate choice in CNS stem cells. *J Cell Biol* **161**, 911–921 (2003).
230. Namihira, M. *et al.* Committed neuronal precursors confer astrocytic potential on residual neural precursor cells. *Dev Cell* **16**, 245–255 (2009).
231. Court, F. A. *et al.* Identity, developmental restriction and reactivity of extralaminar cells capping mammalian neuromuscular junctions. *J Cell Sci* **121**, 3901–3911 (2008).
232. Dupuis, L. & Loeffler, J.-P. Neuromuscular junction destruction during amyotrophic lateral sclerosis: insights from transgenic models. *Curr Opin Pharmacol* **9**, 341–346 (2009).
233. Saroff, D., Delfs, J., Kuznetsov, D. & Geula, C. Selective vulnerability of spinal cord motor neurons to non-NMDA toxicity. *Neuroreport* **11**, 1117–1121 (2000).
234. Rothstein, J. D., Jin, L., Dykes-Hoberg, M. & Kuncl, R. W. Chronic inhibition of glutamate uptake produces a model of slow neurotoxicity. *Proc Natl Acad Sci USA* **90**, 6591–6595 (1993).
235. Ferrarese, C. *et al.* Decreased platelet glutamate uptake in patients with amyotrophic lateral sclerosis. *Neurology* **56**, 270–272 (2001).
236. Maragakis, N. J., Dykes-Hoberg, M. & Rothstein, J. D. Altered expression of the glutamate transporter EAAT2b in neurological disease. *Ann Neurol* **55**, 469–477 (2004).
237. Ghosh, M., Yang, Y., Rothstein, J. D. & Robinson, M. B. Nuclear factor-κB contributes to neuron-dependent induction of glutamate transporter-1 expression in astrocytes. *Journal of Neuroscience* **31**, 9159–9169 (2011).
238. Sari, Y., Prieto, A. L., Barton, S. J., Miller, B. R. & Rebec, G. V. Ceftriaxone-induced up-regulation of cortical and striatal GLT1 in the R6/2 model of Huntington's disease. *J. Biomed. Sci.* **17**, 62 (2010).

239. Neumann, M. *et al.* A new subtype of frontotemporal lobar degeneration with FUS pathology. *Brain* **132**, 2922–2931 (2009).
240. Ling, S.-C. *et al.* ALS-associated mutations in TDP-43 increase its stability and promote TDP-43 complexes with FUS/TLS. *Proc Natl Acad Sci USA* (2010).doi:10.1073/pnas.1008227107
241. Sato, T. *et al.* Axonal ligation induces transient redistribution of TDP-43 in brainstem motor neurons. *Neuroscience* **164**, 1565–1578 (2009).
242. Elvira, G. *et al.* Characterization of an RNA granule from developing brain. *Molecular & cellular proteomics : MCP* **5**, 635–651 (2006).
243. Wegorzewska, I. & Baloh, R. H. TDP-43-based animal models of neurodegeneration: new insights into ALS pathology and pathophysiology. *Neurodegener Dis* **8**, 262–274 (2011).
244. Lagier-Tourenne, C., Polymenidou, M. & Cleveland, D. W. TDP-43 and FUS/TLS: emerging roles in RNA processing and neurodegeneration. *Hum Mol Genet* **19**, R46–R64 (2010).
245. Bilican, B. *et al.* Mutant induced pluripotent stem cell lines recapitulate aspects of TDP-43 proteinopathies and reveal cell-specific vulnerability. *Proc Natl Acad Sci USA* (2012).doi:10.1073/pnas.1202922109
246. Egawa, N. *et al.* Drug Screening for ALS Using Patient-Specific Induced Pluripotent Stem Cells. *Science Translational Medicine* **4**, 145ra104–145ra104 (2012).
247. Zhang, H. *et al.* TDP-43-immunoreactive neuronal and glial inclusions in the neostriatum in amyotrophic lateral sclerosis with and without dementia. *Acta Neuropathol* **115**, 115–122 (2008).
248. Zhang, Y.-J. *et al.* Aberrant cleavage of TDP-43 enhances aggregation and cellular toxicity. *Proc Natl Acad Sci USA* **106**, 7607–7612 (2009).
249. Yang, C. *et al.* The C-terminal TDP-43 fragments have a high aggregation propensity and harm neurons by a dominant-negative mechanism. *PLoS ONE* **5**, e15878 (2010).
250. Wang, X. *et al.* Degradation of TDP-43 and its pathogenic form by autophagy and the ubiquitin-proteasome system. *Neurosci Lett* **469**, 112–116 (2010).
251. Urushitani, M., Sato, T., Bamba, H., Hisa, Y. & Tooyama, I. Synergistic effect between proteasome and autophagosome in the clearance of polyubiquitinated TDP-43. *J Neurosci Res* **88**, 784–797 (2010).
252. Hetz, C. *et al.* XBP-1 deficiency in the nervous system protects against amyotrophic lateral sclerosis by increasing autophagy. *Genes Dev* **23**, 2294–2306 (2009).
253. Zhang, X. *et al.* Rapamycin treatment augments motor neuron degeneration in SOD1 (G93A) mouse model of amyotrophic lateral sclerosis. *Autophagy* **7**, (2011).
254. Dobrowolny, G. *et al.* Skeletal muscle is a primary target of SOD1G93A-mediated toxicity. *Cell Metabolism* **8**, 425–436 (2008).

255. Turner, B. J. & Talbot, K. Transgenics, toxicity and therapeutics in rodent models of mutant SOD1-mediated familial ALS. *Progress in neurobiology* **85**, 94–134 (2008).
256. Gill, A., Kidd, J., Vieira, F., Thompson, K. & Perrin, S. No Benefit from Chronic Lithium Dosing in a Sibling-Matched, Gender Balanced, Investigator-Blinded Trial Using a Standard Mouse Model of Familial ALS. *PLoS ONE* **4**, e6489 (2009).
257. Vargas, M. R. & Johnson, J. A. Astrogliosis in amyotrophic lateral sclerosis: role and therapeutic potential of astrocytes. *Neurotherapeutics* **7**, 471–481 (2010).
258. Friedman, B. A. & Maniatis, T. ExpressionPlot: a web-based framework for analysis of RNA-Seq and microarray gene expression data. *Genome Biol.* **12**, R69 (2011).